DYNAMICS OF MEMBRANE DAMAGE TO SKELETAL MUSCLE CELLS AT SUPRAPHYSIOLOGICAL TEMPERATURES AND THE ROLE OF POLOXAMER 188 IN MINIMIZING MEMBRANE INJURY

by

Joseph T. Padanilam

S.B., Mechanical Engineering
Massachusetts Institute of Technology, 1992

Submitted to the Department of Mechanical Engineering in Partial Fulfillment of the Requirements for the Degree of

MASTER OF SCIENCE
in Mechanical Engineering
at the

Massachusetts Institute of Technology

May 1994

Signature of Author_____
Department of Mechanical Engineering
May 6, 1994

Certified by_____
Mehmet Toner, Assistant Professor of Surgery
Department of Surgery, Harvard Medical School
Thesis Supervisor

Eng.

Accepted by_____
Ain A. Sonin
Chairman, Department Committee on Graduate Students

DYNAMICS OF MEMBRANE DAMAGE TO SKELETAL MUSCLE CELLS AT SUPRAPHYSIOLOGICAL TEMPERATURES AND THE ROLE OF POLOXAMER 188 IN MINIMIZING MEMBRANE INJURY

by

Joseph T. Padanilam

Submitted to the Department of Mechanical Engineering on May 6, 1994, in partial fulfillment of the requirements for the degree of Master of Science in Mechanical Engineering

ABSTRACT

Electrical trauma is a devastating event that affects several thousand people annually with electrical "burns" representing approximately 4% of all admissions to burn units. Electrical trauma victims often suffer extensive skeletal muscle and nerve damage, which is thought to be principally driven by electroporation and electrically-induced Ohmic heating. Previous studies investigating the effects of elevated temperatures on isolated skeletal muscle cells showed the plasma membrane was a major site of damage.

In this study, these two mechanisms were decoupled in order to independently address the relative contribution of Ohmic heating in causing the disruption of skeletal muscle cell membranes. The dynamics of thermal injury to the plasma membrane of isolated rat skeletal muscle cells was quantified using a novel thermal microscopy system. Individual cells loaded with the membrane integrity probe calcein-AM were exposed to temperatures of 40-70° C which caused calcein leakage. An activation energy of 32.9 kcal/mole for 40% calcein leakage which compares favorably to other thermal damage studies was obtained. A model of calcein leakage was developed and showed a time-dependent membrane permeability. This model also accurately predicted calcein leakage from 3T3 mouse fibroblasts and hemoglobin leakage from human erythrocytes.

A concurrent study investigating the effectiveness of Poloxamer 188 (P188) in arresting calcein leakage from isolated skeletal muscle cells exposed to temperatures of 40-60° C was also performed to determine if this surfactant had membrane protective potential. P188 (10 mg/mL) was effective in arresting calcein leakage below 45° C and retarding calcein leakage above 45° C. P188 specificity was demonstrated by the ineffectiveness of dextran in arresting or retarding calcein leakage at 45° C as compared to P188. Further studies, at 42, 50, and 55° C, displayed an unusual yet interesting P188 dose dependence indicating greater effectiveness at 0.1-1 mg/mL, decreased effectiveness at 2 mg/mL, and improved effectiveness at 10 mg/mL. Additional studies conducted at 45° C with P238, P338, P407 indicate no statistically significant difference in effectiveness among them and P188. The beneficial action of P188 on thermally, as well as electrically damaged cells (Lee *et al.*, P.N.A.S. 1989:4524, 1992) makes this polymer a promising candidate in the development of new therapeutic treatments for electrical trauma.

Thesis supervisor: Mehmet Toner, Ph.D.
Assistant Professor of Surgery (Bioengineering)
Harvard Medical School
Lecturer, Department of Mechanical Engineering
Massachusetts Institute of Technology

Acknowledgments

I would like to thank Professor Mehmet Toner for the wonderful research experience he has provided during my graduate studies at MIT. It has been a rather painful and humbling ordeal at times but in the end I view it as my most endearing and rewarding academic experience at MIT. I thank Mehmet especially for all his encouragement, support, and advice throughout the course of this project particularly in the earlier stages when progress seemed unattainable and towards the end when deadlines became increasingly difficult to meet.

I thank Professor Martin Yarmush for his review of this thesis and for the many suggestions he has provided for my experimental studies. I thank Dr. Raphael Lee whose valuable input helped throughout the course of this project and in the preparation of this thesis. I thank Drs. Robert Ezzell and Yimin Ge for the time they have spent teaching me to use various equipment and the ideas and suggestions they have provided. I also thank the following members of the Surgery Research Lab at MGH East for their friendship, help, and stimulating discussions: Bill Thorpe, Will Holmes, Carl Rollins, Diane Casey, Tim Fife, Dr. Carriapa Annaiah, and Dr. Gerald Waneck. Finally, I thank my parents for their love and support during my graduate studies.

This research was funded partially by the Shriners Burns Institute and the Electric Power Research Institute, Empire State Electric Energy Research Company, New York State Electric and Gas Company, Niagara Mohawk Power Corporation, Northeast Utilities Services Company, Public Service Company of Oklahoma, the Public Service Electric and Gas Company of New Jersey, and Wisconsin Electric Power Company.

Table of Contents

List of Figures

List of Tables

Chapter 1. Introduction

The general background of electrical trauma, a discussion of the attendant physical mechanisms of damage, the therapeutic use of surfactants in cellular injury, and the scope of this study are presented in this chapter.

1.1 General Background

Electrical trauma is a devastating event that affects several thousand people annually with electrical "burns" representing approximately 4% of all admissions to burn units.[1] The most serious electrical trauma accidents occur in the work place of the industrialized nations. In the United States, an average of over 4000 nondisabling and over 3600 disabling electrical work-related injuries are recorded annually, according to United States Department of Labor statistics.[2] The mortality rate for accidental electrical shock ranges from 3 to 15%, with about 1000 deaths attributed overall to electrical shock in the United States annually. More than 90% of the injuries occur in males, mostly between the ages of 20 and 34, with 4 to 8 years experiences on the job.[3] According to the Edison Electric Institute, the majority of electrical utility worker accidents involved contact with a 1 to 10 kV electric power line in which the most common circuit path through the victim was hand to hand.[4] Those surviving the shock induced cardiac rhythm disturbances sustained other injuries leading to permanent physical disability. Other common electrical accidents include lightning strikes and domestic accidents. Survivors of lightning strikes who suffer exposure to very intense electric field strengths (> 100 kV/m) often experience unexplained neurological disturbances such as paraplegia that may not manifest until years later; whereas, victims of domestic electrical trauma, namely 2 to 5 year old children, who establish oral contact with an appliance cord undergo disfiguring and disabling damage to the teeth and lower face.

In general, muscle and nerve tissue are most vulnerable to injury by electrical current. A victim of an industrial high voltage accident experiences visible thermal injury at the contact points but the remaining regions in the current path are just slightly swollen and generally display no significant surface damage. However, underneath the skin, the muscles will be in a state of severe and unrelenting spasm or rigor and there will be marked sensory and motor nerve malfunction. The damaged non-viable skeletal muscle of the affected extremity is surgically excised following the first weeks from 25 to 60% of these patients.[43]

The skeletal muscle tissue particularly susceptible to damage by electrical trauma is located adjacent to bone and joints and the muscle tissue in the center of muscle.[5] The unique patterns of muscle tissue injury from electrical shock may provide important information regarding the mechanisms of cellular injury. Extensive clinical data suggests that electrical trauma is similar to a mechanical crush injury.[6] This analogy is justified due to the characteristically large release of intracellular proteins from skeletal muscle into the circulating blood that occurs both in electrical trauma and severe crush injuries. Accumulation of these large macromolecules in the kidney can disrupt the nephrotic filtration apparatus and cause kidney failure, a complication with very high mortality. The additional release of intracellular contents such as hydrogen, potassium, and other ions causes major shifts in the electrolyte balance from normal serum concentrations. The metabolic effects of these alterations are difficult to manage and have not been precisely quantified. This release of myoplasmic contents indicates damage or rupture of the muscle cell membrane. This interpretation is supported by the often observed muscle spasm. Therefore, it is pertinent to investigate how muscle cell membrane damage mediates the muscle tissue damage characteristically found in electrical trauma victims[7] and the physical mechanisms of muscle cell membrane damage.

1.2 Physical Mechanisms of Injury in Electrical Trauma

The extent of electrical damage to skeletal muscle tissue depends on the interaction of power frequency electric fields and skeletal muscle tissue. The nature of this interaction is mediated by the structure and organization of the cells and the extracellular matrix. With the exception of the thin outer cortex of bone and the epidermal layer of the skin, most tissues have power frequency (50-60 Hz) conductivities on the order of 0.1 mS/m. At these frequencies, the resultant tissue current is mostly Ohmic.

The human body when in contact with a 60 Hz source behaves as an almost pure resistive load. The epidermal layer and the metal-skin surface contact impedances dominate the measured resistance of the body. The epidermis is extremely thin, typically a 300 to 500 μm thick layer that covers the body forming a thin electrically insulating shell. The resistance of 1 cm^2 of epidermis ranges from 5 to 50 kΩ. If the skin is not unusually wet at the time of contact with a power source, greater than 95% of the imposed voltage drop may initially occur across the insulating epidermis. Thus, a typical 10 kV contact would then generate an electric field of 1000 to 10000 kV/m in the epidermal layer which exceeds its dielectric breakdown strength. Hence, the epidermal layer vaporizes almost instantaneously compared to the time required to thermally injure subcutaneous tissues. The net result is that, for times great than the epidermal dielectric breakdown time, the body behaves as a 0.5 to 1 kΩ resistive load. Therefore, it is reasonable to predict that a 10 kV contact would produce peak currents ranging from 10 to 20 A.[8]

These currents generated during electrical trauma can disrupt tissue through: (1) pure electrical effects and (2) electrically induced thermal effects. The established mechanisms by which strong electric fields (> 1 kV/m) produce structural damage to cells within just a brief exposure time are membrane dielectric breakdown and membrane electroporation.[7,9]

Skeletal muscle and nerve tissue are most susceptible to damage by these pure electrical mechanisms since the relatively low conductivity of the plasma membrane as compared to the cytoplasm and the relatively large lengths of these cells lead to the imposition of large transmembrane potentials as shown in Figure 1. The electrical power supplied by the generated currents is also dissipated as it passes through the human body via Ohmic heating. In a model of the human upper extremity as shown in Figure 2, the current paths generated impose electrical fields that are roughly parallel to the major tissues in the extremity which include skin, fat, bone, and skeletal muscle. Since the electric fields are aligned nearly in parallel to these tissues, most current will flow through the tissue with the lowest resistance which is skeletal muscle tissue. The Ohmic heating manifests itself within the skeletal muscle tissue as a local temperature rise. The magnitude of this temperature rise depends on the duration of contact with the electrical power source.

The most abundant information regarding the duration of contact for accidental electrical shock is from eyewitness reports which are, however, unreliable. The common observation is that the victim was instantly "blown" or "knocked" away from the contact source. It has been documented that human forearm muscles experience involuntary spasm when more than 16 mA at 60 Hz are passed through the upper extremity.[10] Hence, a victim holding onto a conductor at the initiation of a 10 A current flow would be unable to release this contact. The circuit would remain closed until broken at other contact points and the duration of contact under these circumstances would depend on several circumstantial variables that it is impossible to reliably predict. If, however, the victim approaches a "live" conductor, then the current flow will begin when arcing occurs prior to mechanical contact. Within 10 to 100 milliseconds, the excitation-contraction coupling response time of human skeletal muscles, the muscles located in the current path will contract. Depending on the relative hand-conductor position, involuntary mechanical contact may be established or the victim may be propelled away from the contact. Based on

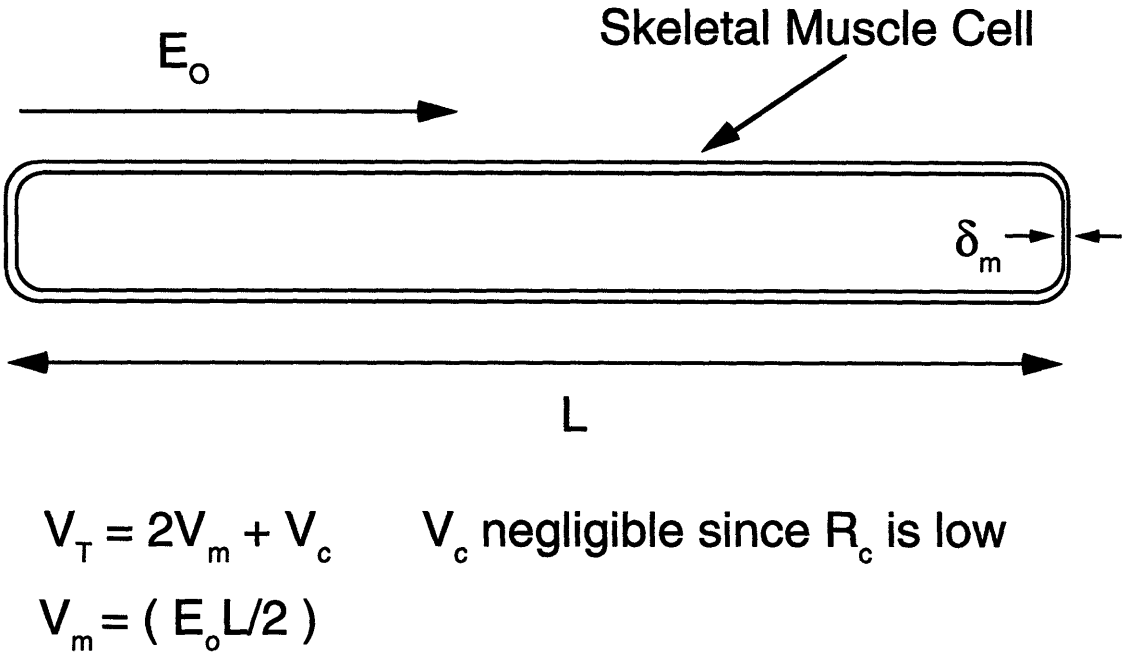

Figure 1. Dependence of transmembrane potential, V_m, on cell length, L, and electric field strength, E_O. V_T is the total potential, V_C is the cytoplasmic potential, and R_C is the cytoplasmic resistance.

eyewitness reports, the latter seems to be more common since most victims experience generalized muscle contraction throughout. Under these circumstances, it is reasonable to predict contact duration times on the order of 100 milliseconds. Hence, electrically induced Ohmic heating that generates supraphysiological temperatures within skeletal muscle tissue is another mode of damage that may occur during electrical trauma.

Since skeletal muscle tissue is susceptible to damage during electrical trauma directly through cell membrane dielectric breakdown and membrane electroporation and indirectly through Ohmic heating, it is relevant to describe the nature and extent of damage caused by these various mechanisms and present the theoretical models developed to predict damage caused by these various mechanisms. By comparing these various damage mechanisms,

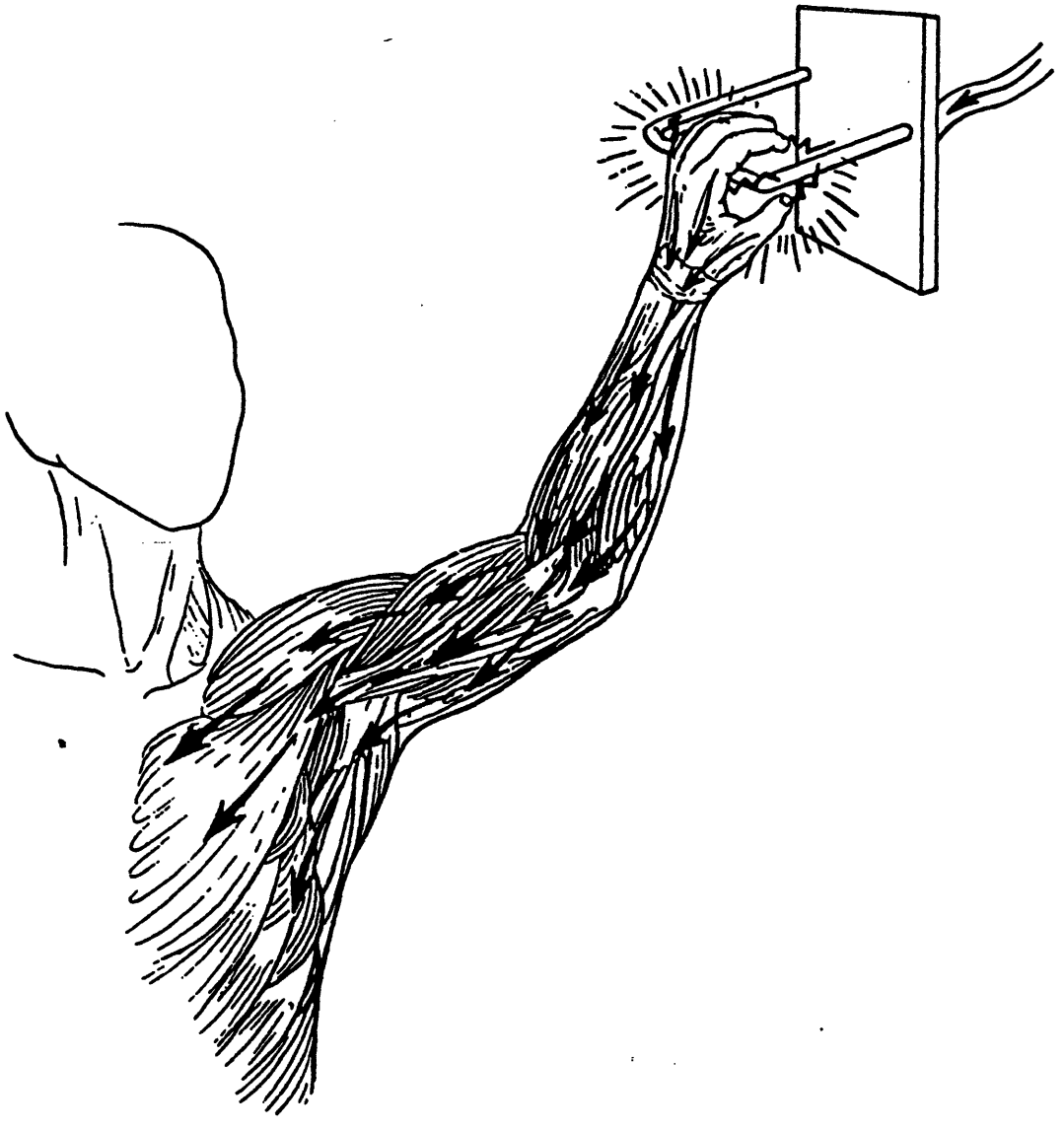

Figure 2. Typical current paths and resultant electric field lines that are roughly parallel to the muscle tissue in the upper extremity during a hand contact. (Reproduced from Tropea and Lee[12]).

an idea of the relative damage caused by each mechanism can be obtained which will enhance our understanding of how electrical trauma is manifested in skeletal muscle tissue.

1.2.1 *Ohmic Heating*

The passage of current through skeletal muscle tissue causes energy dissipation when charges that produce the current collide with the molecules within the skeletal muscle tissue. This energy dissipation or Ohmic heating can be mathematically expressed through the following equation:

$$P = JE \tag{1}$$

where P is the power dissipation per unit volume of skeletal muscle tissue (W/m^3), J is the current density (A/m^2), and E is the electric field strength (V/m). Ohm's law states the current density is related to the electric field by the conductivity of the material (σ) such that

$$J = \sigma E \tag{2}$$

which then permits the following expression:

$$P = \sigma E^2 = \frac{J^2}{\sigma} \tag{3}$$

The relative contribution of Ohmic heating in skeletal muscle tissue can be estimated by determining the tissue temperature as a function of time. Lee and Kolodney[11] and Tropea and Lee[12] numerically simulated the Ohmic heating response using the finite element method to solve the Bioheat transfer equation given by the following expression:

$$\rho c \frac{dT(t)}{dt} = \kappa \nabla^2 T(t) + \rho_b c_b \omega_b \left(T_b - T(t)\right) + q_m + \frac{J^2}{\sigma} \tag{4}$$

where ρ is the tissue density (kg/m^3), c is the tissue specific heat (J/kg °C), κ is the thermal conductivity (W/m °C), T_b is the blood temperature (°C), ρ_b is the blood specific density

(kg/m^3), c_b is the specific heat of blood (J/kg °C), ω_b is a proportionality constant related to the tissue perfusion rate (s^{-1}), and q_m is the rate of metabolic heating per unit volume (W/m^3). For the range of temperatures that appear to be relevant to subcutaneous tissue injury, the temperature dependence of σ can be neglected. This equation states that the local rate of temperature rise in skeletal muscle tissue per unit volume of tissue is balanced by diffusion of heat per unit volume into the tissue, the net power per unit volume convected by blood flow from the tissue, the power per unit volume contributed by metabolic heating, and the power per unit volume generated by Ohmic heating. Results of numerical simulations in the upper extremity for a 10 kV worst case hand-to-hand contact with a 1 second duration of contact predict the generation of muscle core temperatures ranging from 40 to 55° C. Since the extent of thermal damage to skeletal muscle tissue is thought to be correlated to cellular membrane damage based on clinical evidence which reports the release of myoplasmic contents as a typical condition in electrical trauma victims, it is crucial to determine the damaging effects of supraphysiological temperatures on the plasma membrane of skeletal muscle cells.

Several thermal injury studies have been performed by exposing cell populations to supraphysiological temperatures to determine the kinetics of thermal damage. These investigations characterized thermal damage in a variety of cell types with a variety of damage criteria such as blister formation in HeLa S-3 cells,[13] 1%[14] and 5%[15] hemolysis in human erythrocytes, ghosting of human erythrocytes,[16] 5% carboxyfluorescein dye leakage from isolated rat skeletal muscle cells,[17,18] 63% calcein dye leakage from 3T3 fibroblasts,[19] and clonogenic assays in Chinese hamster cells[20] and pig kidney cells.[21] Due to the wide range of cell types involved, the arbitrarily chosen damage criteria for each particular cell type, and the various temperature ranges for each particular study, the results of these studies can only be qualitatively compared. When the data from these studies were analyzed in an Arrhenius format, that is by plotting the time required to satisfy the particular

damage criteria as a function of inverse absolute temperature, the activation energies obtained from the studies in which the damage criterion was based on some type of membrane disruption ranged from 30 to 60 kcal/mole. This range of activation energies suggests a number of possible damage mechanisms including denaturation of membrane proteins, disruption of the phospholipid bilayer, and cytoskeletal depolymerization. The study by Cravalho *et al.*[18] using isolated rat skeletal muscle cells provided preliminary evidence that plasma membrane damage occurs due to exposure to supraphysiological temperatures. However, given the limited range of temperature and number of time points, it is difficult to draw firm conclusions about the precise nature of the damage mechanisms involved.

1.2.2 *Electroporation*

Electroporation is theorized to occur when strong electrical forces drive polar water molecules into molecular scale defects in the lipid bilayer component of the cell membrane causing them to enlarge.[22,23] If the pores become large enough, they will continue to grow until the membrane ruptures. Rupture occurs in pure bilayer lipid membranes exposed to 0.2 to 0.5 V for longer than 0.1 msec.[22]

Electroporation has been demonstrated within intact muscle tissue. Using cooled rat *biceps femoris* muscles, Bhatt *et al.*,[24] have shown that the probability of muscle cell membrane rupture by electroporation increases with the square of the electric field strength and is proportional to the duration of cell exposure to the applied field. Electric fields greater than 6 kV/m and exposure durations greater than 0.1 msec were required to cause membrane damage. This study indicated that membrane rupture was caused directly by the imposed transmembrane potential and was not spontaneously reversible. Human skeletal muscle

cells can be expected to be more susceptible since they are larger than the rat muscle cells used in this study and will thus have higher imposed transmembrane potentials.

A number of theories have been developed to model electroporation.[22,23,25] Powell and Weaver[22] based their model on the work of Litster[26] who introduced the idea that the Brownian motion of molecules of the plasma membrane created transient molecular defects or pores to form in bilayer lipid membranes. These defects are restrained by the interfacial forces at the edge of a pore. The energy ΔE required to create a pore of radius r is the energy associated with the creation of the edge of the pore minus the eliminated surface area. Assuming a cylindrical geometry for the pore, the following expression is obtained:

$$\Delta E = 2\pi\gamma r - \pi\Gamma r^2 \tag{5}$$

where Γ is the surface tension of the membrane and γ is the strain energy per unit length of the membrane pore edge. Powell and Weaver added a term to this equation to account for the electrostatic energy effects associated with the transmembrane potential V_m such that the following expression was obtained:

$$\Delta E = 2\pi\gamma r - \pi r^2[\Gamma + \alpha(V_m)^2] \tag{6}$$

where α is a positive parameter dependent on the permitivities of the membrane and the intracellular and extracellular fluids and the membrane thickness δ_m. Thus, V_m tends to decrease the stability of the membrane by decreasing the amount of energy required to form a pore. Taylor and Michael[27] suggested that axisymmetric holes in thin sheets of fluid where surface tension forces predominate will expand if their initial radii are larger than the thickness of the sheet, while holes with radii smaller than this thickness will close. Rupturing a soap bubble with a pinprick is a common example. This is due to the action of

surface tension that acts to reduce the surface area. An applied V_m acts to lower the critical pore radius beyond which mechanical forces at the edge of the pore cannot restrain the pore from expanding until cell rupture.

1.2.3 *Dielectric Breakdown*

Another mechanism of pure electrical damage, membrane dielectric breakdown, occurs when the electric field strength within the membrane exceeds the critical value above which the force on atoms in the electric field pull the electrons out of their orbital shells. To observe dielectric breakdown, the membrane voltage must be raised to the dielectric breakdown potential more rapidly than electroporation can occur. Dielectric breakdown has been shown to occur in pure bilayer lipid membranes when transmembrane potentials exceed 0.5 to 1 V.[23] Dielectric breakdown manifests itself as a large drop in membrane resistivity. For mammalian cell membranes, 0.8 to 1 V is required for cell rupture via dielectric breakdown.[23]

1.3 Use of Surfactants in Preventing Membrane Injury

The various mechanisms attendant to skeletal muscle cell damage during electrical trauma have been discussed. Based on these mechanisms and the body of clinical evidence suggesting compromised membrane integrity, it is prudent to address and explore therapeutic schemes that may either repair and/or stabilize disrupted membranes to prevent loss of myoplasmic contents and to provide sufficient time for any inherent cellular repair mechanisms to reconstruct the damaged membrane. The effectiveness of polyol block copolymer surfactants in minimizing cellular injury will therefore be discussed.

1.3.1 *Polyol block copolymers*

Polyol block copolymers are a series of surfactants that consist of a hydrophobic core comprised of polyoxypropylene flanked on both sides by hydrophilic tails comprised of polyoxyethylene as shown in Figure 3. In a number of applications that will be discussed shortly, these block copolymers have been successful in preventing various types of damage at the cellular level. It is postulated that the fundamental biological interaction of these copolymers is to block weak adhesion caused by pathologic hydrophobic interactions. Pathologic hydrophobic interactions occur when mobile elements in body fluids such as blood nonspecifically adhere thereby restricting the physiological motion of these elements and promoting undesired adhesion of cells and molecules. In damaged cells, hydrophobic phospholipid domains normally located within the plasma membrane may become exposed to aqueous extracellular media to produce these pathologic hydrophobic interactions which compound the extent of damage. It is hypothesized that the hydrophobic polyoxypropylene core of the block copolymer binds noncovalently by surface tension to the exposed hydrophobic phospholipid domains of a damaged cell thereby converting it to a non-adhesive hydrated surface since the hydrophilic polyoxyethylene tails now opposing the aqueous extracellular media form hydrogen bonds with extracellular water molecules. This non-adhesive hydrated surface closely resembles that of a normal cell.

1.3.1.1 *Poloxamer 188*

The polyol block copolymer that has been most widely utilized in biomedical applications is Poloxamer 188 (P188). P188 is an 8.4 kDa amphipathic, non-ionic blood compatible surfactant consisting of a 30 unit polyoxypropylene core flanked on both sides by 75 unit polyoxyethylene tails. P188 has been approved by the Food and Drug Administration for

human use orally, as a topical wound cleanser, and it was shown to be safe for intravenous use in a series of studies with animals and humans.[29-32] At low concentrations, P188 is thought to form unimolecular micelles in which a single P188 molecule wraps around itself.[33] At higher concentrations, it has been reported to form micelles consisting of 2-8 molecules[34,35] at 0.1 to 0.2 wt % however it is now thought that these molecules aggregate to form micelles over a range of concentrations near 1 mg/mL leading to a saturation point.[36]

P188 has been used as a mild detergent to cleanse wounds,[37] as an emulsifier for non-polar lipids, a laxative; it was also used to coat the surface of early membrane oxygenators to reduce erythrocyte lysis during cardiopulmonary bypass operations in the 1960's.[38] P188 has been shown to reduce friction resulting from non-specific physicochemical adhesion between erythrocytes and blood vessel walls[28] and decrease pathologic elevations in blood viscosity due to the adhesion of soluble fibrin molecules that are present in the circulatory system of patients following surgery, trauma, shock, and myocardial infarction.[39] It is relatively non-toxic except at high concentrations when used to retard formation of an acute thrombosis[40] and is excreted in the urine unmetabolized.[38]

P188 was recently used to protect electropermeabilized skeletal muscle cells and tissue. In an attempt to circumvent the deleterious effects of electroporation the effectiveness of P188 in sealing electropermeabilized membranes was investigated by Lee *et al.*[41] These results showed that P188 (8 mg/mL) was capable of arresting the leakage of the fluorescent membrane integrity probe carboxyfluorescein from the cytoplasm of isolated rat skeletal muscle cells exposed to a single 20 kV/m, 4-ms-duration field pulse as compared to a control without P188. The effectiveness of P188 was also assessed *in vivo* in the rat *biceps femoris* flap attached by its arteriovenous pedicle which was electropermeabilized.[41] Histopathologic examination indicated that postshock P188 administration reduced tissue

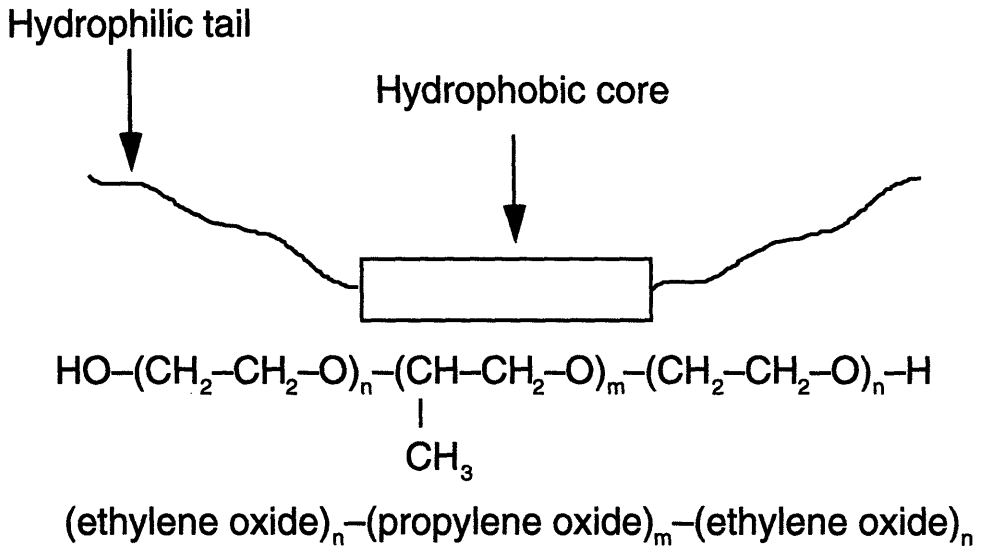

Figure 3. Typical structural formula of a polyol block copolymer with a hydrophilic polyoxypropylene core flanked on both sides by hydrophilic polyoxyethylene tails.

inflammation and damage in comparison to control tissues. All these studies were performed at 37° C to decouple the thermal and electrical effects. These results suggest that P188 may have potential success in sealing membranes permeabilized by direct electrical effects.

1.4 Scope of This Study

Skeletal muscle cell rupture may occur via Ohmic heating[11,12] and/or electroporation.[7,9] In this study, these two mechanisms were decoupled in order to independently address the relative contribution of thermal damage in causing the disruption of skeletal muscle cell membranes which is hypothesized to mediate skeletal muscle tissue damage. The kinetics of thermal injury to the plasma membrane of isolated rat skeletal muscle cells was quantified using a novel thermal microscopy system. Individual cells loaded with the membrane integrity probe calcein-AM were exposed to temperatures ranging from 40 to 70°

C which caused calcein leakage. The Arrhenius dependence of 40% calcein leakage yielded an activation energy of 32.9 kcal/mole which compares favorably with those of previous thermal damage studies. A model of calcein leakage kinetics was developed and revealed a time and temperature dependent hyperpermeability state of the plasma membrane. This model also accurately predicted calcein leakage from 3T3 mouse fibroblasts and hemoglobin leakage from human erythrocytes.

A concurrent study investigating the effectiveness of P188 in arresting calcein leakage from isolated skeletal muscle cells exposed to supraphysiological temperatures ranging from 40 to 60° C was also performed to determine if this surfactant had membrane protective potential. The results showed P188 (10 mg/mL) was effective in arresting intracellular leakage of calcein below 45° C. Above 45° C, P188 retarded the leakage of calcein in the thermally damaged membranes. These results demonstrate the first successful action of P188 in retarding calcein leakage from thermally damaged cells. The specificity of P188 was demonstrated by the ineffectiveness of neutral dextran in arresting or retarding calcein leakage at 45° C as compared to P188. Other studies solely utilizing the hydrophobic core constituent represented by polypropylene glycol (PPG) and the hydrophilic tail constituent represented by polyethylene glycol (PEG) indicated the relative ineffectiveness of both PPG nor PEG alone as compared to P188.

Further studies determined the dependence of calcein leakage kinetics on P188 concentration as a function of temperature. The results display an unusual yet interesting dose dependence which indicate greater effectiveness at concentrations of 0.1 to 1 mg/mL, decreased effectiveness at 2 mg/mL, and improved effectiveness at 10 mg/mL. Additional studies conducted at 45° C with the poloxamers P238, P338, P407 indicate no statistically significant difference in effectiveness among them and P188.

Chapter 2. Materials and Methods

The experimental materials and methods used for this study which include a protocol for isolating individual skeletal muscle cells, a novel thermal microscopy system, and a procedure for making membrane permeability measurements are presented in this chapter.

2.1 Isolation of Skeletal Muscle Cells

The skeletal muscle cells used in this study were isolated from the *flexor digitorum brevis* muscle from the hind foot of 3 month old adult, female Sprague-Dawley rats weighing 150-200 grams as described in detail elsewhere.[17] Briefly, cells were harvested by surgical removal of the *flexor digitorum brevis*, digestion in 0.3% collagenase (type II; Worthington Biochemical, Freehold, NJ) for 3 hours at 37° C, and subsequent trituration and extensive washing in Dulbecco's Modified Eagle's Medium (DMEM; Gibco, Grand Island, NY) supplemented with 10% horse serum (Gibco), 1% penicillin/streptomycin (JRH Biosciences, Lenexa, KS), and 5 μg/mL cytosine-ß-D-arabinofuranoside (Sigma, St. Louis, MO), a DNA inhibitor, that prevents the proliferation of dedifferentiated fibroblasts in culture. The isolated cells were then diluted in DMEM culture media, plated onto non-tissue culture petri dishes (Falcon, Becton Dickinson, Lincoln Park, NJ), and cultured in a 95% air and 5% CO_2 incubator at 37°C for 5 to 7 days. Experiments were performed between two days post isolation to allow the cells to recover from the digestion in collagenase and not after five days post isolation when cell survival began declining.

2.2 Thermal Microscopy System

A thermal microscopy system consisting of a thermal microperfusion stage and fluorescent microscopy and image analysis system was used for the thermal damage experiments and subsequent data analysis. A depiction of this integrated system is shown in Figure 4.

2.2.1 *Thermal Microperfusion Stage*

A thermally controlled microperfusion stage was designed to conduct thermal injury experiments on skeletal muscle cells.[44] A schematic of this stage is shown in Figure 5. The stage contained a microperfusion chamber (8 mm x 2 mm x 1 mm) into which cells were loaded. The chamber temperature was controlled by a custom designed proportional integral feedback thermal controller (Interface Techniques Company, Cambridge, MA).[45] The lower surface of the chamber consists of a highly conductive sapphire (16 mm x 16 mm x 1mm) piece mounted on a heating window which is a glass coverslip (18 mm x 18 mm) with two thin deposited gold films (18 mm x 2 mm) on opposite sides that dissipate electrical energy supplied by leads from the thermal controller. Between the sapphire and the heating window is a thin, foil feedback thermocouple (Omega, Stamford, CT).

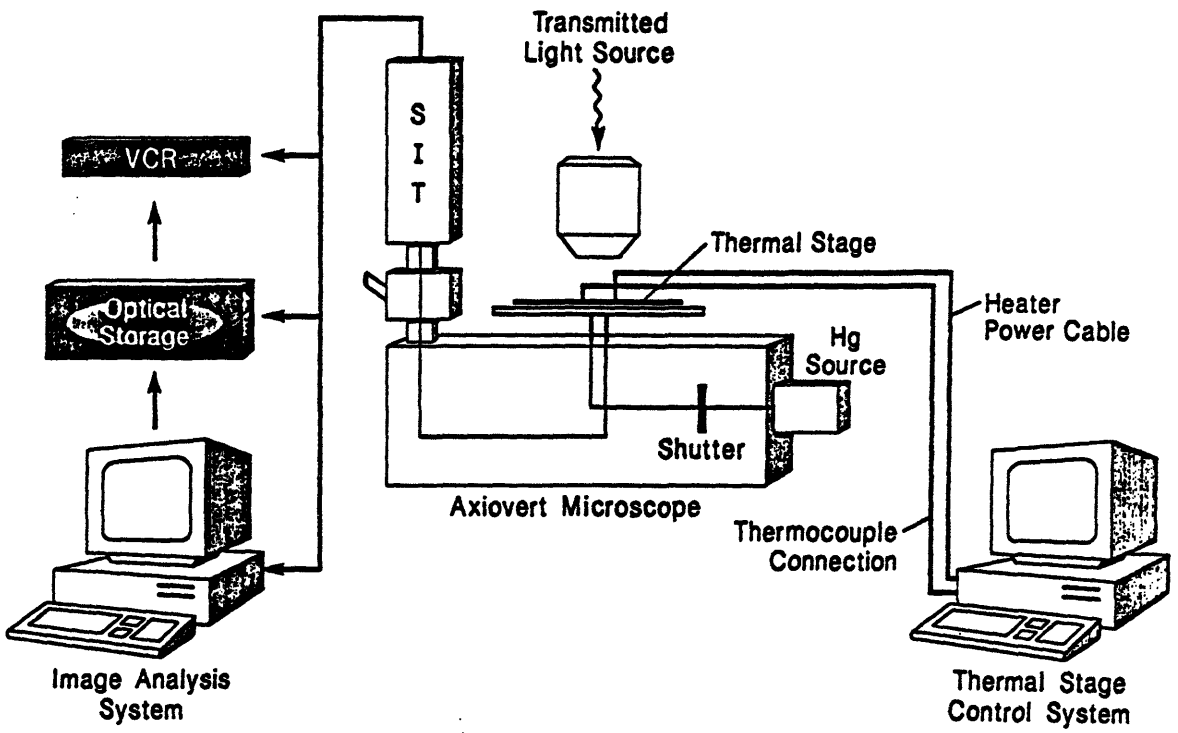

Figure 4. Depiction of the integrated thermal microscopy system consisting of a thermal microperfusion stage and fluorescent microscopy and image analysis system.

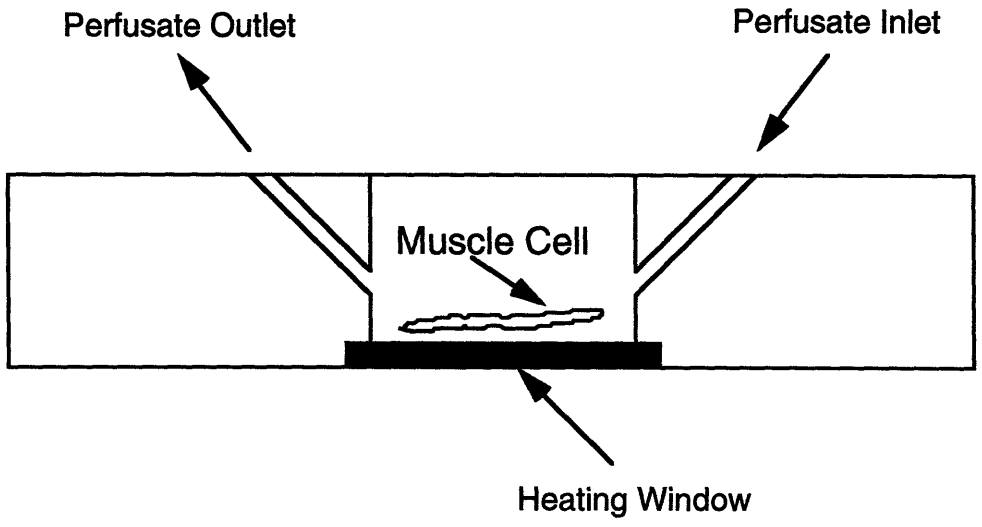

Figure 5. Schematic of the thermally controlled microperfusion stage.

To characterize the thermal field in the chamber, the thermal controller was calibrated using Tempilstik (Tempil Div, South Plainfield, NJ) paraffin standards which melt at specific temperatures (38, 45, 55, and 66° C). A thin strip of these standards was placed within the chamber and the temperature was gradually increased (4° C/min) until the sample melted at which time the temperature on the screen of the thermal controller was recorded.

To characterize the flow conditions in the chamber, both dispersion and flow analysis were performed. For dispersion analysis, the chamber was initially filled with distilled, deionized water (dd$H_2$0). The chamber was then perfused with dd$H_2$0 at the following flow rates: 1, 2, and 3 mL/min. The outlet flow tubing from the chamber was connected to a flow through cuvette mounted inside a spectrophotometer (Beckman, DU-65, Fullerton, CA). At time zero, a 0.1 mL 0.4% trypan blue (Sigma) solution was injected as a plug into the inlet tubing and its absorbance history in the outlet stream was continuously monitored at 540 nm. For flow analysis, the stage was mounted on a Zeiss Axiovert (Germany)

microscope and the chamber was placed in the field of a 2.5 X objective connnected to a video camera (Hamamatsu, Nuvicon, Japan) supplying light microscopic images which were recorded by a VCR (Panasonic, AG-7500A, Japan). The chamber was then filled with ddH_20 and perfused continuously with 0.4% trypan blue solution at the same flow rates used for dispersion analysis. The bright field video recordings were later analyzed using Image-1 (Universal Imaging, West Chester, PA) software to determine the normalized brightness of trypan blue in the chamber as a function of time at various flow rate.

2.2.2 *Fluorescent Microscopy and Image Analysis System*

Fluorescent images of skeletal muscle cells exposed to supraphysiological temperatures in the microperfusion chamber were observed and recorded using a Zeiss Axiovert microscope equipped with a Hg lamp regulated by a programmable shutter (AZI, Avon, MA), a low light camera (Hamamatsu, Silicon Intensified Transmittance [SIT]), and an Optical Memory Disk Recorder (OMDR) (Sony, LVR-5000, Japan). This configuration allows images to be acquired in a programmable fashion, with Image-1 software controlling all aspects of image acquisition, and analysis of the intracellular fluorescent intensity. For measurement of intracellular calcein fluorescence, a region was traced around the cell and the average intensity within the traced region was quantified. The background intensity of the image was measured in rectangular region just outside the cell.

2.3 Membrane Permeability Measurements

To facilitate and perform membrane permeability measurements on skeletal muscle cells, hypertonic media and the membrane integrity probe, calcein-AM, were utilized.

2.3.1 *Use of Hypertonic Media*

Individual skeletal muscle cells used in these studies were suspended in Dulbecco's Phosphate Buffered Saline (PBS) (Gibco) with 1.5 mM $CaCl_2$ (Sigma) rendered hypertonic (900 mosm) by the addition of 180 g/l of sucrose (Sigma). The hypertonic PBS solution arrested the characteristic contraction process that occurs in skeletal muscle cells exposed to supraphysiological temperatures thereby decoupling membrane damage occurring due to excessive contraction.[46,47]

2.3.2 *Use of Calcein-AM as A Membrane Integrity Probe*

Structural integrity or permeability of the plasma membrane was determined through the use of the vital fluorescent dye calcein-AM (Molecular Probes, Eugene, OR). Calcein-AM is a neutral, hydrophobic molecule that can readily diffuse across the plasma membrane of skeletal muscle cells. Once inside, non-specific intracellular esterases catalyze the hydrolysis of the AM portion of the molecule and produce a fluorescent calcein which weighs 623 Da and has a net negative charge of -6 if completely deesterifed that renders it membrane impermeant. All experiments performed lasted less than 18 minutes, a time in which the passive leakage of calcein from cells was found to be negligible. To prevent intensity loss due to photobleaching, a shuttering scheme was adopted which kept total exposure of calcein to the excitation beam equal to one minute or less during image acquisition, a time which led to less than 10% fluorescence loss during continuous exposure (data not shown). Since the intensity of the excitation beam was further attenuated through the use of neutral density filters, this negligible photobleaching effect was not corrected in our calculations. Given the volume of the chamber was much larger than the cell volume, the background intensity remained constant during the experiments and reflected the amount of autofluorescence. Thus, the measured and constant

background fluorescence was subtracted from the intracellular fluorescence. These measurements were then normalized with respect to the initial corrected intracellular fluorescence.

Prior to experimentation, an aliquot of 5 μl of 5 mM calcein-AM in acetone was added to 2 mL of hypertonic PBS solution. Individual skeletal muscle cells were transferred from DMEM culture media to this hypertonic PBS solution containing calcein-AM. The cells were then allowed to incubate at room temperature for 30 minutes to allow uptake and hydrolysis of calcein-AM. Cells chosen for eventual experimentation had visible myonuclei and characteristic striation patterns. These cells were loaded into the perfusion chamber and the chamber was then sealed from the ambient environment with silicone grease and a glass (12 mm x 12 mm) coverslip. Calcein-AM free hypertonic PBS solution was then perfused for about 6 seconds until the chamber was full. Given the large size of skeletal muscle cells and the relatively slow rates, the cells remained in their location during the perfusion. The cells were then subjected to a step change in temperature (1000° C/min) from ambient temperature to various elevated temperatures and the image acquisition system was simultaneously initiated. Experiments were run either for 17 minutes or until all the dye leaked out, whichever occurred first.

2.4 Use of Polyol Block Copolymer Surfactants

Polyol block copolymer surfactants, namely Poloxamers 188, 238, 338, and 407 (BASF, Parsippany, NJ), and their basic constituent compounds, PEG and PPG (Aldrich, Milwaukee, WI), were used in this study to prevent excessive intracellular calcein leakage.

2.4.1 *Use of Poloxamer 188*

Poloxamer 188 (P188) is an 8.4 kDa amphipathic, non-ionic blood-compatible copolymer consisting of a hydrophobic core of 30 units of propylene oxide (PO) flanked on both sides by hydrophilic tails consisting of 75 units of ethylene oxide (EO). The EO/PO ratio and structural formula of P188 is shown in Table 1. In a concurrent set of studies, calcein-AM free hypertonic PBS solution containing P188 (10 mg/mL) was perfused into the chamber just prior to exposure to supraphysiological temperatures ranging from 40 to 60° C to determine if this surfactant could arrest leakage of calcein. Another set of studies was performed utilizing P188 at concentrations from 0.1 to 2 mg/mL at temperatures of 42, 50, 50° C to characterize the relative effectiveness of P188 as a function of concentration at various temperatures.

2.4.2 *Use of Other Poloxamers*

A set of studies was conducted at 45° C with P238, P338, and P407 at 10 mg/mL to determine how various PO hydrophobic core lengths and EO hydrophilic tail lengths different from that of P188 affect the kinetics of calcein leakage. The EO/PO ratios, chemical formulas, and molecular weights of these poloxamers are shown in Table 1.

2.4.3 *Use of Polyethylene Glycol, Polypropylene Glycol, and Dextran*

Two sets of studies were performed utilizing polyethylene glycol (PEG) and polypropylene glycol (PPG) to determine the mechanism by which P188 may arrest calcein leakage. PEG (3.4 kDa) which represents the hydrophilic tail region of P188 was used at 20 mg/mL and PPG (2 kDa) which represents the hydrophobic core of P188 was used at 10 mg/mL at 42 and 50° C. Another study was performed utilizing neutral dextran (Pharmacia, Sweden),

an 11 kDa polysaccharide, at 0.5, 2, and 10 mg/mL at 45° C in order to demonstrate the specificity of P188 in arresting calcein leakage from thermally damaged skeletal muscle cells. The structural formulas of PEG, PPG, and dextran are shown in Table 1.

Table 1. Structural formulas, molecular weights, and EO/PO ratios of the various block copolymers, PEG, PPG, and dextran.

Compound	Structural Formula	EO/PO ratio	Mol. Wt. (kDa)
P188	$H\text{-}(EO)_{75}\text{-}(PO)_{30}\text{-}(E0)_{75}\text{-}OH^{\dagger}$	5	8.4
P238	$H\text{-}(EO)_{105}\text{-}(PO)_{40}\text{-}(E0)_{105}\text{-}OH$	5.25	11.6
P338	$H\text{-}(EO)_{150}\text{-}(PO)_{55}\text{-}(E0)_{150}\text{-}OH$	5.45	16.4
P407	$H\text{-}(EO)_{105}\text{-}(PO)_{70}\text{-}(E0)_{105}\text{-}OH$	3	13.3
PEG	$H\text{-}(O\text{-}CH_2\text{-}CH_2)_{77}\text{-}OH$	-	3.4
PPG	$H\text{-}(O\text{-}CH(CH_3)\text{-}CH_2)_{34}\text{-}OH$	-	2
Dextran	$(C_6H_{12}O_6)_{61}$	-	11

† -(EO)- represents $-(O\text{-}CH_2\text{-}CH_2)-$ and -(PO)- represents $-(O\text{-}CH(CH_3)\text{-}CH_2)-$

2.5 Data Analysis and Statistics

The dispersion, flow, and thermal calibration experiments were performed once per flow rate and three times per temperature. For all normalized intracellular fluorescence measurements at supraphysiological temperatures, each data point is an average of 6-10 skeletal muscle cells and the error bars represent the standard error of the mean (SEM).

Chapter 3. Theoretical Model

The mathematical models that characterize the hyperpermeability state of the plasma membrane of skeletal muscle cells exposed to supraphysiological temperatures are derived, discussed, and presented in this chapter.

3.1 Two-Compartment Diffusion Model

The hyperpermeability state of the plasma membrane at supraphysiological temperatures was observed as an increased rate of intracellular calcein leakage. The diffusion of calcein across the thermally disrupted plasma membrane of a cell modeled as a cylinder can be modeled by the following mass conservation equation:

$$V\frac{dC_i}{dt} = -PA(C_i - C_o) \tag{7}$$

where V is the cell volume, A is the cell surface area, C_i and C_O are the intra- and extracellular dye concentrations, respectively, and P is the membrane permeability. Axial dye leakage occurring through the ends of the cylindrically modeled cell is assumed negligible relative to radial dye leakage occurring through the core. It is further assumed that C_i is much greater than C_O since the cell volume is much less than the microperfusion chamber volume. A calcein calibration experiment obtained elsewhere[19] showed that $C_i = kI$ where k is a proportionality constant and I is the intracellular calcein intensity. If these two assumptions are incorporated into Eq. (7), the following expression relating calcein intensity to the permeability of the membrane to calcein is obtained:

$$\frac{dI}{I} = -\frac{PA}{V}dt \tag{8}$$

3.1.1 *Constant and Time-dependent Permeability*

In order to integrate Eq. (8) to obtain analytical solutions for the intracellular calcein intensity as a function of time, it is necessary to assume a specific functional form for the permeability. If the permeability is assumed constant, the following expression can be obtained:

$$\frac{I}{I_o} = exp\left(-\frac{AP}{V}t\right) \tag{9}$$

where I_O is the initial intracellular calcein fluorescence.

If the permeability is assumed to be time-dependent (i.e. $P = \alpha t + \beta$), the following expression can be obtained:

$$\frac{I}{I_o} = exp\left(-\frac{At}{2V}(\alpha t + 2\beta)\right) \tag{10}$$

where α and β are two empirical constants to be determined from measurements. The value of A/V for a cylindrical cell is $2/r$ where r is the average radius of a skeletal muscle cell which is approximately 5 μm. Eqs. (9) and (10) were concurrently fit by a nonlinear regression to all the calcein leakage curves at supraphysiological temperatures in the absence of P188 and will be presented and compared in Chapter 4.

3.1.1.1 *Statistical Comparison of Constant and Time-Dependent Permeability Fits*

In order to determine whether Eq. (10) was statistically superior to Eq. (9), the F-test was performed to evaluate whether an additional parameter was justified based on the following

relationship from Bevington:[48]

$$F_{\chi} = \frac{(\chi_c^2 - \chi_{td}^2)(N-m-1)}{\chi_c^2} \tag{11}$$

where the parameter F_{χ} is related to the difference of the chi squared values for the two analytical solutions and is assumed to follow the F distribution, χ^2_c is the chi squared value for Eq. (9), χ^2_{td} is the chi squared value for Eq. (10), N is the number of data points, and m is the number of parameters in the linear fit (i.e. m = 1). Based on the N value per temperature and the corresponding F_{χ} value, it is possible to determine the error (P value) incurred by using a higher order fit which is Eq. (10) for this case. Provided the error value is small (≤ 5%), the more likely Eq. (10) is statistically superior to Eq. (9). The results of the F test and the corresponding P values will be presented in Chapter 4.

3.1.1.2 *Use of Time-Dependent Permeability Model in Other Cell Types*

The relative success of fitting Eq. (10), as shown in Section 4.11.2, to calcein leakage in skeletal muscle cells exposed to supraphysiological temperatures suggested potential success in applying this model to other cell types in which thermal disruption of the plasma membrane was assessed by the leakage of a membrane integrity probe. Hence, Eq. (10) was fit to experimental membrane integrity probe leakage curves obtained by other investigators for calcein leakage from 3T3 fibroblasts[19] and hemoglobin leakage from human erythrocytes.[49] These curve fits will be presented in Chapter 4.

3.1.2 *First-Order Reaction Model for Diffusional Permeability*

The relative success of the time-dependent permeability assumption strongly suggested a

time-dependent breakdown of the plasma membrane when exposed to supraphysiological temperatures. Although this time-dependent assumption was empirical, it motivated further speculation so that a more kinetic model describing the time-dependency of the permeability of the plasma membrane could be formulated. To develop this model, it is worthwhile to discuss the basic nature of the plasma membrane.

One of the principal functions of the plasma membrane is to regulate the transport of various molecules between the intra- and extracellular regions. It has been proposed by Tien,[50] Kotyk and Janacek,[51] and Chizmadzhev *et al.*[52] that a possible mechanism for the transport of a molecule across the plasma membrane is passage of the molecule through microscopic defects (or holes) in the phospholipid bilayer. When the bilayer separates regions of high and low permeant concentration, its ability to permit passage of a permeant along the concentration gradient can be characterized according to Tien,[50] and Kashchiev and Exerowa,[53] as follows:

$$P = p\frac{D}{\delta} \tag{12}$$

where P is the plasma membrane permeability, p is the porosity or ratio of hole surface area to total cell surface area, D is the diffusivity of a specified permeant, and δ is the characteristic diffusion length for a given cell.

Eq. (12) provides the basic, fundamental definition of permeability. The only parameter in this expression which can exhibit time-dependency to reflect a time-dependent permeability is the porosity. Hence, the porosity is assumed to be described in the following manner typical of a first-order chemical reaction:

$$np \xrightarrow{k_1} p$$

where np represents a relatively "non-porous" state typical of physiological porosity, $k1$ is the forward rate constant that characterizes the increasing porosity as a function of time during exposure to supraphysiological temperatures, and $p(t)$ is the now time-dependent porosity. By solving the appropriate conservation of species equations, the following expression for the porosity as a function of time is obtained:

$$p = 1 + [p_o - 1](exp(-k_1 t)) \tag{13}$$

where p_O is the initial, physiological porosity. When this expression is substituted into Eq. (12), the following time-dependent expression for the permeability is obtained:

$$P = \frac{D}{\delta}[1 + [p_o - 1](exp(-k_1 t))] \tag{14}$$

When this expression for the permeability is substituted into the two-compartment model as described by Eq. (8) and integrated, the following analytical solution is obtained for the normalized intracellular intensity as a function of time:

$$\frac{I}{I_o}(t) = exp\left[-\frac{AD}{V\delta}\left[t + \left(\frac{p_o - 1}{k_1}\right)(1 - exp[-k_1 t])\right]\right] \tag{15}$$

By using a simplified version of the Stokes-Einstein relation,[54] an estimated value for D of 2.8 x 10^{-10} m^2/s can be obtained which compares well to the measured diffusivity of 2 x 10^{-10} m^2/s for the fluorescent probe 2,7-bis-(2-carboxyethyl)-5-(and 6-)-carboxyfluorescein which weighs 436 Da which is less than calcein (623 Da) but has the same net negative charge of -6 when completely deesterifed.[82] The value of δ is assumed to equal the radius of the skeletal muscle cell whose value is approximately 5 μm. The value of p_O used, 1 x 10^{-6}, was iteratively determined as the optimal choice based on the

qualitative accuracy of the curve fits and the values of their correlation coefficients (R values). This model was fit using a nonlinear regression to all the calcein leakage curves for skeletal muscle cells exposed to supraphysiological temperatures and these fits will be presented in Chapter 4.

Chapter 4. Results

The results of the thermal microscopy system characterization, the experimental results and subsequent analyses of the thermal damage studies, and the results of the curve fits of the previously developed analytical solutions are presented in this chapter.

4.1 Thermal Microperfusion Stage Characterization

The thermal and fluid flow properties of the microperfusion stage were each separately characterized to ensure reproducible, uniform thermal and flow conditions within the microperfusion stage during experimentation.

4.1.1 *Thermal Characterization*

In order to characterize the thermal field in the chamber, a calibration curve was generated by plotting the nominal melting temperatures of Templistik standards (38, 45, 55, and 66° C) against the screen temperature of the temperature controller at which these standards melted. A line fit to these data showed a good correlation with $R^2 = 0.98$ (data not shown). The sample also melted uniformly on the surface of the chamber (8 mm x 2 mm) over a temperature increase of only 0.5° C indicating the absence of undesired thermal gradients. Based on these results, the thermal conditions of the microperfusion stage were considered well characterized and acceptable for the subsequent thermal injury experiments.

4.1.2 *Flow Characterization*

To ensure that the microperfusion chamber in the thermal stage was well perfused and free of stagnant flow regions, dispersion analysis of the chamber was conducted. A dispersion

coefficient was calculated using $\sigma^2 = 2N_D + 8(N_D)^2$, where σ^2 is the nondimensionalized variance of the outlet dye concentration as measured by a spectrophotometer and N_D is the dispersion number.[55] Theoretical N_D values range from 0 for plug flow to ∞ for complete back-mixing. N_D values obtained for the various flow rates are shown in Table 2. A value of $N_D << 1$ indicates a near-plug flow. Since the N_D values for all flow rates were less than 0.04, the chamber was indeed well perfused and free of stagnant flow regions. Direct microscopic observations of chamber flow, in which a flat front of trypan blue dye was visualized flowing through the chamber as a uniform front with no significant broadening, confirmed our results. To determine the time for the chamber concentration to equal the concentration of incoming perfusate, perfusion analysis of the chamber was conducted. The brightness of trypan blue as a function of time was found to be exponential for all flow rates tested and τ (time required to reach 63% of the steady state value) decreased with increasing flow rates. The values of τ are shown in Table 2. A typical experimental flow rate of 3 mL/min would require approximately 4 seconds for the concentration inside the chamber to equal that of the incoming perfusate. Based on these results, the flow conditions of the microperfusion stage were considered to be suitable for experimental studies with isolated skeletal muscle cells.

Table 2. Dispersion number and time for the chamber to reach 63% of the steady state concentration of the incoming perfusate as a function of flow rate.

Flow rate (mL/min)	N_D	τ (sec)
1	0.033	2.3
2	0.024	1.5
3	0.027	1.0

4.2 Fluorescent Microscopy System Characterization

The normalization scheme utilized for all calcein leakage data presented in this study will be discussed. To ensure that intracellular fluorescence measurements of calcein leakage from isolated skeletal muscle cells exposed to supraphysiological temperatures were accurate, studies were conducted to demonstrate negligible intensity loss due to photobleaching and natural dye leakage. Additional studies and analyses were conducted to demonstrate: (1) the proportionality of intracellular calcein intensity to intracellular calcein concentration, (2) the validity of the two-compartment model, Eq. (9), (3) the relative uniformity of calcein leakage from the center and ends of the cell, and (4) the relative uniformity of the digitized field on which the intracellular fluorescence of a skeletal muscle cell was observed.

4.2.1 *Normalization Scheme*

Normalized intracellular calcein intensity was determined in the following manner. First, a region was traced along the outer border of a cell and the intensity within this region was quantified. The background intensity was then quantified in a square shaped region just outside the cell. The shape and size of this region were arbitrarily chosen and are not important since the background intensity was relatively invariant. The background intensity was then subtracted from the intensity within the region traced along the outer border of the cell. This corrected intensity was then normalized with respect to the initial (t = 0 min) corrected intensity for each individual experiment. This method of quantifying the two-dimensional intracellular intensity of a three-dimensional cell was considered reasonable since the average diameter of a skeletal muscle cell is 10 μm whereas its average length is 1000 μm indicating that radial dye mass transfer is approximately 4 orders of magnitude faster than axial dye mass transfer.

4.2.2 *Photobleaching and Natural Dye Leakage*

The relative contribution of photobleaching of calcein in skeletal muscle cells was determined by continuously exposing calcein loaded skeletal muscle cells to the fluorescent excitation beam at 37° C. These characterization experiments were performed in the presence of neutral density filters which attenuate the magnitude of the excitation beam and homogenize the exposure field of the sample. The results of this study shown in Figure 6A indicates less than 5% intensity loss occurs after a minute of continuous exposure. Hence, a shuttering scheme was adopted accordingly to keep total exposure less than 1 minute during a calcein leakage experiment. The relative contribution of natural dye leakage of calcein in skeletal muscle cells was determined by exposing calcein loaded skeletal muscle cells to 37° C for 30 minutes during which intensity measurements were made every 15 minutes in order to prevent photobleaching. The results of this study shown in Figure 6B indicate less than 3% intensity loss due to natural dye leakage following continuous exposure at 37° C for 30 minutes. Since all calcein leakage experiments conducted lasted 17 minutes or less, the effect of natural dye leakage was negligible for our intensity measurements.

4.2.3 *Proportionality of Calcein Intensity to Calcein Concentration*

It was assumed that intracellular calcein intensity was proportional to intracellular calcein concentration. To test this assumption, various calcein-AM concentrations were hydrolyzed in a 1:1 KOH and methanol mixture. To ensure reproducible volumes, a lithographically fabricated hemocytometric slide was used to hold 2 μl of solution. The results showed a linearly proportional relationship (R^2 = 0.985) between intracellular calcein intensity and intracellular calcein concentration for calcein concentrations ranging from 5 to 60μM as described elsewhere.[19]

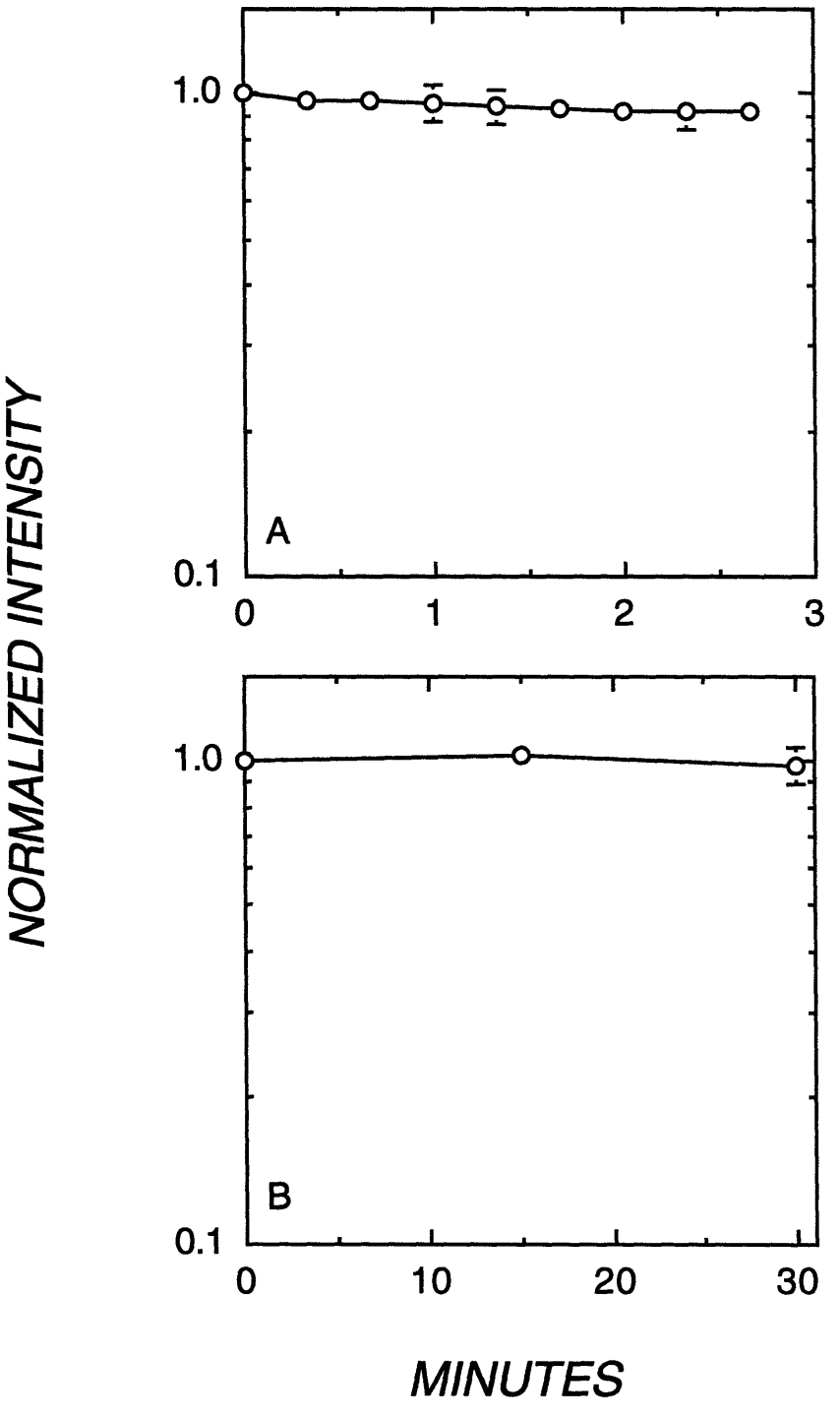

Figure 6. Normalized intracellular calcein intensity as a function of time for photobleaching (A) and natural dye leakage (B) at 37° C. Error bars represent the standard error of the mean (SEM).

4.2.4 *Validity of Two-compartment Model*

The two compartment model Eq. (9) was considered valid with an error < 5% if the Sherwood number,[83] Sh = PL/D is < 0.1, where P is the permeability, L is the characteristic length of the cell (V/A), and D is the diffusivity of a molecular species. Sh compares the transmembrane diffusion of a molecular species to the intracellular diffusion of the same molecular species. If $P < 2 \times 10^{-6}$ m/s, the model was considered valid. The permeabilities calculated in this study ranged from 1 to 100 $\times 10^{-9}$ m/s so the two compartment model was indeed valid for this study as described elsewhere.[19]

4.2.5 *Differential Calcein Leakage Analysis*

Calcein dye leakage from skeletal muscle cells was analyzed at 42 and 50° C, a typical low and high temperature, to determine the relative permeability of different regions of a thermally damaged cell. The relative amounts of dye leakage from the center and end regions of a cell were determined and these results shown in Figure 7 indicate that dye leakage is relatively uniform from the center and end regions of the cell. Thus, the use of intracellular calcein intensity was adequate for an overall permeability measurement.

4.2.6 *Uniformity of the Digitized Field*

For a typical thermal injury experiment, a calcein loaded skeletal muscle cell nearly traversed the entire length of the digitized field. Hence, it was important to ensure that the fluorescent detection characteristics of the SIT camera (Hamamatsu) were uniform and not overly sensitive in one region and less sensitive in other regions. To characterize the uniformity of the digitized field, a line intensity scan was conducted along the length of a cell and the variation in intensity from the center to the two ends was less than 5% (data not

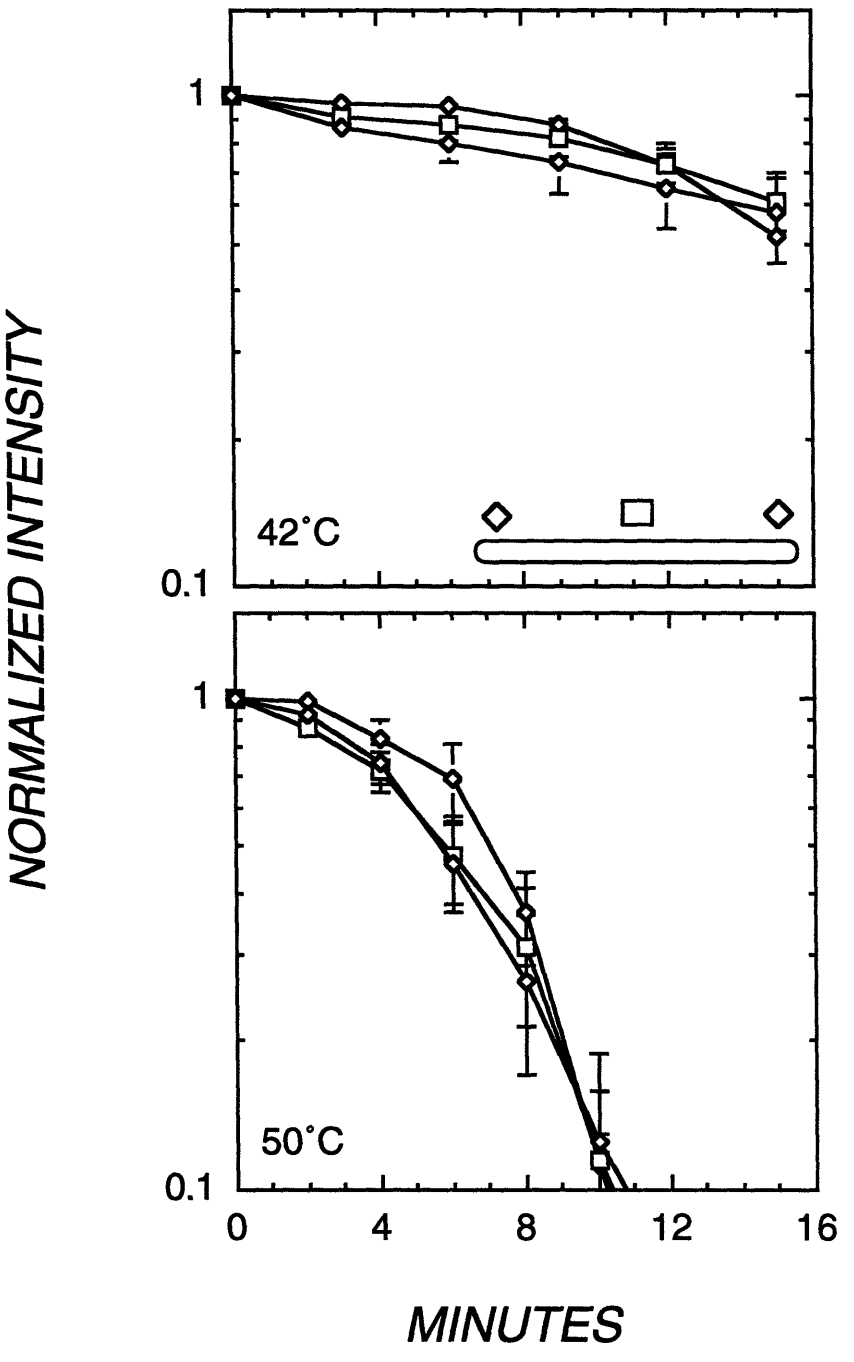

Figure 7. Normalized intracellular calcein intensity as a function of time for differential dye leakage studies at 42 and 50° C. Error bars represent the SEM.

shown). The digitized field was therefore assumed to be sufficiently uniform for reliable measurements of intracellular calcein fluorescence.

4.3 Kinetics of Calcein Leakage

The kinetics of calcein leakage in individual skeletal muscle cells exposed supraphysiological temperatures were determined to characterize the effects of elevated temperatures on the plasma membrane. The two left panels in Figure 8 show a typical experiment with two skeletal muscle cells at 50° C at t = 0 and t = 6 min. A noticeable intracellular fluorescence loss has occurred after 6 minutes of exposure at 50° C indicating damage to the plasma membrane. Calcein dye leakage from skeletal muscle cells exposed to temperatures ranging from 37 to 70° C is shown in Figure 9 by plotting normalized intracellular fluorescent intensity of the skeletal muscle cells on a logarithmic scale as a function of time.

The physiological response of these calcein loaded cells at 37° C indicates a negligible intracellular fluorescence loss of 7% due to photobleaching after 17 minutes. At 40 and 42° C, the shapes of the curves are similar and show a slight delay or shoulder before the onset of dye leakage. The final normalized intracellular fluorescence losses at these two temperatures were 30% and 50%, respectively. At 45° C, the shape of the curve was linear for the entire duration of exposure and the final normalized fluorescence loss was 75%. This linear shape deviated markedly from the shapes of the curves of all the other supraphysiological temperatures. At 50, 55, 60, and 70° C, the shapes of the curves are similar and dye leakage is rapid with little or no delay or present. The times at which 90% normalized intracellular fluorescence loss occurred at 50, 55, 60, and 70° C were 11, 5, 3, and 0.5 minutes, respectively.

4.4 Arrhenius Dependence of Calcein Leakage

To determine the activation energy (E_a) for thermal damage to the plasma membrane of

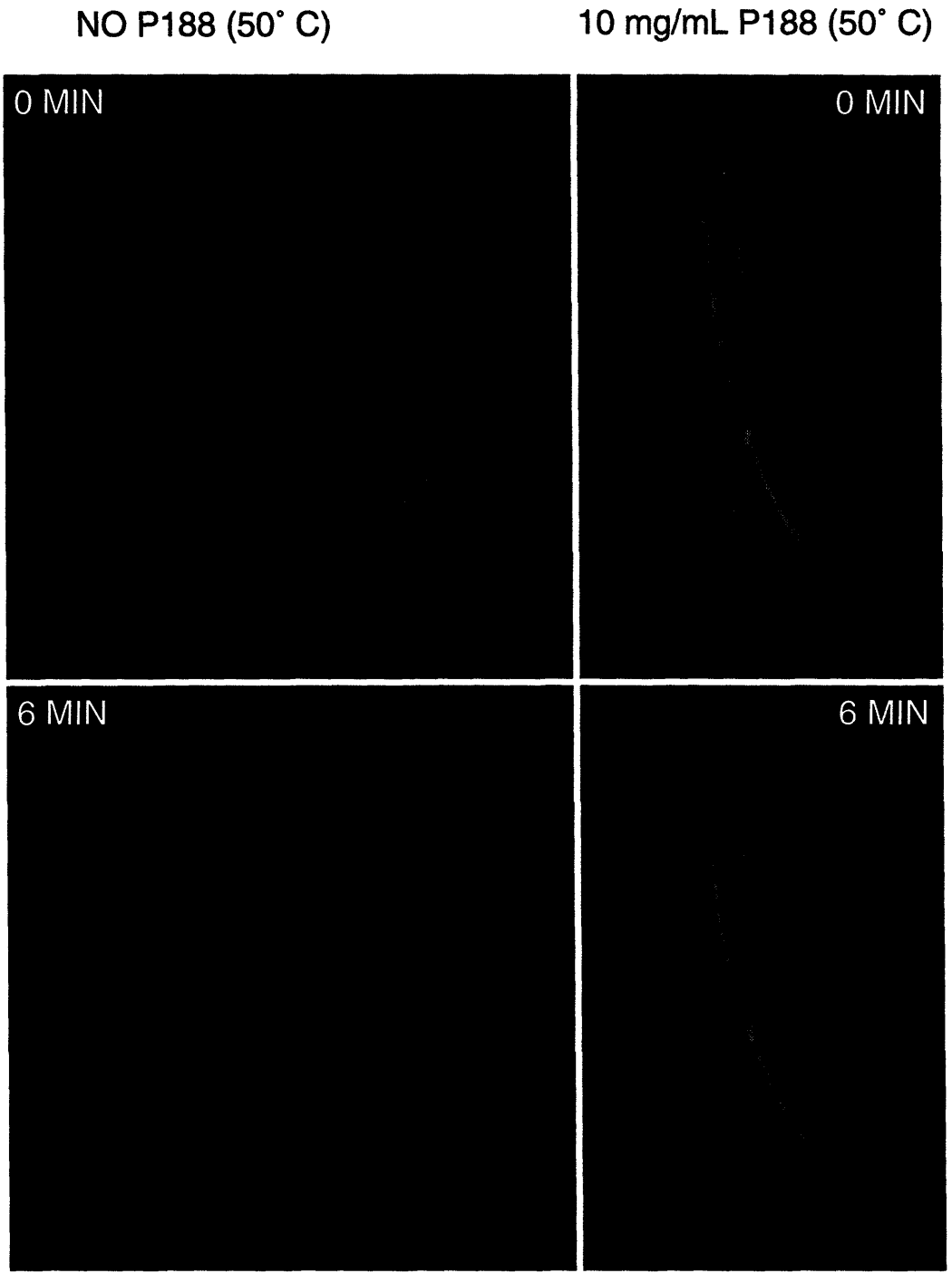

Figure 8. Intracellular calcein fluorescence in skeletal muscle cells exposed to 50° C in the presence and absence of P188 (10 mg/mL) for t = 0 min and t = 6 min.

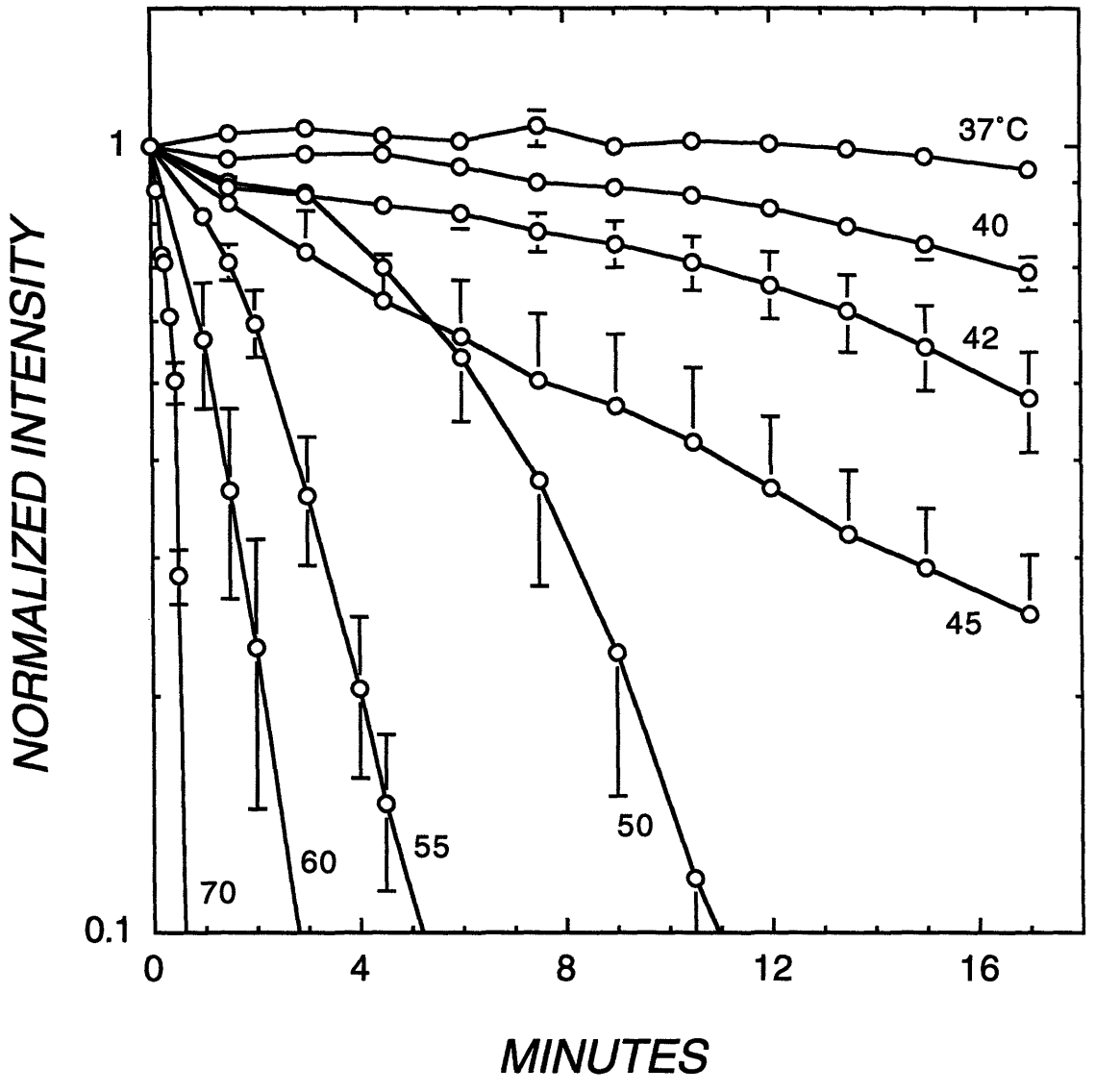

Figure 9. Normalized intracellular calcein intensity as a function of time for skeletal muscle cells exposed to 37-70° C. Error bars represent the SEM.

skeletal muscle cells exposed to supraphysiological temperatures, an Arrhenius plot shown in Figure 10 was constructed by plotting the times required to reach 40% normalized intracellular fluorescence loss on a logarithmic scale as a function of inverse absolute temperature for the temperature range of 40 to 70° C. This time used in the Arrhenius plot is arbitrary and varies according to the experiment and specific damage criteria. This time

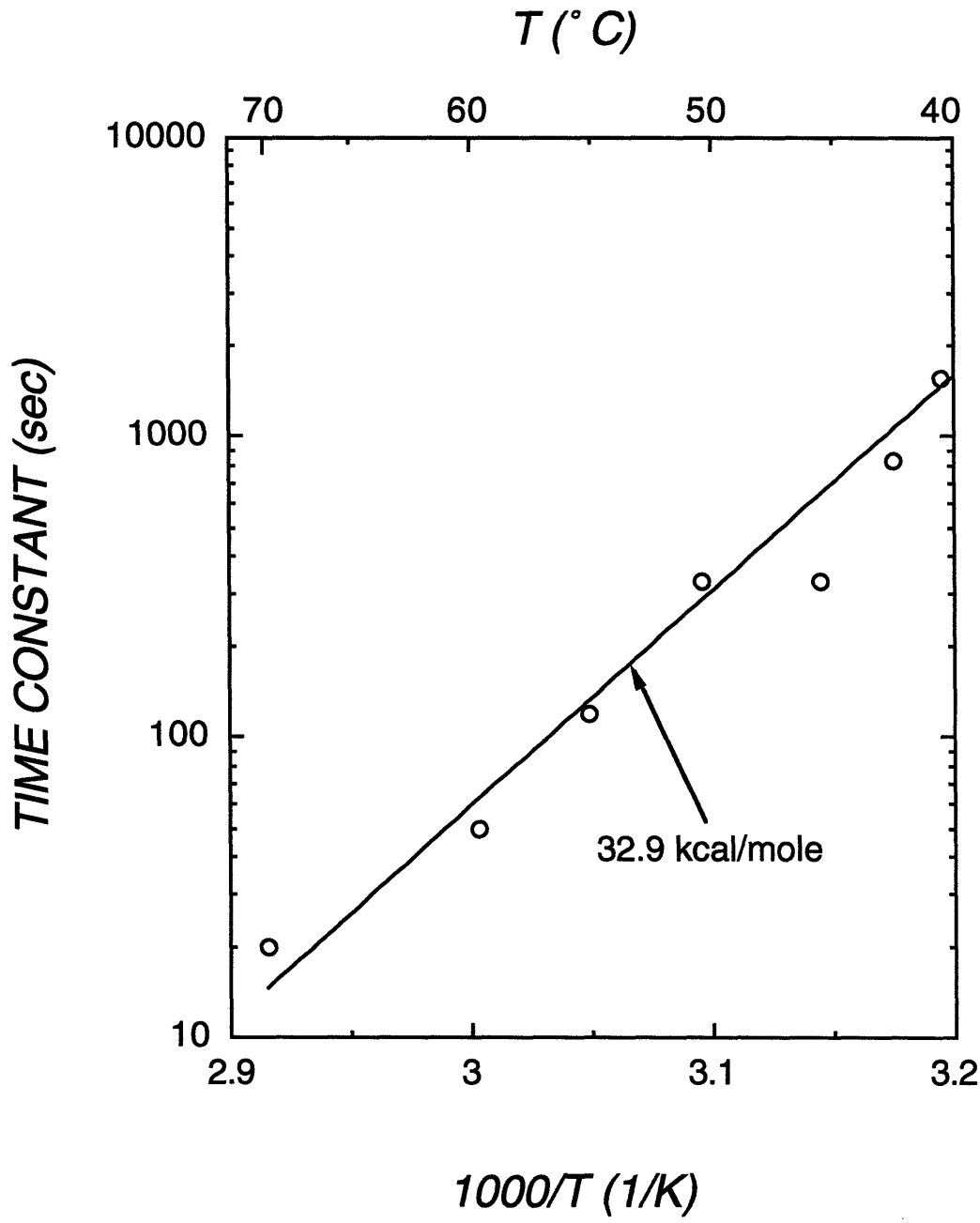

Figure 10. The Arrhenius dependence of the kinetics of calcein leakage shown by the time constant for 40% calcein leakage as a function of inverse absolute temperature from 40 to 70° C.

was chosen since sufficient membrane damage was assumed to have occurred to permit 40% calcein leakage and this particular choice also provided 4 data points for the line fit to

the results in the presence of P188 at 10 mg/mL as discussed below. The slope of the line fit to this data by a least squares regression ($R^2 = 0.99$) in the absence of P188 yielded an E_a of 32.9 kcal/mole which indicates the energetic threshold required to produce 40% dye leakage. Although this choice of 40% dye leakage differs from the traditional choice of 63% dye leakage, the activation energy for 63% dye leakage was 28 kcal/mole which is in close agreement to 32.9 kcal/mole with a relative variation of only 15%.

4.5 Effect of P188 on the Dynamics of Calcein Leakage

The kinetics of calcein leakage from skeletal muscle cells exposed to supraphysiological temperatures ranging from 40 to 60° C in the absence and presence of P188 at 10 mg/mL was determined and compared in Figure 11 where the normalized intracellular fluorescence was plotted as a function of time. Similar experiments were conducted at 37° C to determine how much intensity loss was caused by photobleaching and whether P188 permeabilized an intact membrane. The results (data not shown) indicated a 7% normalized fluorescence loss due to photobleaching and a 7% normalized fluorescence loss due to membrane permeabilization by P188 in 17 minutes. In Figure 8, a micrograph comparing the intracellular fluorescence of two isolated skeletal muscle cells exposed to 50° C in the presence of 10 mg/mL P188 and a control without P188 at t = 0 min and t = 6 min is shown. The fluorescence has noticeably decreased in 6 minutes for the control whereas the fluorescence has not changed significantly in the presence of P188 after 6 minutes which qualitatively suggests that P188 was preventing calcein leakage from the cells. At 40 and 42° C, P188 completely arrested dye leakage when compared to the corresponding controls whose normalized fluorescence losses were 30% and 50% at 17 minutes respectively. At 45° C, the P188 successfully blocked dye leakage up to 10 minutes as compared to the control which exhibited steady leakage. After 17 minutes at 45 °C, the P188 effectiveness lessened as evidenced by a normalized fluorescence loss of 40% as compared to 75% in the

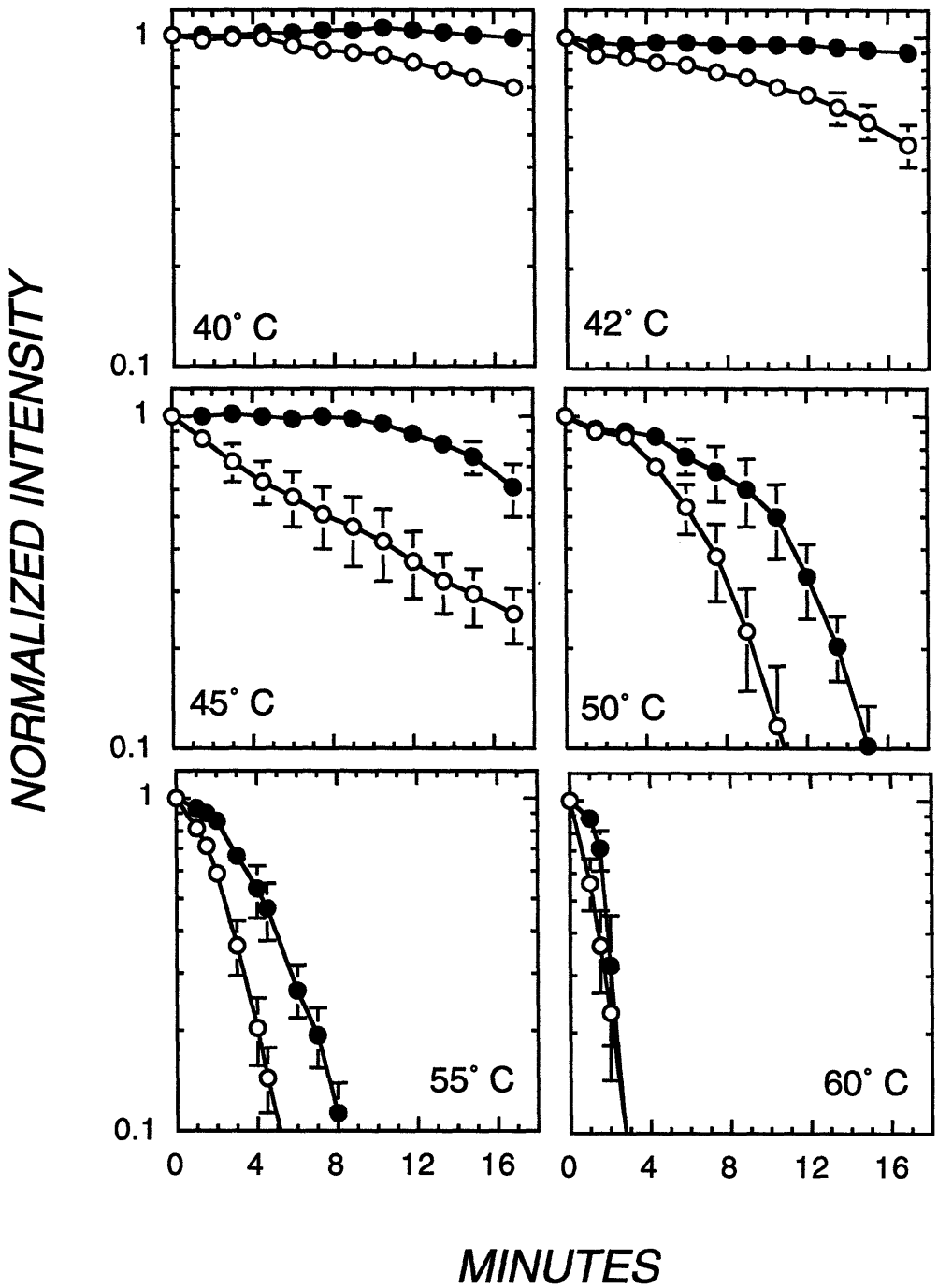

Figure 11. Normalized intracellular calcein intensity as a function of time in skeletal muscle cells exposed to 40-60° C in the presence (black circles) and absence (white circles) of P188 at 10 mg/mL. Error bars represent the SEM.

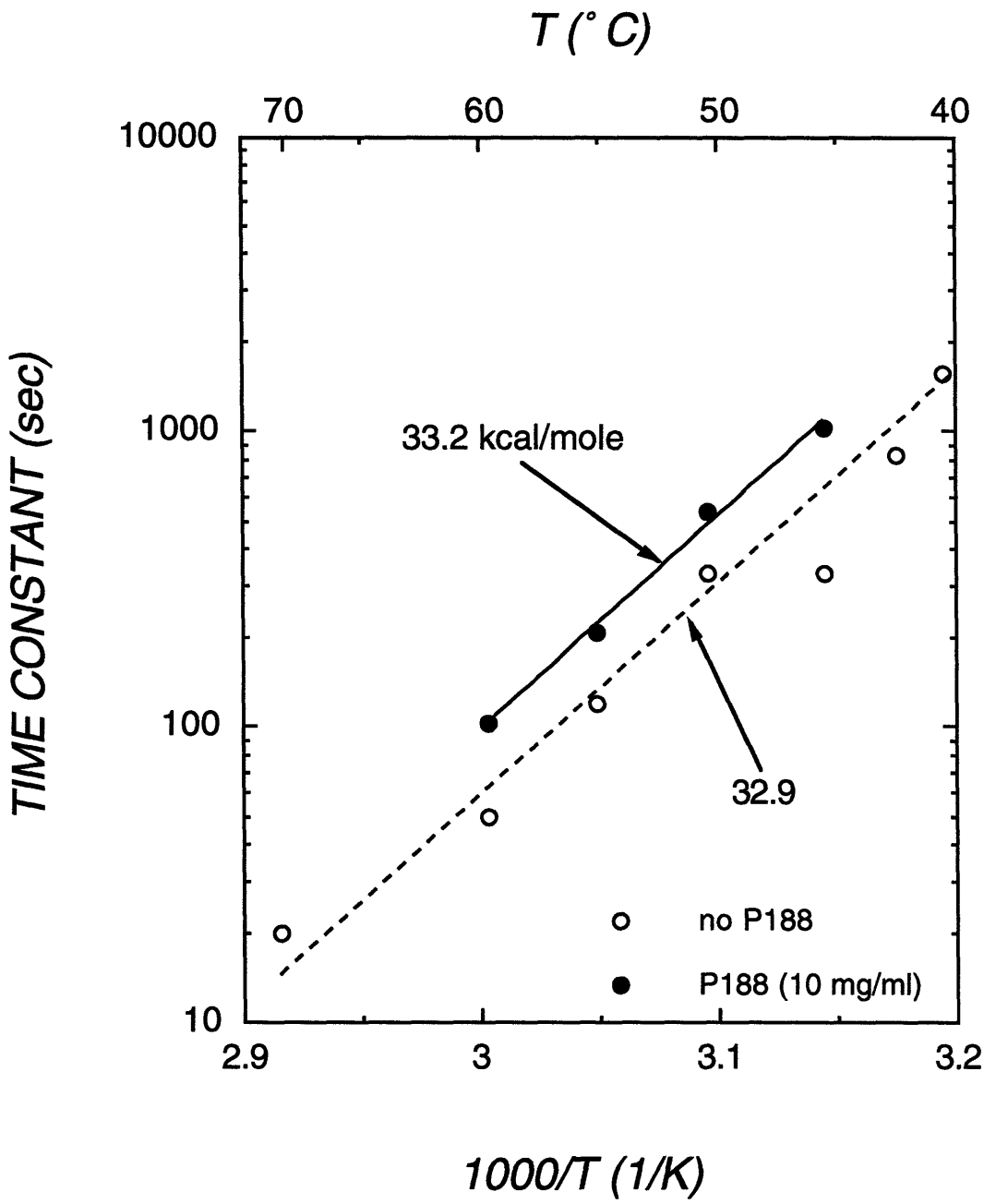

Figure 12. Arrhenius dependence of the kinetics of calcein leakage in the presence and absence of P188 (10 mg/mL) as shown by plotting the time constant for 40% calcein leakage as a function of inverse absolute temperature.

control. Above 45° C, P188 generally both delayed and retarded the onset of dye leakage. At 50° C, the time required for a normalized fluorescence loss of 90% was 14 minutes with

P188 and 10 minutes for the control. At 55° C, the time for 90% leakage was 7.5 minutes for P188 and 4.5 minutes for the control. At 60° C, no clear difference is noted between the P188 and control dye leakage, thereby indicating this temperature as the approximate threshold for P188 effectiveness.

4.6 Effect of P188 on the Activation Energy of Calcein Leakage

To determine the activation energy (E_a) for thermal damage to the plasma membrane of skeletal muscle cells exposed to supraphysiological temperatures in the presence of P188 at 10 mg/mL, an Arrhenius plot shown in Figure 12 was constructed by plotting the time constant (time required to reach 40% normalized fluorescent intensity loss) on a logarithmic scale as a function of inverse absolute temperature for the temperature range of 45 to 60° C. The slope of the line fit to this data by a least squares regression ($R^2 = 0.99$) yielded an E_a of 33.2 kcal/mole. Figure 12 also shows the result with no P188 which yielded an E_a of 32.9 kcal/mole. The two lines are essentially parallel to one another.

4.7 Effect of P188 Concentration on Calcein Leakage

All calcein leakage experiments conducted thus far utilized P188 at a concentration of 10 mg/mL which was above the critical micelle concentration (CMC) of 1 mg/mL as measured at 25° C.[38] Experiments were conducted at 42, 50, and 55° C with P188 concentrations ranging between 0.1 and 10 mg/mL P188 in order to determine the dose response to P188. In Figure 13, the results of these experiments are shown by comparing the kinetics of calcein leakage for the various P188 concentrations at 42, 50, and 55° C. For all temperatures, P188 prevents calcein leakage as effectively as it did at 10 mg/mL for concentrations at and below the CMC; whereas, at 2 mg/mL, P188 is relatively ineffective when compared to the other doses. These calcein leakage data are presented in another

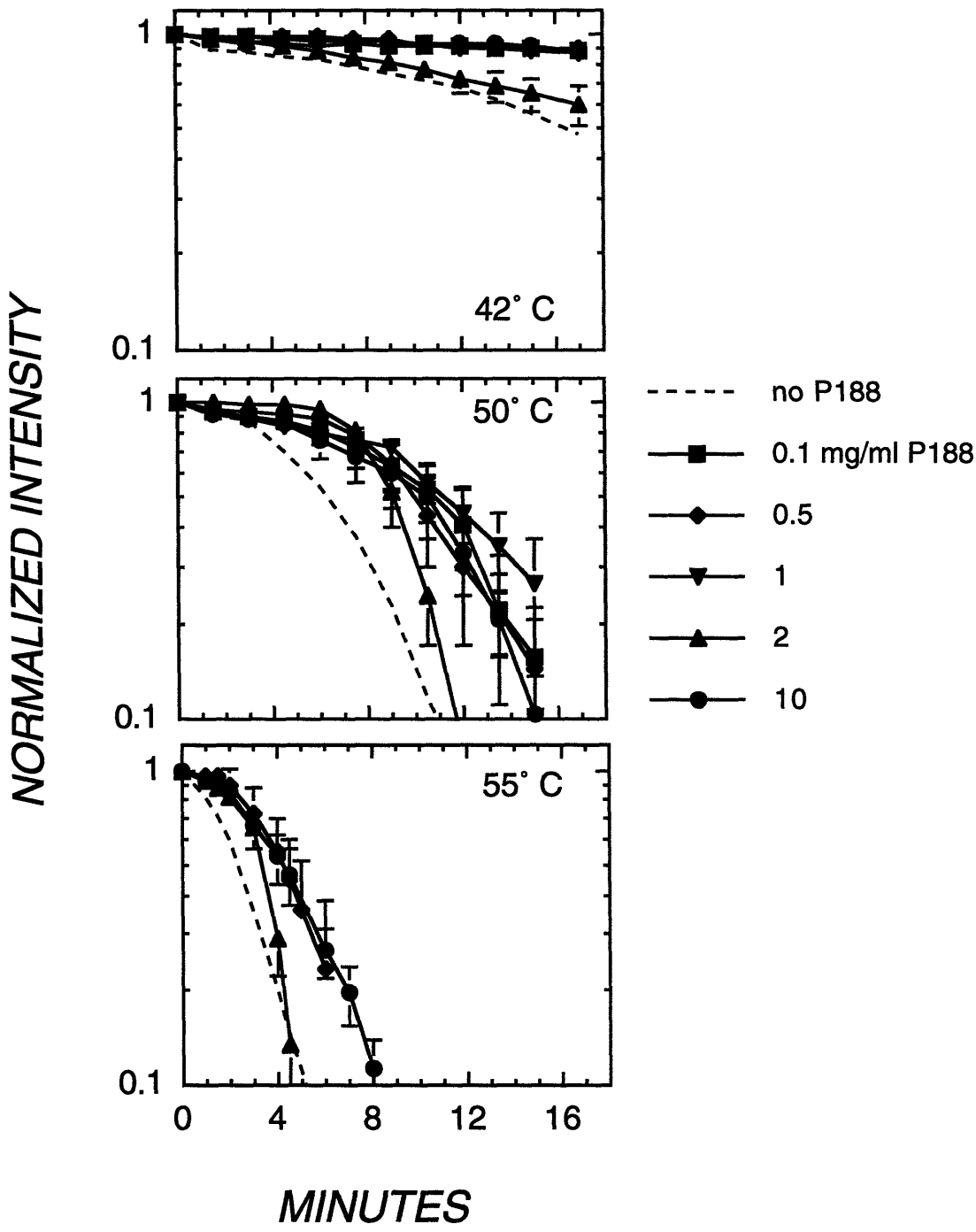

Figure 13. Normalized intracellular calcein intensity as a function of time for skeletal muscle cells exposed to 42, 50, and 55° C at various P188 concentrations. Error bars represent the SEM.

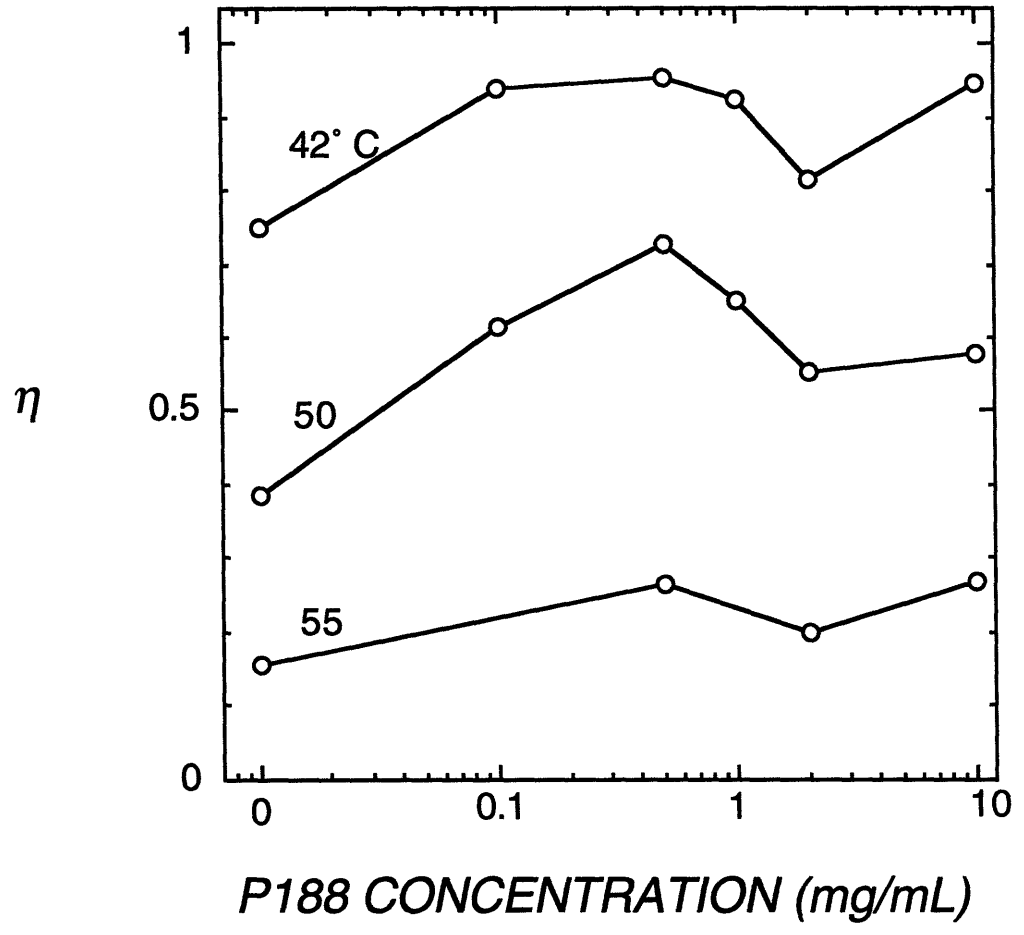

Figure 14. P188 effectiveness as a function of P188 concentration on a logarithmic scale for skeletal muscle cells exposed to 42, 50, and 55° C.

format in Figure 14 that displays the unusual yet interesting trend of P188 effectiveness as a function of concentration at 42, 50, 55° C. The relative effectiveness, η, is defined as follows:

$$\eta = \frac{\int_0^t I(t)dt}{I_o \Delta t} \tag{16}$$

where Δt (= 17 min) is the total duration of the experiment. The value of η which varies from 0 to 1 is the ratio of the area under the calcein leakage curve to the maximum possible

area under the curve which occurs when the normalized intensity equals 1.0 for the entire 17 min exposure time. The general trend for the η values at 42, 50, and 55° C indicated a rise from an absolute minimum with no P188 to a maximum at 0.5 mg/mL followed by a decrease to a relative minimum at 2 mg/mL and then a rise at 10 mg/mL. These results indicate that 0.5 mg/mL was the most effective P188 concentration and that 0.2 mg/mL was the least effective P188 concentration at 42, 50, and 55° C.

4.8 Effect of Dextran on Calcein Leakage

In order to demonstrate the specificity of P188 in sealing the plasma membrane of skeletal muscle cells, experiments were conducted with neutral dextran at 45° C. In these experiments, hypertonic PBS was supplemented with dextran at 0.5, 2, and 10 mg/mL. The results of these experiments shown in Figure 15 compare the effect of dextran at 3 different concentrations to P188 and no P188. The final normalized intracellular fluorescent losses in the presence and absence of P188 were 40% and 75%, respectively. The final normalized intracellular fluorescent losses in the presence of dextran at 0.5, 2, and 10 mg/mL were 70%, 80%, and 90%, respectively, which demonstrate that dextran is relatively ineffective at 3 different concentrations as compared to P188.

4.9 Effect of Various Poloxamers on Calcein Leakage

In order to determine how various PO core lengths and EO tail lengths different from that of P188 affect the kinetics of calcein leakage, experiments were conducted at 45° C with poloxamers P238, P338, and P407 at 10 mg/mL. The EO/PO ratios for P238, P338, and P407 were 5.25, 5.45, and 3, respectively, with the absolute sizes of the PO core and EO tails varying as shown in Table 2. The total EO/PO ratio for P188 was 5. The calcein

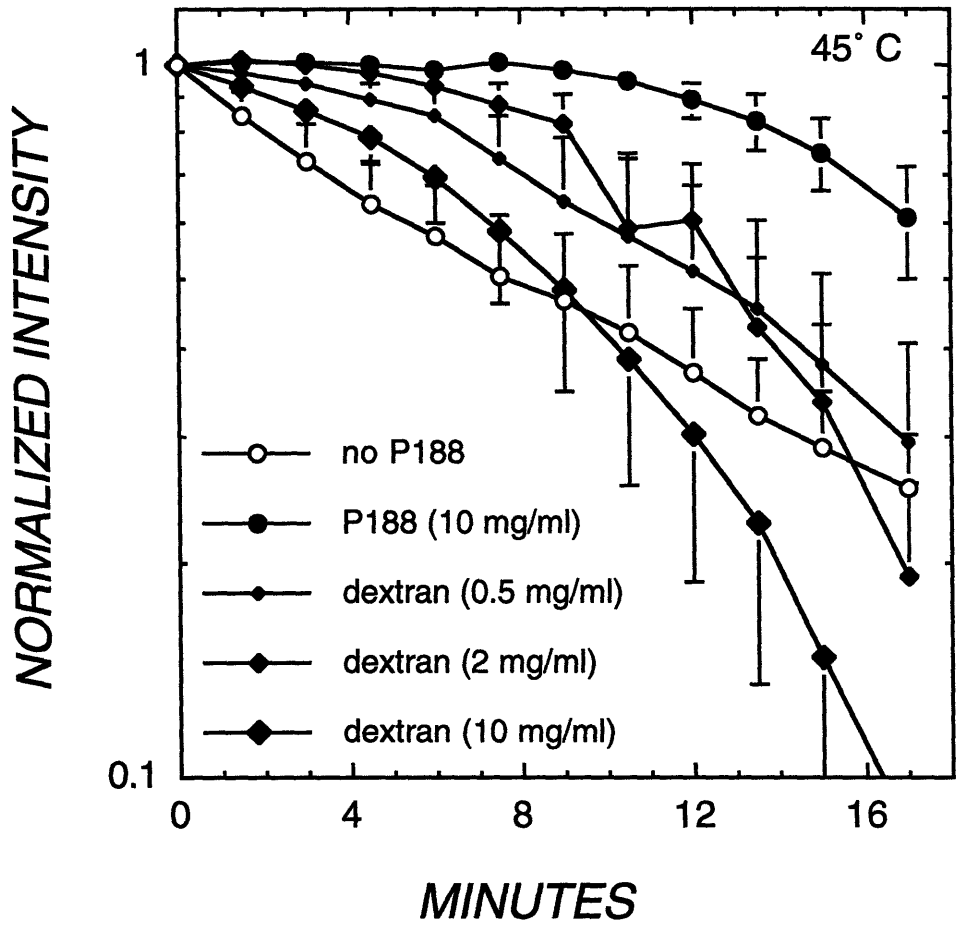

Figure 15. Normalized intracellular calcein intensity as a function of time for skeletal muscle cells exposed to 45° C in the presence and absence of P188 at 10 mg/mL and in the presence of dextran at 0.5, 2, and 10 mg/mL. Error bars represent the SEM

leakage curves in Figure 16 show that P238, P338, and P407 at 10 mg/mL were as effective as P188 at 10 mg/mL.

4.10 Effect of Polyethylene and Polypropylene Glycol on Calcein Leakage

In order to determine the mechanism of P188 action and whether utilizing solely the hydrophobic or hydrophilic portions of P188 was sufficient to arrest calcein leakage,

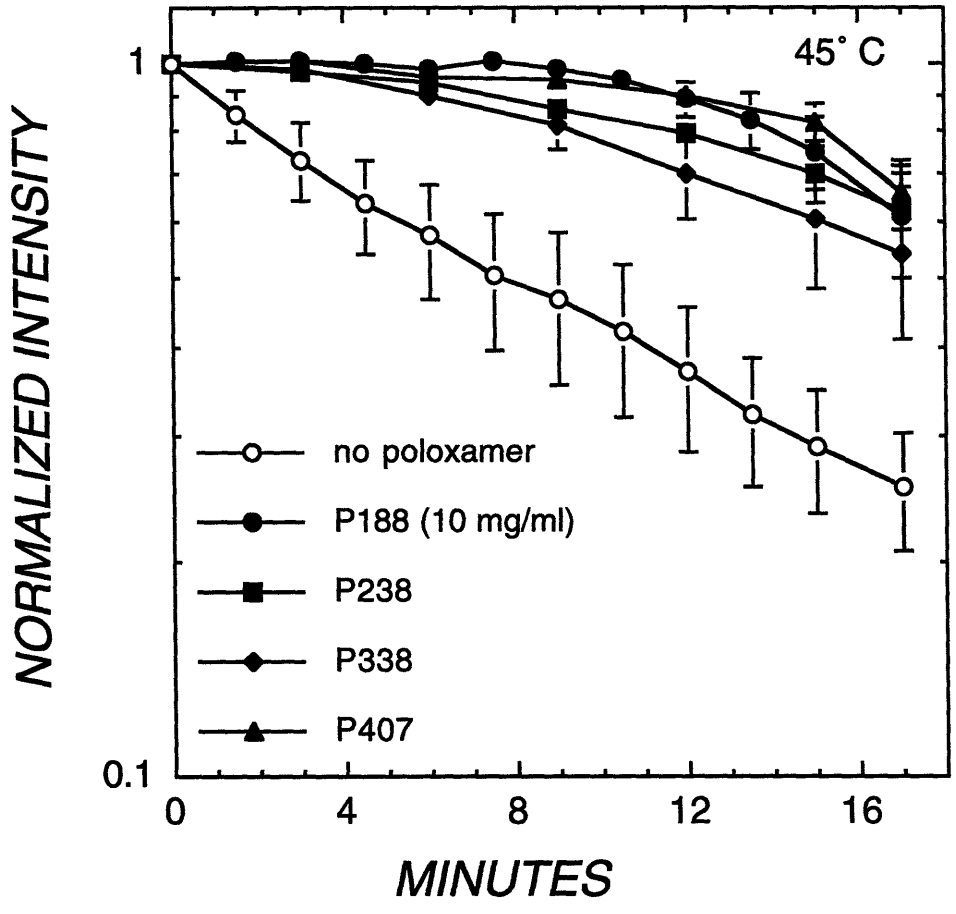

Figure 16. Normalized intracellular calcein intensity as a function of time for skeletal muscle cells exposed to 45° C in the presence of P188, P238, P338, and P407 at 10 mg/mL and in the absence of poloxamer. Error bars represent the SEM.

experiments were conducted at 42 and 50° C with PEG at 20 mg/mL and PPG at 10 mg/mL. PEG was used at a concentration of 20 mg/mL in order to appropriately represent each P188 molecule containing 2 hydrophilic ethylene oxide tails at a concentration of 10 mg/mL. The results in Figure 17 demonstrate that neither PEG nor PPG alone was able to arrest or even retard calcein leakage as effectively as P188 at 42 and 50° C.

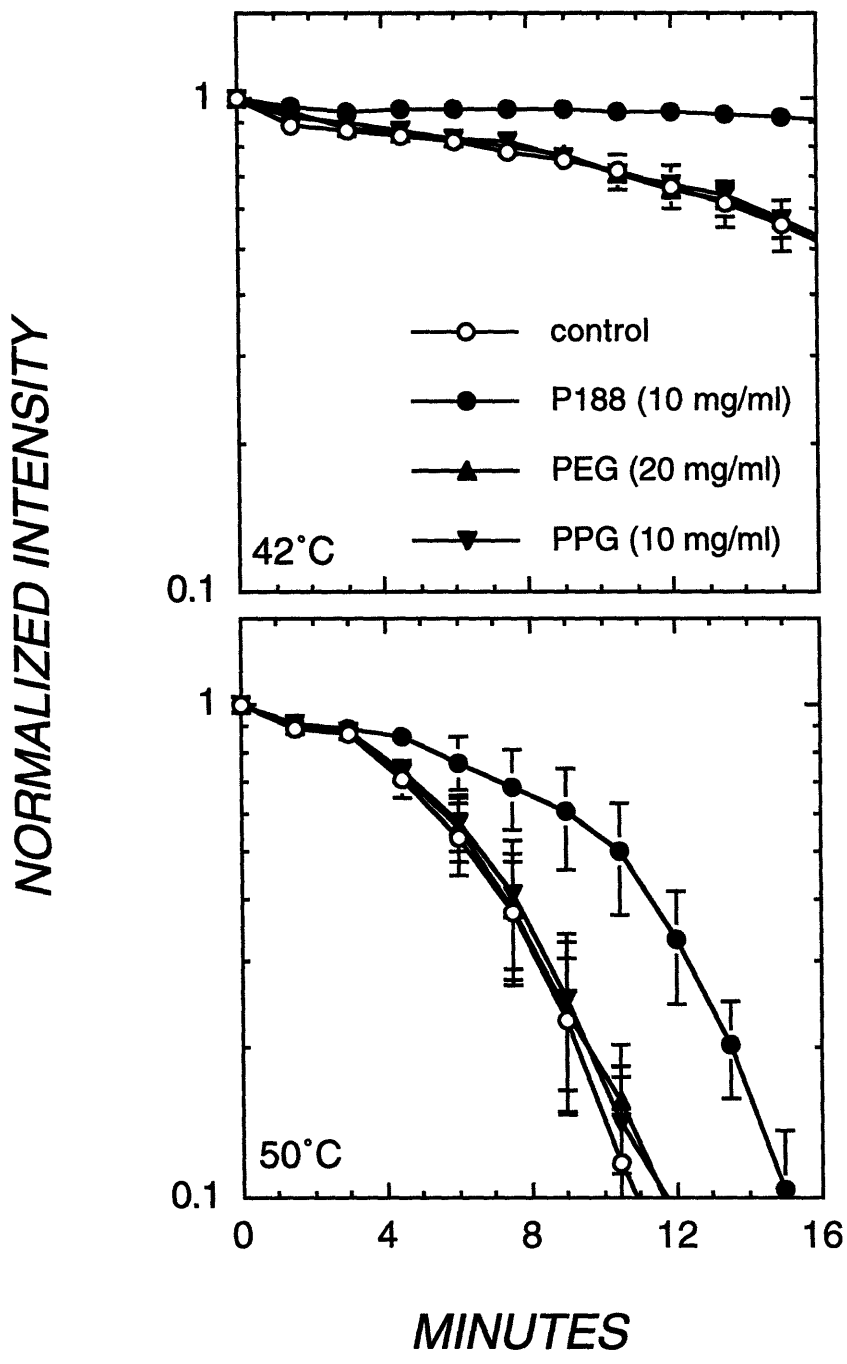

Figure 17. Normalized intracellular calcein intensity as a function of time for skeletal muscle cells exposed to 42 and 50° C in the presence of PEG and PPG at 20 and 10 mg/mL, respectively. Error bars represent the SEM.

4.11 Determination of Model Parameters

The mathematical models Eqs. (9) and (10) were concurrently fit to the calcein leakage curves for skeletal muscle cells exposed to supraphysiological temperatures in the absence of P188. The Arrhenius dependence of the permeability at 63% leakage and the empirical parameters α and ß were determined as well. These two models were compared using the F-test to determine which model was statistically superior. Eq. (10), the statistically superior model as will be presented shortly, was then applied to thermal damage studies in other cell types with various membrane integrity probes. The kinetic model, Eq. (15), was also fit to the calcein leakage curves for skeletal muscle cells exposed to supraphysiological temperatures in the absence of P188 and the Arrhenius dependence of the rate constant k_1 was determined.

Table 3. R values for the two separate curve fits and the values of α and ß for the linearly time-dependent permeability for skeletal muscle cells exposed to temperatures from 40-70° C.

T (° C)	R_c	R_{td}	α (10^9 m/s^2)	ß (10^9 m/s
40	0.93248	0.98839	0.0014	0.1934
42	0.97394	0.97887	0.0008	1.2189
45	0.99447	0.99863	-0.0019	4.2063
50	0.92378	0.99545	0.0276	-0.4413
55	0.97660	0.99862	0.0854	6.3088
60	0.99080	0.99966	0.2038	18.635
70	0.93414	0.98093	6.1038	15.9429

where the subscripts "c" and "td" represent constant and time-dependent, respectively.

4.11.1 *Models Assuming Constant and Linearly Time-Dependent Permeability*

The two different solutions of the two-compartment model were formulated by assuming that the plasma membrane permeability was constant and linearly time-dependent during exposure to supraphysiological temperatures. These two solutions, Eqs. (9) and (10), were concurrently fit to the calcein dye leakage curves from skeletal muscle cells exposed to supraphysiological temperatures ranging from 40 to 60° C in the absence of P188 as shown in Figures 18A, B. The correlation coefficients (R values) for the two separate curve fits and the values of the empirical parameters α and ß for the linearly time-dependent permeability fit as a function of temperature are shown in Table 3.

For all temperatures, the linearly time-dependent fit had higher R values than the constant permeability fit which indicates a closer agreement between the actual data and the curve fit values. The time-dependent fits, in general, also better represent the kinetics and trends of the dye leakage curves than the constant permeability fits. At 40 and 42° C, the time-dependent fit (solid line) predicts the slight delay before the onset of leakage and the shape of the leakage curves whereas the constant fit (dotted line) does not. At 45° C, the two fits are nearly indistinguishable and predict the kinetics equally well. At 50° C, the time-dependent fit clearly describes the shape of the leakage curve more accurately than the constant fit whose pure exponential decay poorly portrays the kinetics of the leakage curve. At 55 and 60° C, the time-dependent fit continues to better depict the data as seen by comparing the curve fits and the R values. The α values were anomalous from 40 to 45° C since they decreased from 0.0014×10^9 m/s^2 to a rather unusual negative value of -0.0019×10^9 m/s^2. The values of α from 50 to 70° C were more reasonable since they displayed an expected increase. The ß values showed at first an increasing trend from 40 to 45° C but a physically inadmissible negative value of -0.4413×10^9 m/s at 50° C. The ß values at 60 and 70° C are relatively anomalous as well since a decrease is observed from

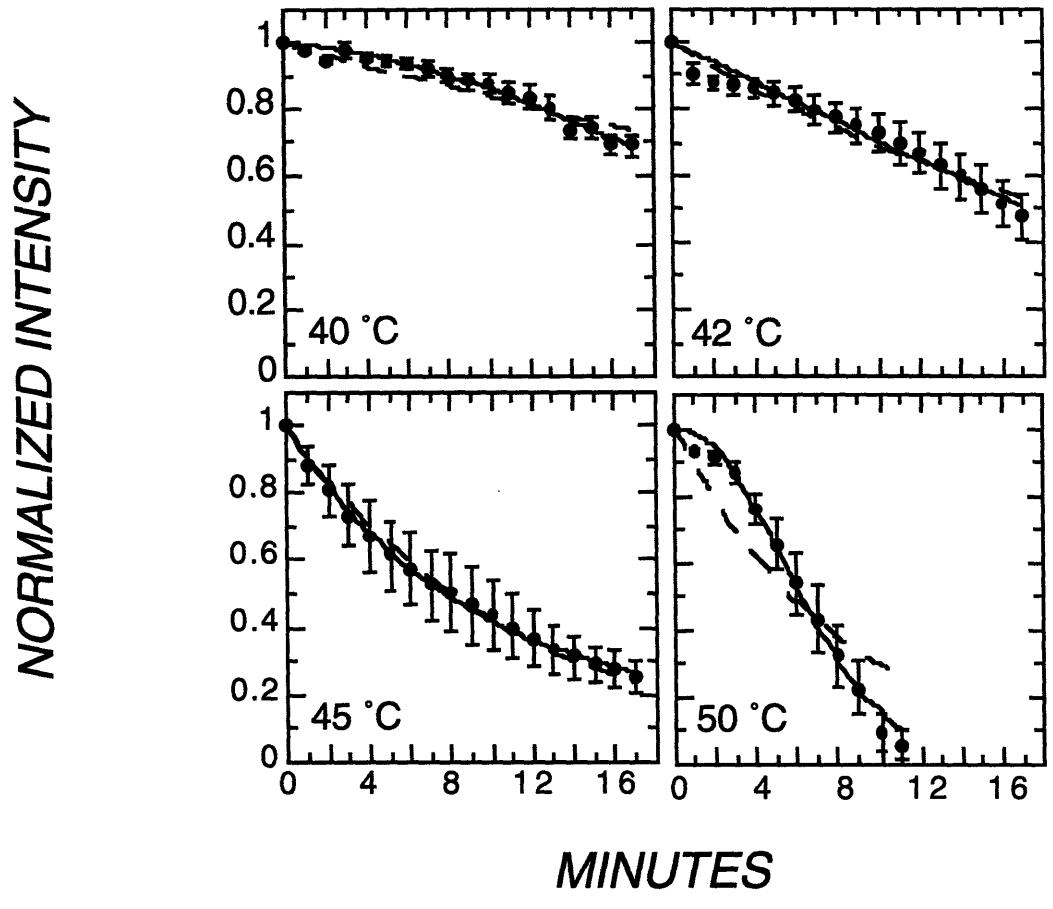

Figure 18A. Curve fits of Eq. (9) (dotted line) and Eq. (10) (solid line) to calcein leakage curves of skeletal muscle cells exposed to temperatures from 40-50° C. Error bars represent the SEM.

18.635 x 10^9 m/s to 15.9429 x 10^9 m/s. Despite these anomalies, this analysis has provided the ability to accurately predict the dynamics of plasma membrane damage at elevated temperatures.

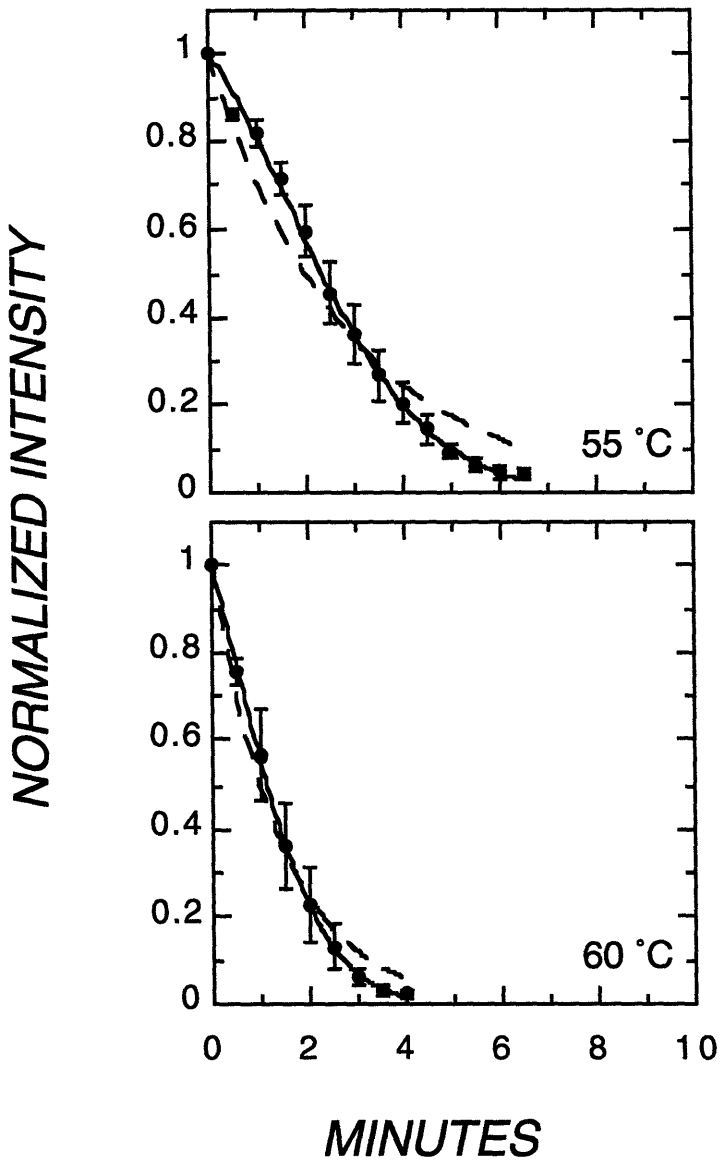

Figure 18B. Curve fits of Eq. (9) (dotted line) and Eq. (10) (solid line) to calcein leakage curves of skeletal muscle cells exposed to 55 and 60° C. Error bars represent the SEM.

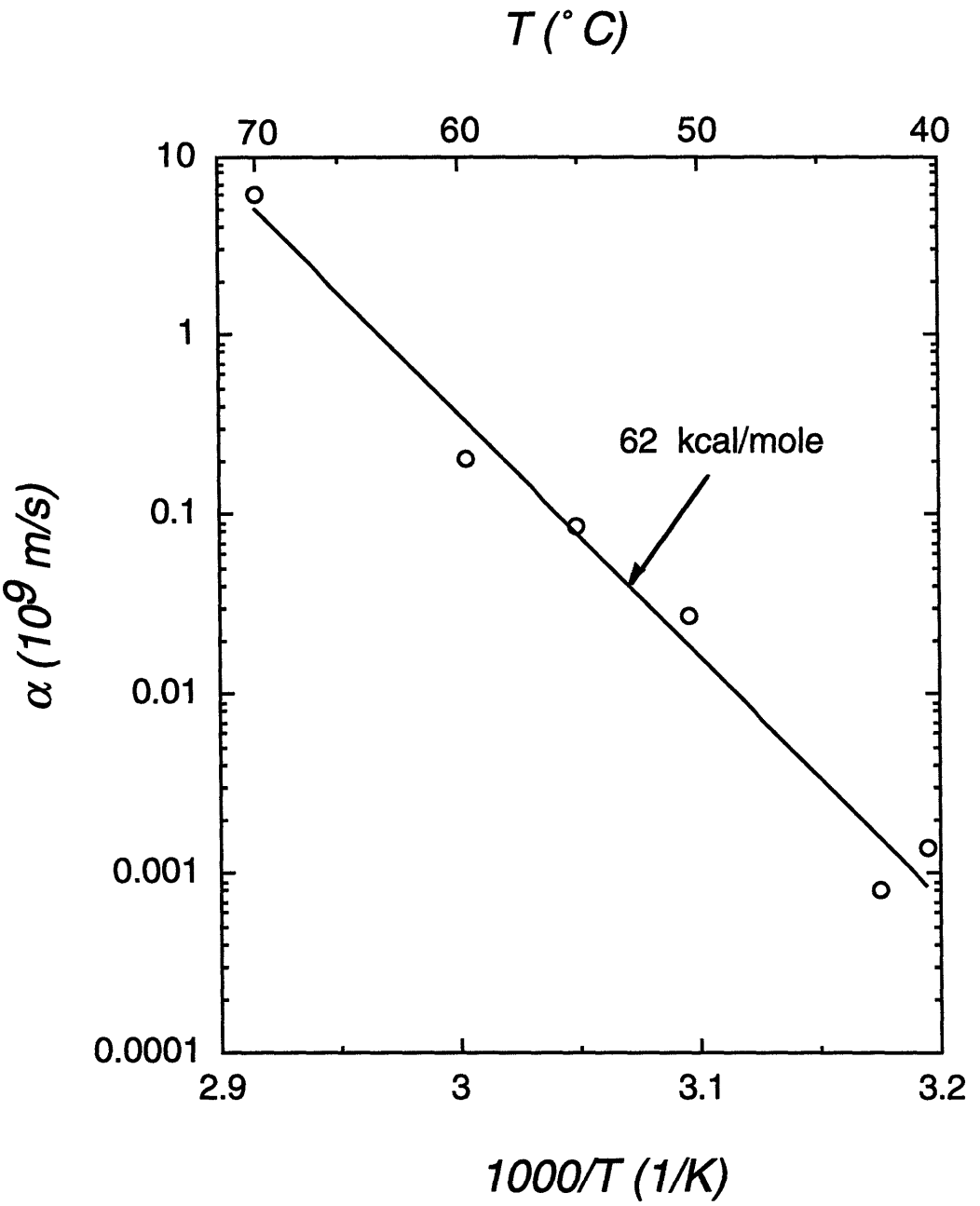

Figure 19. Arrhenius dependence of the empirical parameter α for skeletal muscle cells as shown by plotting α as a function of inverse absolute temperature.

4.11.1.1 *Arrhenius Dependence of Empirical Parameters and Permeability*

In order to determine the E_a's associated with the empirical parameters of the time-dependent solution and the permeability, Arrhenius plots were constructed by plotting the

empirical parameter α and the permeability at 63% dye leakage, respectively, on a logarithmic scale as a function of inverse absolute temperature. In Figure 19, α exhibited a general increase with increasing temperature except from 40 to 42° C. The value of α at 45° C was not included in the plot since it was negative. The slope of the line fit to the data by a least squares regression (R^2 = .979) yielded an E_a of 62 kcal/mole. In Figure 20, the permeability at 63% dye leakage also exhibited a general increase with increasing temperature again except from 40 to 42° C. The slope of the line fit to the data by a least squares regression (R^2 = .974) yielded an E_a of 34 kcal/mole.

Table 4. Results of the F-test to determine which analytical solution was statistically superior.

T(°C)	Fχ	N	χ^2_c	χ^2_{td}	P
40	29.4	35	0.037	0.004	0.001
42	6.18	35	0.018	0.014	0.05
45	25.7	35	0.009	0.002	0.001
50	46.1	51	0.184	0.011	0.001
55	38.6	43	0.068	0.004	0.001
60	24.0	27	0.018	0.0007	0.001
70	5.62	10	0.147	0.044	0.05

4.11.1.2 *Statistical Comparison of Mathematical Models*

In order to determine whether the time-dependent fit was statistically superior to the constant fit, the F-test, Eq. (11), was performed to evaluate whether an additional parameter was justified. The results of this analysis are summarized in Table 4 which

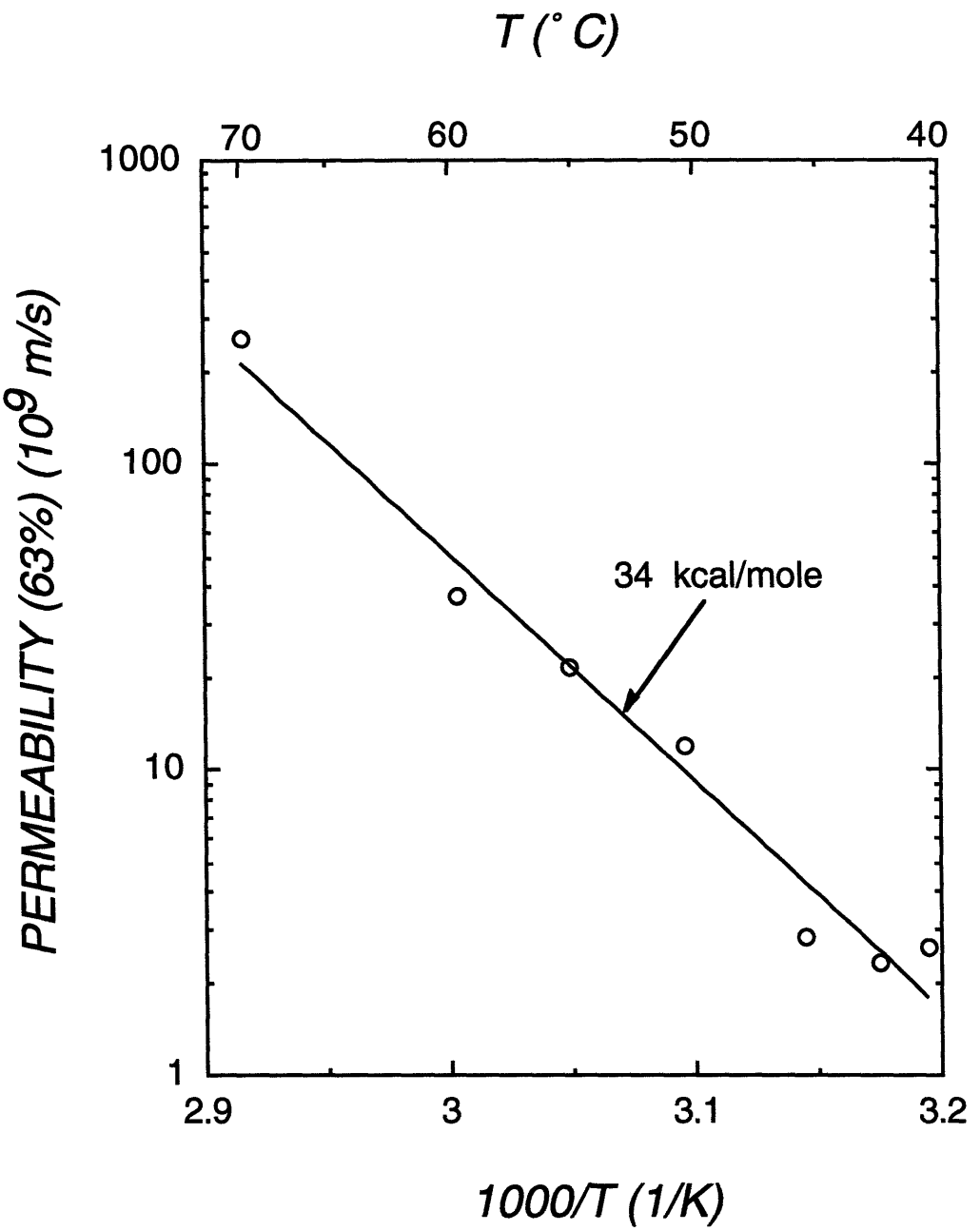

Figure 20. Arrhenius dependence of the permeability for skeletal muscle cells as shown by plotting the permeability at 63% calcein leakage as a function of inverse absolute temperature.

show the probability of error (P value) as a function of temperature. If the P value is ≤ .05, the more likely the time-dependent fit is statistically superior. Based on the P values, the time-dependent fit was indeed statistically superior to the constant fit for all supraphysiological temperatures.

4.11.1.3 *Application of Time-Dependent Solution in Other Thermal Damage Studies*

Because of the relative success of the time-dependent solution, Eq. (10), in accurately predicting the kinetics of calcein dye leakage from skeletal muscle cells, this model was fit to similar kinetic leakage curves from other thermal damage studies with other cell types. In Figure 21A, B, Eq. (10) was fit to calcein leakage curves from 3T3 mouse fibroblasts exposed to 40-70° C obtained from Bischof *et al.*[19] The model successfully describes the kinetics of calcein leakage with both qualitative accuracy as shown by the curves themselves and quantitative accuracy as shown by the R values in Table 5 with the lowest R value being 0.96322 at 70° C. The α values for the 3T3 fits are shown in Table 5 and discussed in detail in Bischof *et al.*[19]

In Figure 22A, B, the model slightly modified was fit to hemoglobin leakage curves from human erythrocytes exposed to 47.5-54.5° C obtained from Lepock *et al.*[49] The modification involved setting $\beta = 0$ given the relatively large size (an ellipsoid measuring approximately 64 x 55 x 50 Å) and large mass (64-68 kDa) of hemoglobin,[81] and therefore, relatively low initial permeability. The model again showed success in predicting the kinetics of hemoglobin leakage. The R values shown in Table 5 were relatively low from 47.5-50.5° C ranging from 0.94596 to 0.96565 but increased from 51.6-54.5° C. The general trend of α shown in Table 5 was an increase with increasing temperature from a low of 0.492×10^{14} m/s^2 at 47.5° C to a high of 60.1×10^{14} m/s^2 at 53.5° C with the only exception being a decrease from 53.5-54.5° C.

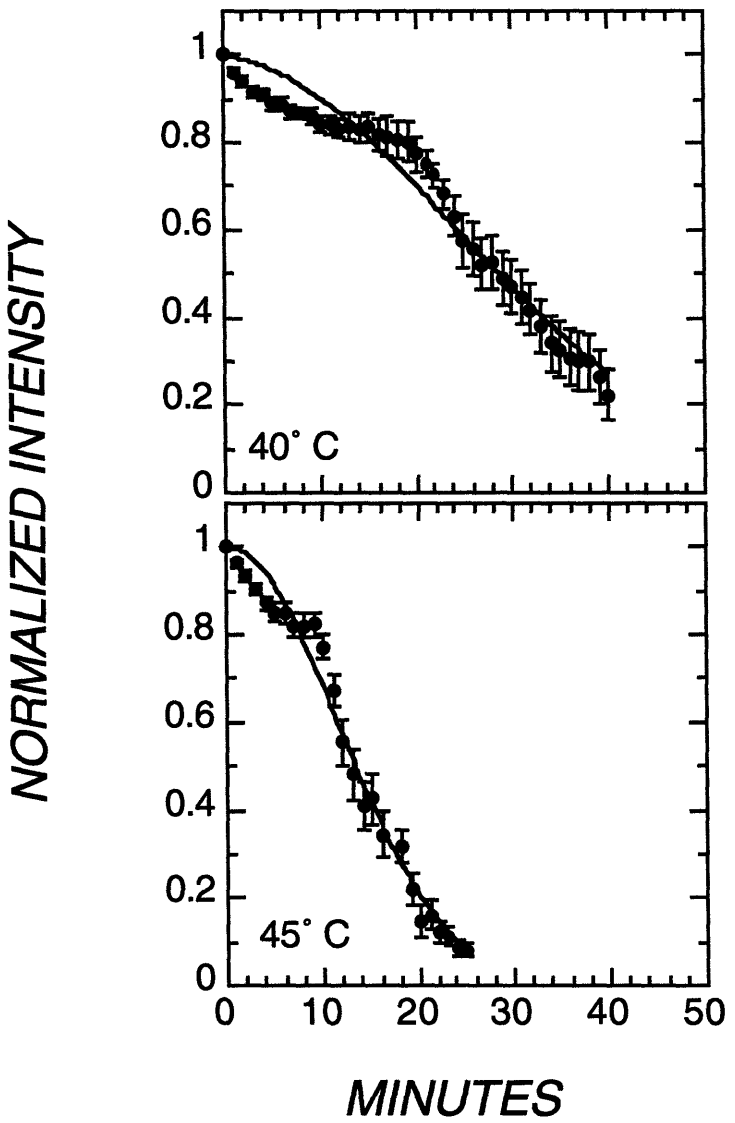

Figure 21A. Curve fit of Eq. (10) to calcein leakage curves of 3T3 mouse fibroblasts exposed to 40 and 45° C. Error bars represent the SEM.

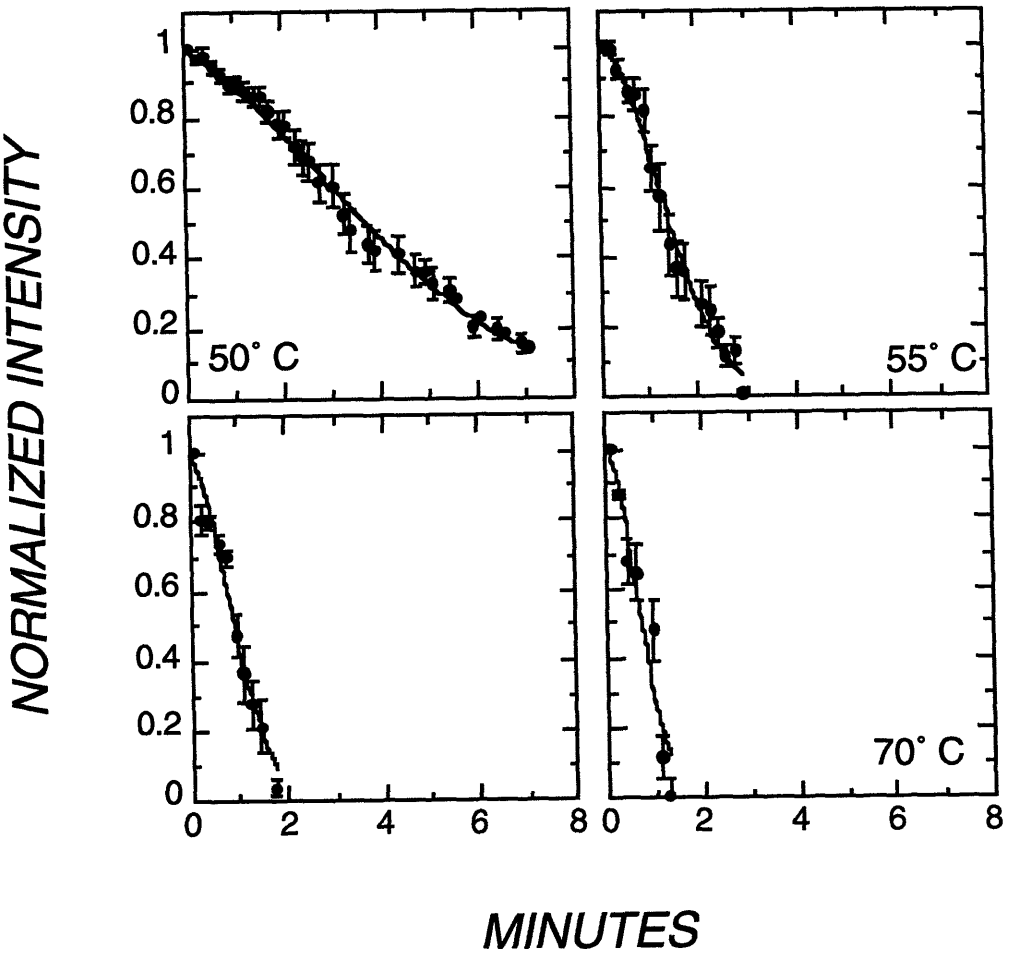

Figure 21B. Curve fit of Eq. (10) to calcein leakage curves of 3T3 mouse fibroblasts exposed to temperatures from 50-70° C. Error bars represent the SEM.

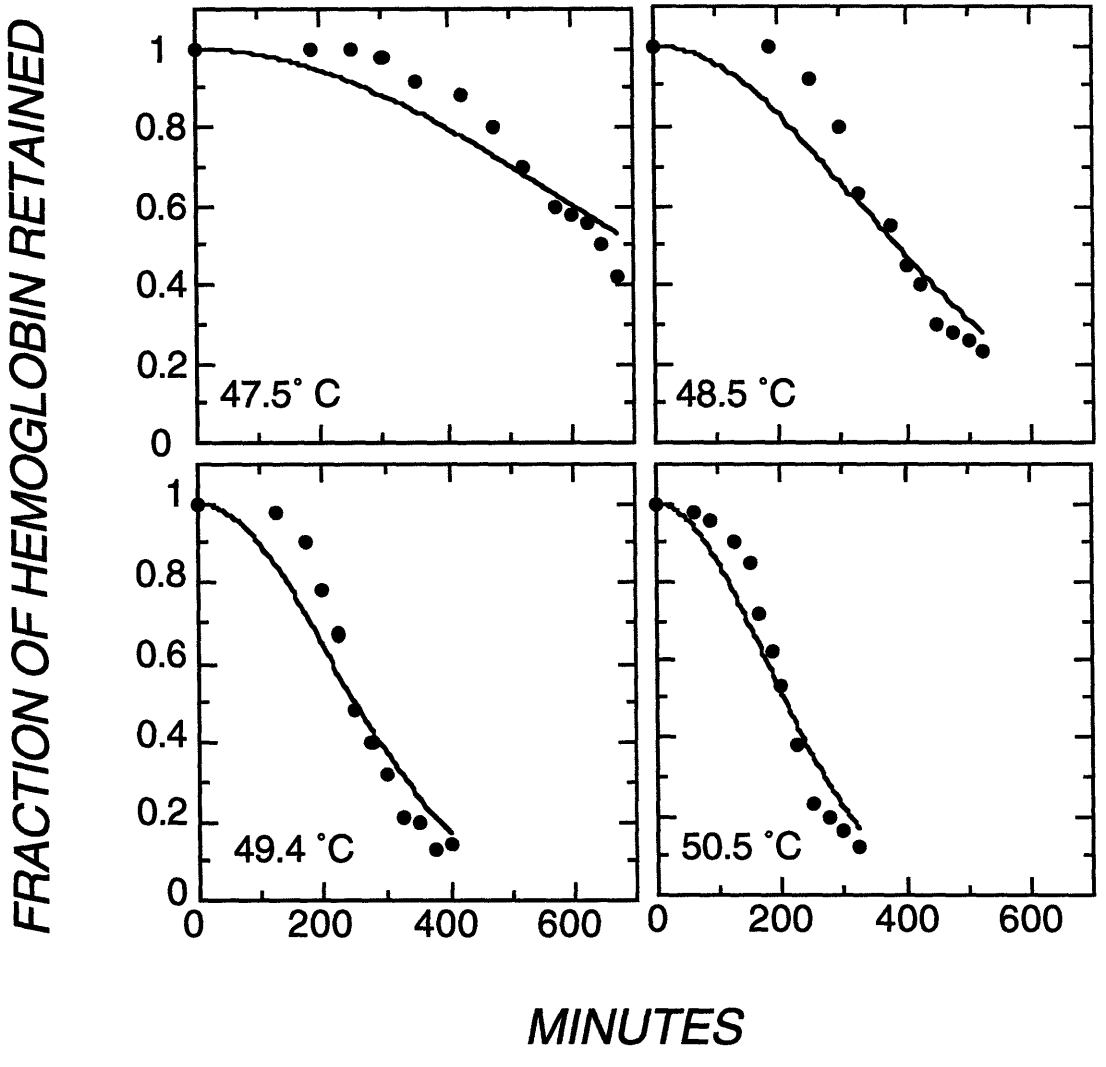

Figure 22A. Curve fit of Eq. (10) to hemoglobin leakage curves of human erythrocytes exposed to temperatures from 47.5-50.5° C. Error bars represent the SEM.

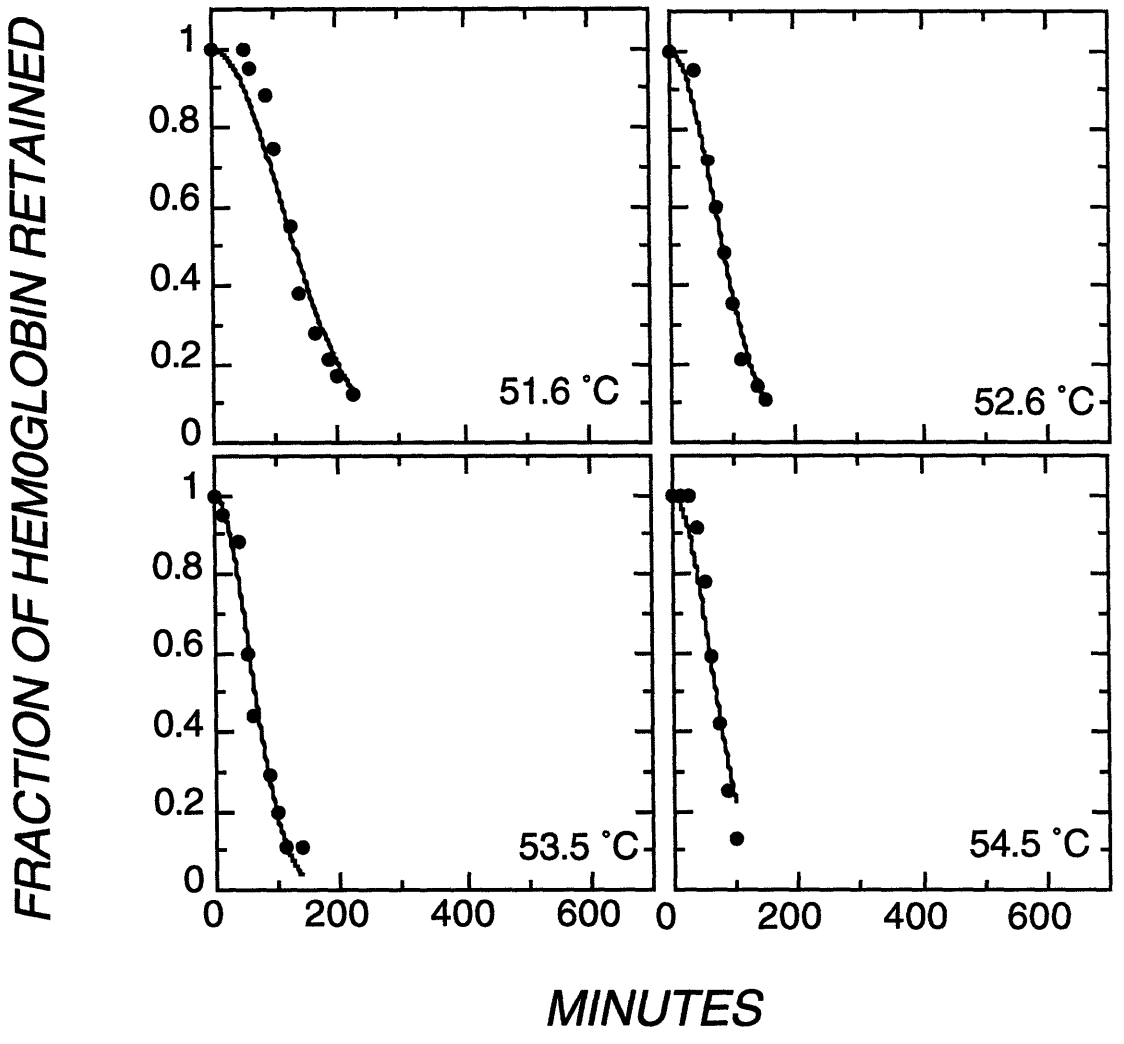

Figure 22B. Curve fit of Eq. (10) to hemoglobin leakage curves of human erythrocytes exposed to temperatures from 51.6-54.5° C. Error bars represent the SEM.

Table 5. R and α values for the time-dependent fits for 3T3 mouse fibroblasts and human erythrocytes.

T(° C)	R_{td} (3T3)	$\alpha(10^9$ m/s$^2)$	T(° C)	R_{td} (HE)	$\alpha(10^{14}$ m/s$^2)$
40	0.98077	0.002	47.5	0.94596	0.492
45	0.99044	0.011	48.5	0.95012	1.63
50	0.99623	0.077	49.4	0.95499	3.86
55	0.99245	0.863	50.5	0.96565	5.85
60	0.98481	3.179	51.6	0.97572	14
70	0.96322	1.782	52.6	0.99148	34.9
			53.5	0.98891	60.1
			54.5	0.97644	52.3

4.11.1.4 *Arrhenius Dependence of the Permeability Coefficients*

In order to determine the E_a's associated with α and the permeability, Arrhenius plots were constructed by plotting α and the permeability at 63% hemoglobin leakage, respectively, on a logarithmic scale as a function of inverse absolute temperature. In Figure 23, α exhibited a general increase with increasing temperature except from 53.5 to 54.5° C. The slope of the line fit to the data by a least squares regression (R^2 = .963) yielded an E_a of 137 kcal/mole. In Figure 24, the permeability at 63% hemoglobin leakage also exhibited a general increase with increasing temperature again except from 53.5 to 54.5° C. The slope of the line fit to the data by a least squares regression (R^2 = .957) yielded an E_a of 76 kcal/mole. The E_a values for α and the permeability at the time of 63% calcein leakage from 3T3 cells are discussed in detail in Bischof *et al.*[19] Briefly, the values are 70 and 34 kcal/mole for α and the permeability, respectively.

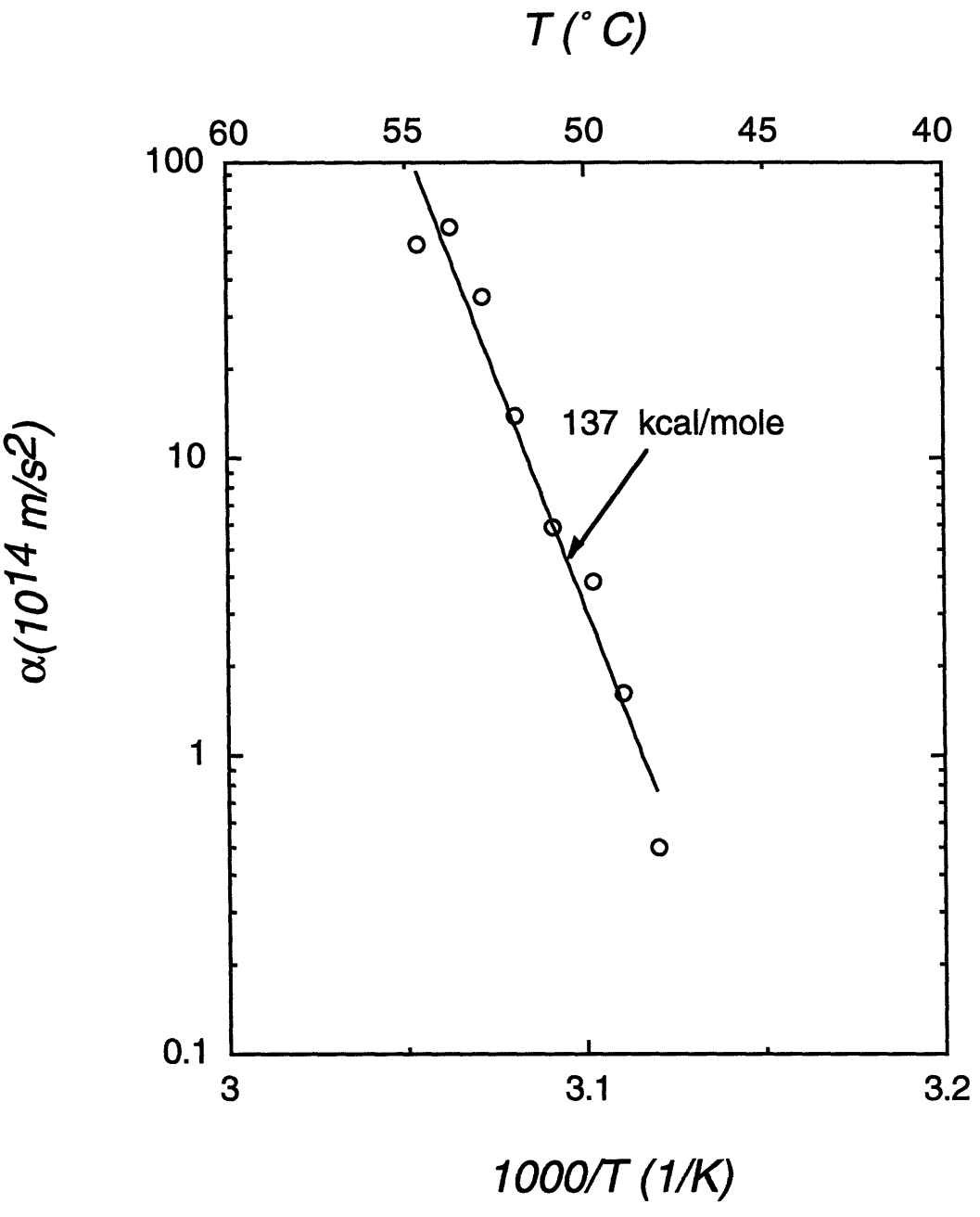

Figure 23. Arrhenius dependence of the empirical parameter α for human erythrocytes as shown by plotting α as a function of inverse absolute temperature.

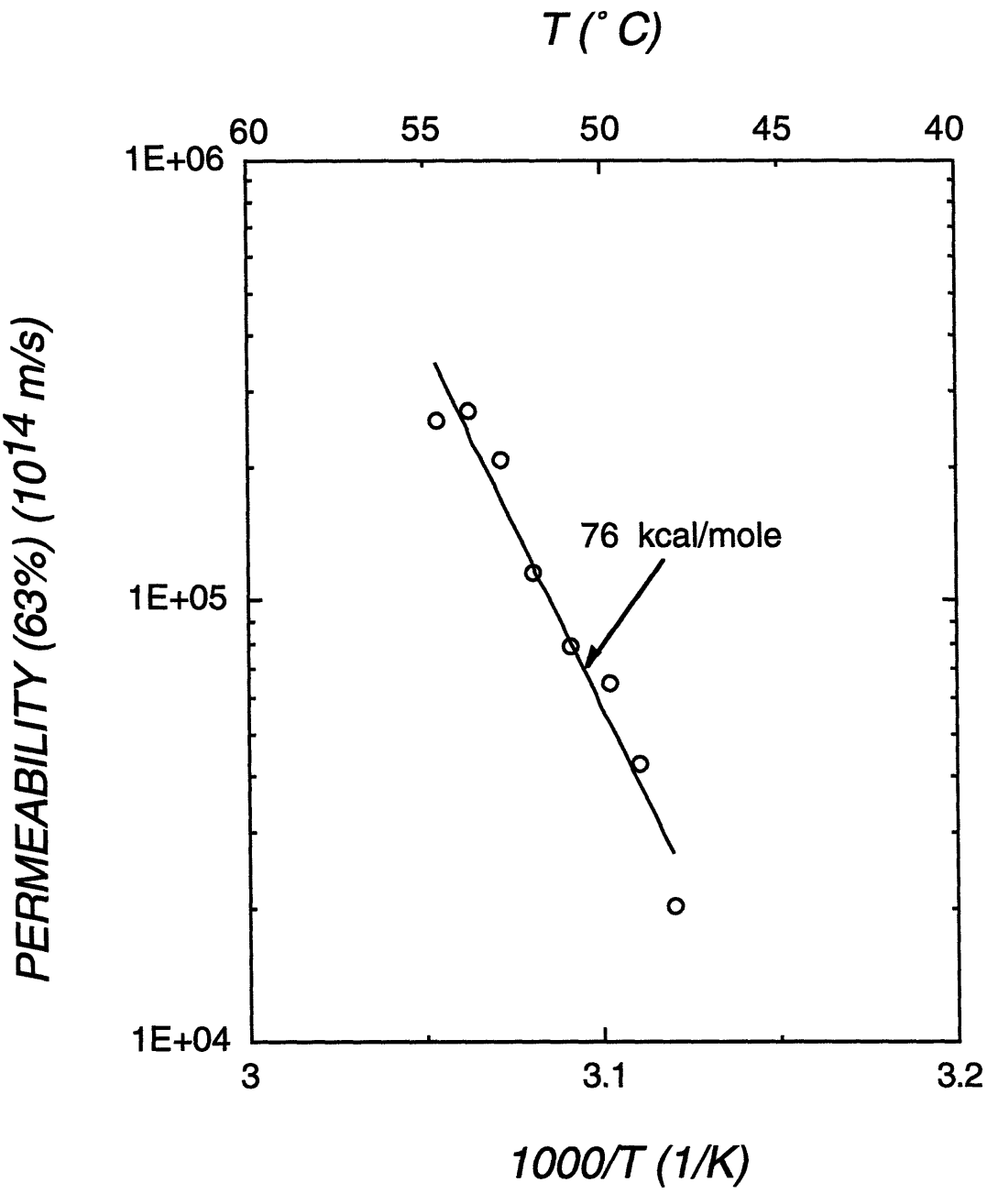

Figure 24. Arrhenius dependence of the permeability for human erythrocytes as shown by plotting the permeability at 63% hemoglobin leakage as a function of inverse absolute temperature.

4.11.2 *Model Assuming a First Order Reaction in the Membrane Porosity*

Eq. (15) formulated by assuming that the plasma membrane porosity was altered during high temperature exposure in a kinetic scheme typical of a first order chemical was fit to the calcein leakage curves for skeletal muscle cells exposed to 40-70° C. The resultant curve fits are shown in Figure 25A, B, and the R and k_1 values for each temperature are shown in Table 6. The R values were relatively high (≥ 0.978) for all temperatures except 42 and 45° C where the values were 0.89633 and 0.79594, respectively. The model accurately characterized the kinetics of calcein leakage at 40° C and from 50-70° C. Despite a relatively low R value at 42° C, the shape of the curve fit corresponded qualitatively well except for the initial 20% leakage. At 45° C, the model did not predict very well the calcein leakage kinetics. The k_1 values consistently increased with temperature as should be expected from a low of 1.943×10^{-6} s^{-1} at 40° C to a high of 8.486×10^{-3} s^{-1} at 70° C.

Table 6. R and k_1 values for the fits of Eq. (15) to the calcein leakage curves from skeletal muscle cells.

T(° C)	R	$k_1(s^{-1})$
40	0.98283	1.943×10^{-6}
42	0.89633	4.272×10^{-6}
45	0.79594	1.222×10^{-5}
50	0.99498	2.689×10^{-5}
55	0.98878	1.715×10^{-4}
60	0.98205	6.936×10^{-4}
70	0.97859	8.486×10^{-3}

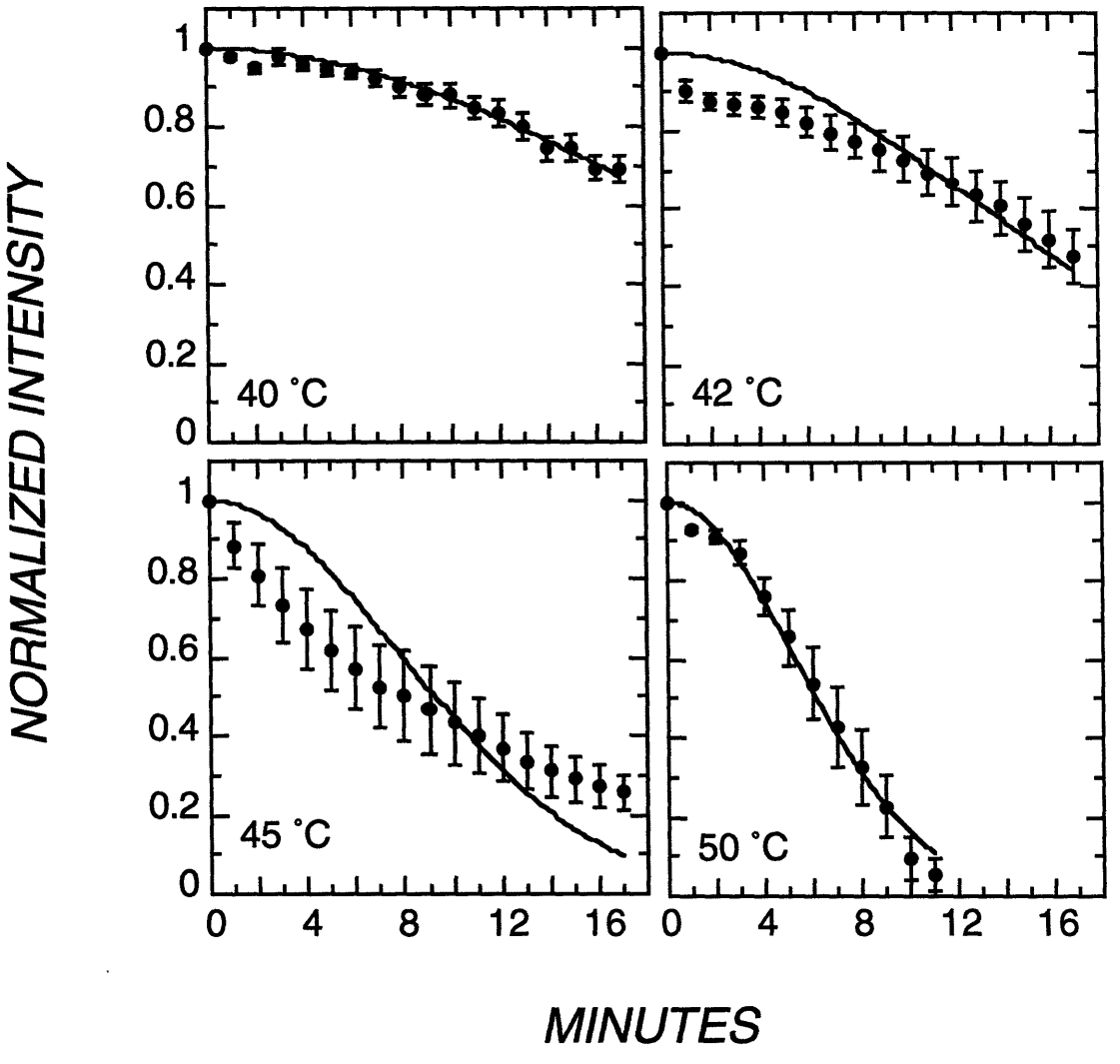

Figure 25A. Curve fit of Eq. (15) to calcein leakage curves of skeletal muscle cells exposed to temperatures from 40-50° C. Error bars represent the SEM.

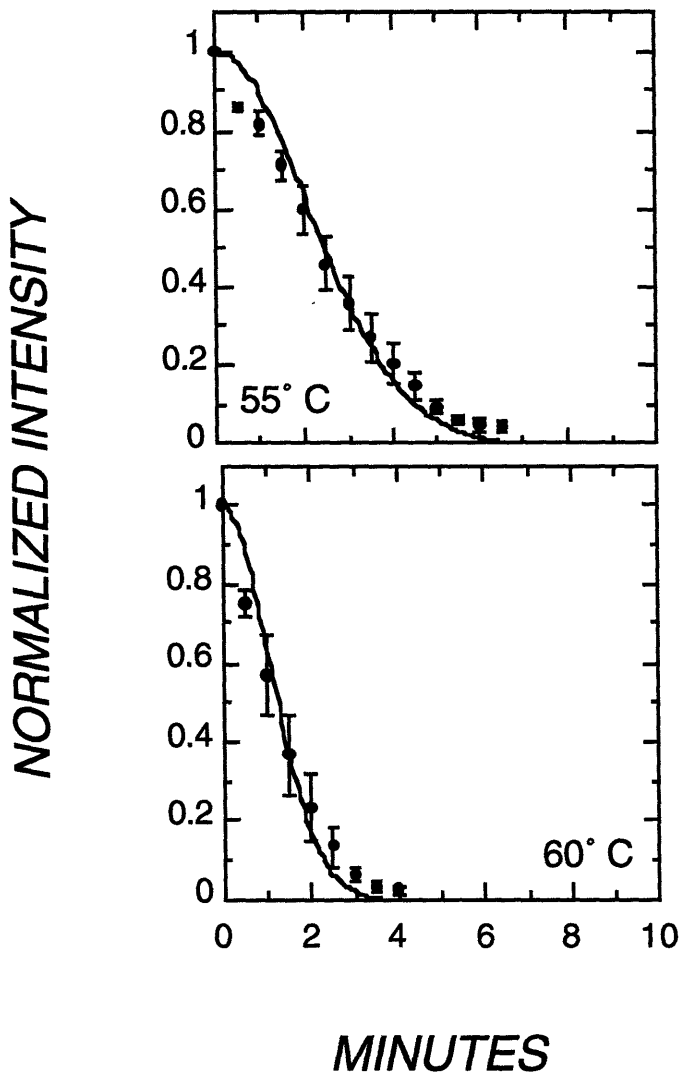

Figure 25B. Curve fit of Eq. (15) to calcein leakage curves of skeletal muscle cells exposed to 55 and 60° C. Error bars represent the SEM.

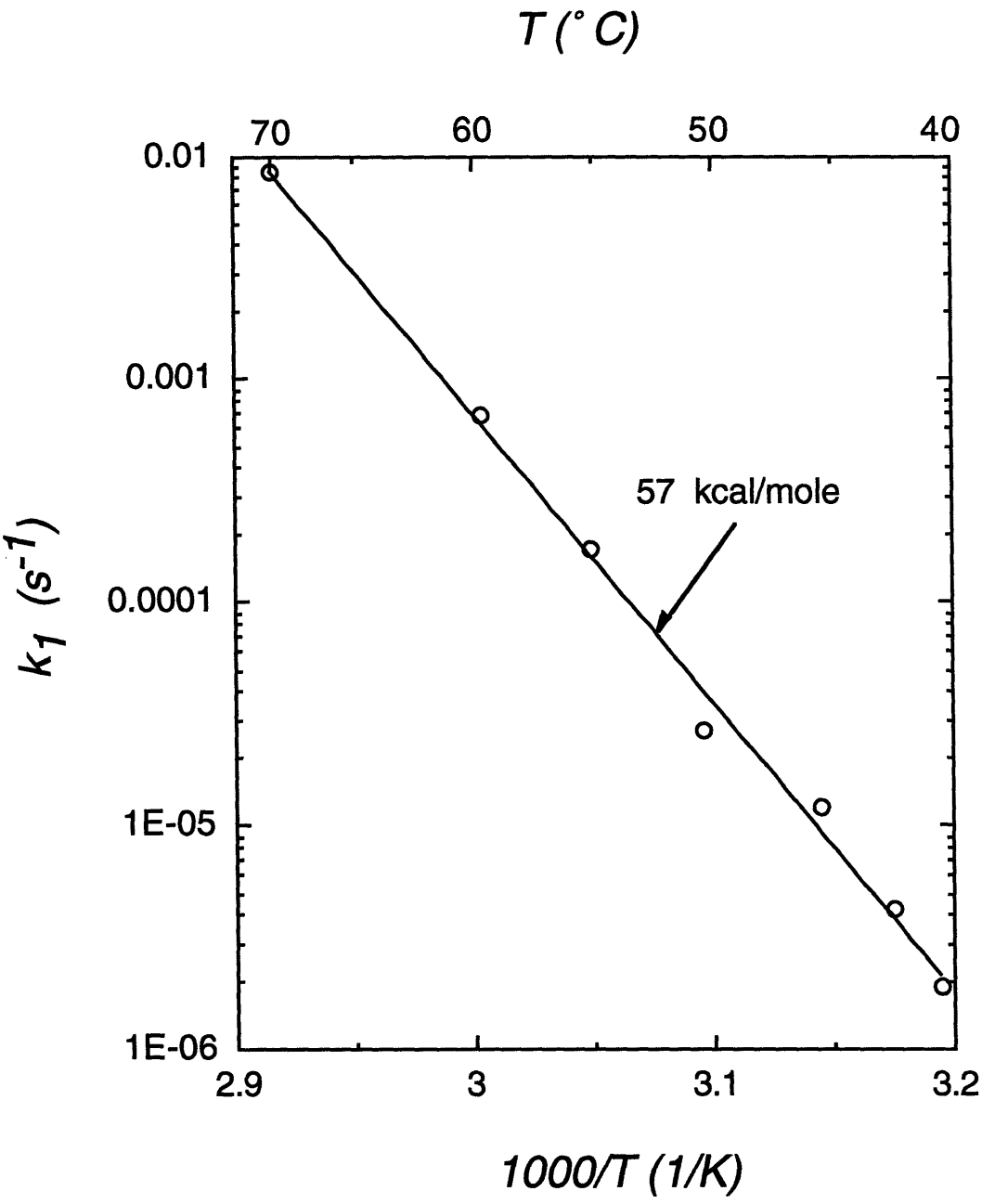

Figure 26. Arrhenius dependence of the rate constant k_1 for skeletal muscle cells as shown by plotting k_1 as a function of inverse absolute temperature.

4.11.2.1 *Arrhenius Dependence of k_1*

In order to determine the E_a associated with k_1, an Arrhenius plot shown in Figure 26 was constructed by plotting k_1 on a logarithmic scale as a function of inverse absolute temperature. The slope of the line fit to the data by a least squares regression ($R^2 = .995$) yielded an E_a of 57 kcal/mole.

Chapter 5. Discussion

This study has shown that the plasma membrane integrity is compromised in skeletal muscle cells during exposure to elevated temperatures and that P188 was effective in minimizing the extent of this membrane injury. These two major findings will be discussed in this chapter. A novel thermal microscopy system was developed and employed to quantify dynamic changes in plasma membrane permeability in skeletal muscle cells.

5.1 Thermal Damage to the Plasma Membrane

Compromised plasma membrane integrity at elevated temperatures was evidenced by supraphysiological leakage of the membrane integrity probe calcein. The calcein leakage curves indicated that the kinetics and extent of plasma membrane damage increased as temperature increased. To assess the possible mechanisms of damage, an Arrhenius plot was constructed to determine the activation energy, E_a, which indicates the amount of work required to satisfy an arbitrarily specified damage criterion which, for this study, was the time for 40% dye leakage. The E_a of 32.9 kcal/mole (Figure 13) obtained in this study compares favorably with those obtained in other cell types using various damage criteria. The E_a of 32.9 kcal/mole obtained in skeletal muscles (without P188) is of the same order of magnitude as the E_a of 38 kcal/mole obtained by Bischof *et al.*[19] for 63% calcein dye leakage from 3T3 fibroblasts exposed to temperatures between 40 and 70°C, and 58.8 kcal/mole obtained by Gaylor *et al.*[17] for 5% carboxyfluorescein leakage from skeletal muscle cells exposed to temperatures ranging from 45 to 60° C. The E_a value of 32.9 kcal/mole is also of the same order of magnitude as the E_a's of 59.5 kcal/mole obtained by Moussa *et al.*[13] for blister formation in HeLa S-3 fibroblasts, 30 kcal/mole obtained by Gershfeld and Murayama[14] for 1% hemolysis of human erythrocytes, 46.3 kcal/mole obtained by Moussa *et al.*[15] for 5% hemolysis of human erythrocytes, and 50.4 kcal/mole

obtained by Lloyd *et al.*[16] for ghosting of human erythrocytes. The temperature ranges for these studies varied but, in general, overlapped with our temperature range of 40 to 60° C. Since no apparent break point was present in the Arrhenius plot for 40% calcein leakage from skeletal muscle cells, it is possible that the same mechanism of damage acted throughout the entire temperature range. E_a values ≥ 50 kcal/mole may indicate damage to the phospholipid bilayer as well as membrane proteins. Lepock *et al.*[49] has shown that membrane protein denaturation takes place however damaging the phospholipid bilayer requires less energy. Indirect evidence based on the effectiveness of P188 in this study and in arresting carboxyfluorescein leakage from electroporated skeletal muscle cells[41] suggests that the majority of the damage is caused by disruption of the phospholipid bilayer. However, it is noteworthy to mention that temperature affects the entire cell and not just the plasma membrane so the precise nature of the damage measured may not be solely a membrane event.

To further understand the dynamics of membrane permeability changes at elevated temperatures, the calcein leakage models (i.e. constant and time-dependent permeability) were fit concurrently to the calcein leakage curves from 40 to 60° C (Figure 21A, B). Based on the qualitatively better accuracy, higher R values, and statistical superiority of Eq. (10), the plasma membrane permeability is most likely being degraded in a time-dependent manner. The finding is novel and exciting since other studies investigating thermal damage to the plasma membrane have assumed the permeability to be constant. A time-dependent permeability also is intuitively logical since prolonged exposure to high temperatures would ultimately lead to cell lysis and a permeability that approaches ∞.

In order to better understand the time-dependent plasma membrane permeability, the two empirical parameters, α and ß, which physically represent the rate of change of the permeability and the initial permeability, were analyzed. An E_a value of 62 kcal/mole was

obtained in the Arrhenius plot of α values (Figure 22). This E_a value compares favorably with the E_a values presented in the previous paragraph and to the E_a of 70 kcal/mole for α for 3T3 mouse fibroblasts in the range of 40-55° C.[19] This E_a however is not as straightforward as to interpret as the other E_a's which generally reflected the work required to satisfy arbitrarily chosen damage criteria. A possible meaning of this E_a may be the work required to alter the plasma membrane such that the permeability exhibits time dependence. An E_a value of 34 kcal/mole was obtained in the Arrhenius plot of the permeability values at the time of 63% calcein leakage (Figure 23). This value compares well to the E_a value of 42 kcal/mole obtained by Cravalho *et al.*[18] which assumed a solely temperature dependent permeability. This 34 kcal/mole value for the permeability is in close quantitative agreement with the 32.9 kcal/mole value 40% calcein leakage and matches the E_a of 34 kcal/mole for the permeability at the time of 63% leakage obtained for 3T3 fibroblasts in the range of 40-55° C.[19] The E_a value of 34 kcal/mole probably represents the work needed to sufficiently permeabilize the membrane to permit 63% dye leakage.

Given the success of Eq. (10) in accurately predicting the kinetics of plasma membrane degradation for skeletal muscle cells, this model was fit to calcein leakage from 3T3 mouse fibroblasts[19] (Figure 24A, B) and hemoglobin leakage from human erythrocytes[49] (Figure 25A, B). All the fits for the 3T3 fibroblasts and human erythrocytes were qualitatively successful and agreed well with the data. An E_a value of 76 kcal/mole was obtained in the Arrhenius plot of the permeability values at the time of 63% hemoglobin leakage (Figure 27). This value is also more than twice the E_a value for permeability of skeletal muscle cells since hemoglobin is larger (an ellipsoid measuring approximately 64 x 55 x 50Å) and heavier (64-68 kDa) than calcein (a sphere with an estimated diameter of 28 Å and weighing 623 Da). This value is of the same order magnitude as the E_a values of 30 kcal/mole obtained by Gershfeld and Murayama[14] for 1% hemolysis of human

erythrocytes, 46.3 kcal/mole obtained by Moussa *et al.*[15] for 5% hemolysis of human erythrocytes, and agrees well with 72.4±5.2 kcal/mole obtained by Lepock *et al.*[49] for hemoglobin leakage from human erythrocytes. The success of Eq. (10) for these other cell types definitely suggests a time-dependent thermal degradation of the plasma membrane in 3T3 fibroblasts and human erythrocytes. This analysis also indicates that, despite the kinetic variations and various membrane integrity probes, the process of thermal degradation of the plasma membrane in various cell types is qualitatively similar and may involve the same types of mechanisms of damage.

The success of the time-dependent permeability assumption strongly suggested a time-dependent thermal degradation of the plasma membrane. Given the time-dependent assumption was empirical, a kinetic model describing the time-dependency of the plasma membrane permeability was formulated and incorporated into the two-compartment diffusion model to obtain the analytical solution of Eq. (15). This model only employed one parameter, instead of two as Eq. (10), for the curve fit since the initial porosity, p_o, value was fixed at 1×10^{-6} as described in Chapter 3. The model was qualitatively successful at all temperatures except 45° C where the observed exponential calcein leakage differed markedly from all other temperatures. An Arrhenius plot of the parameter k_1 (Figure 29) yielded an E_a value of 57 kcal/mole. This value probably represents the amount of energy needed to effect a time-dependent increase in the porosity. The success of this model for most temperatures further strengthens the hypothesis of time-dependent thermal degradation of the plasma membrane. Given the success of Eq. (15) for skeletal muscle cells, it can probably be successfully employed for 3T3 fibroblasts and human erythrocytes but this further analysis was not done in this study.

The experimental and subsequent analytical results strongly suggest that the plasma membrane was a specific site of thermal damage and was being thermally degraded in a

time-dependent manner. The precise nature of this damage and the mechanisms which mediate this damage are however still unclear. Based on the structure of the plasma membrane, it is proposed that time-dependent membrane permeability changes may be mediated by the following mechanisms: (1) direct disruption of the phospholipid bilayer, (2) denaturation of membrane proteins, (3) depolymerization of the cytoskeleton, and (4) activation of secondary messengers by cytoplasmic free Ca^{2+}. It is worthwhile to explore the relative likelihood and subsequent contributions of these plausible mechanisms leading to time-dependent membrane permeability.

Direct thermal disruption of the phospholipid bilayer may be driven either by the formation of microsized defects or by phase transitions from the gel to liquid crystalline state. Kashchiev and Exerowa[53] and Exerowa and Kashchiev[57] modeled thermally driven nucleation of these defects in phospholipid bilayer of the plasma membrane which augment membrane permeability. This nucleation process may be driven by vacancies or voids in the plasma membrane or by inclusion of foreign bodies and/or proteins. Wiegel[58] also modeled pore formation and the resultant pore size distribution in a pure phospholipid bilayer. Both models show a temperature dependent pore size distribution with increasing pore numbers and pore sizes as the temperature increases. The two parameters governing the thermodynamics of this defect formation process are σ, the surface tension of the membrane, and γ, the edge free energy of a pore in the phospholipid bilayer. If these two parameters could be altered in a time-dependent manner during high temperature exposure, then the defect distribution could be altered in a time-dependent manner and lead to a time-dependent permeability that accounts for the calcein leakage curves at elevated temperatures. If this is true, then the E_a measured for 40% calcein leakage, 32.9 kcal/mole, may be a reasonable estimate for hole-mediated diffusion of calcein through the plasma membrane during high temperature exposure. The E_a for pure bulk diffusion of water is 6 kcal/mole. The E_a for hole-mediated diffusion of calcein should consist of the

work required to form the hole, steric hindrance to calcein in the pore, and 6 kcal/mole for bulk diffusion. This hypothesis is further supported by an E_a of 11.9±11.7 kcal/mole obtained by Lepock *et al.*[49] for hemoglobin leakage from liposomes consisting of only erythrocyte lipids. Since these liposomes required only 11.9±11.7 kcal/mole for hemoglobin leakage, the phospholipid bilayer is more prone to damage than proteins at elevated temperatures. The values of 30-72.4 kcal/mole for hemoglobin leakage from human erythrocytes may then reflect a stabilizing effect due to membrane proteins and the cytoskeleton. Therefore, the phospholipid bilayer may the primary site of thermal damage.

Another explanation for thermal disruption of the phospholipid bilayer is a phase transition from the gel to liquid crystalline state for the phospholipid bilayer of the plasma membrane. The phospholipid bilayer has been extensively studied for augmenting permeability at high temperatures, especially near the transition from the gel to liquid crystalline state, in experimental as well as theoretical models by Kanehisa and Tsong,[59] Mantsch *et al.*,[60] Cruzeiro-Hansson *et al.*[61,62] The precise transition temperature, T_m, is unknown for skeletal muscle cells and would not be straightforward to predict since T_m depends strongly on the types of phospholipids contained in the plasma membrane.[65] T_m for a pure phospholipid bilayer or liposome tends to be very sharp; whereas, the T_m of the plasma membrane is much broader due to the presence of other constituents (e.g. proteins). Given that these transitions occur over a broad range of temperatures, it is plausible that this mechanism can account for the time-dependent permeability observed in this study. In fact, it may be a possible explanation for the exponential calcein leakage observed at 45° C. Since exponential leakage requires a constant membrane permeability, a gel to liquid crystalline transition with T_m at 45° C would occur relatively quickly and exponential calcein leakage would commence.

The denaturation of membrane proteins has also been studied for increasing permeability at high temperatures. Denatured or thermally altered membrane proteins could create hyperpermeability in the membrane by acting themselves as a site of increased transport, by increasing permeability at the interface with the phospholipid bilayer, or by activating a secondary system that leads to further membrane degradation. Several protein phase transitions have been reported in erythrocyte plasma membranes using DSC in the range of 40-80 °C.[64,66-68] The E_a's for 40% calcein leakage obtained in this study and those obtained in other thermal damage studies for various damage criteria are consistent with the energy for protein denaturation.[18,67] It is therefore reasonable to assume some proteins in plasma membrane of skeletal muscle cells were denatured during exposure at 40-70° C. The kinetics of protein denaturation may progress slowly (i.e. in a time-dependent manner) at lower supraphysiological temperatures and may occur rapidly at higher temperatures. A time-dependent denaturation of membrane proteins would certainly lead to a time-dependent permeability that accounts for the dye leakage curves from 40-42° C and 50-70° C.

A number of studies have documented the disruption and collapse of cytoskeletal proteins following heat shock. Welch and Suhan[70] show a collapse of the vimentin containing intermediate filaments around the nucleus, along with considerable alterations in the structural integrity and relaxation state of the nucleoli after a heat shock to rat fibroblasts. Coss *et al.*[71] investigated the damage and reassembly of microtubules in heat stressed CHO cells, finding that the severity of disruption and disassembly correlated directly with the thermal dose. Roti Roti and Laszlo[72] proposed the following sequential model for cellular injury: (1) disruption of critical membrane structures, presumably the plasma membrane cytoskeletal attachment points; (2) collapse of the cytoskeleton towards the nucleus; (3) adsorption of protein onto nuclear matrix; and (4) disruption of nuclear and metabolic functions. Spectrin, the main cytoskeletal protein of erythrocytes, has been shown to denature at temperatures above 40° C.[69,74,75] If the major cytoskeletal proteins

in skeletal muscle cells also denature above 40° C, then it is possible that a hyperpermeability state in the plasma membrane will be imposed by damaging the attachment sites on the plasma membrane. Also, the denatured cytoskeletal proteins may activate secondary messenger systems to effect more membrane degradation. Since these effects would be time dependent, the propagation of cytoskeletal damage to the plasma membrane would also be time dependent which could then account for the calcein leakage curves at all temperatures except 45° C. If cytoskeletal depolymerization were a sudden event leading to a constant, hyperpermeable state, then this mechanism could explain the exponential calcein leakage at 45° C.

Finally, thermal degradation of the plasma membrane (i.e. either the phospholipid bilayer or membrane proteins) can occur indirectly by the activation of phospholipases, proteases, and kinases through a Ca^{2+} modulated secondary messenger system.[73,76,77] The Ca^{2+} secondary messenger system may additionally depolymerize cytoskeletal elements instead of solely the plasma membrane. Thermal damage to the plasma membrane has been observed to lead to an increase in intracellular-free Ca^{2+} and cause stimulation of phosphoinositide turnover in HA1 cells.[78,79] The expression of these degradative enzymes is a kinetic process and so their effects on the plasma membrane should show time dependence. Therefore this mechanism may explain the calcein leakage curves effected by a time-dependent hyperpermeability in the plasma membrane.

The mechanisms proposed above may act in concert to effect thermal degradation of the plasma membrane. Also, one mechanism may increase the likelihood of damage via another mechanism. Clearly, each mechanism needs to be separately investigated to determine their relative effects and ranges of temperature in which each may be more prevalent. This will greatly aid understanding of the thermal membrane damage process and in developing methods for minimizing this damage.

5.2 Effectiveness of Poloxamer 188

The results of this study indicate that P188 was effective in arresting transmembrane calcein leakage from thermally damaged skeletal muscle cells below 45° C and in retarding transmembrane calcein leakage above 45° C. The apparent threshold for P188 effectiveness seemed to be 60° C since calcein leakage in the presence and absence of P188 was nearly the same. To assess the possible mechanisms of thermal damage in the presence of 10 mg/mL P188, the results with P188 from 45 to 60° C were graphed in an Arrhenius format and the E_a for the time for 40% calcein leakage was 33.2 kcal/mole. This value is in close agreement with the E_a of 32.9 kcal/mole obtained without P188. This E_a of 33.2 kcal/mole in the presence of P188 (10 mg/mL) also compares favorably with the previously mentioned E_a's from other studies. One plausible explanation is that P188 slows down calcein leakage without altering the mechanism (i.e., activation energy) of the thermal damage process.

The study with various P188 concentrations at 42, 50, and 55° C showed that P188 at 0.1-1 mg/mL was as and oftentimes more effective than 10 mg/mL; whereas, 2 mg/mL P188 was always ineffective relative to 0.1-1 mg/mL and 10 mg/mL with 0.5 mg/mL consistently being the most effective for all temperatures. The asymmety of P188 effectiveness may be explained by considering that P188 has a CMC of about 1 mg/mL at 25° C.[41] At low concentrations, P188 is thought to form unimolecular micelles in which a single P188 molecule wraps around itself[33] as shown in Figure 28A. At higher concentrations, it has been reported to form micelles consisting of 2-8 molecules[34,35] as shown in Figure 28B at 0.1 to 0.2 wt % however it is now thought that these molecules aggregate to form micelles over a range of concentrations near 1 mg/mL leading to a saturation point.[36] Thus, from 0.1-1 mg/mL P188, most P188 molecules probably interacted individually and not as micelles with the plasma membrane as depicted in Figure

27. At 10 mg/mL, both micelles and individual molecules of P188 probably interacted with the membrane . It is unclear which of the two forms were more prevalent since the actual CMC of P188 at elevated temperatures is unknown. At 2 mg/mL, most P188 molecules probably interacted as micelles with the plasma membrane. Hence, this asymmetry of P188 effectiveness may result from a dominant contribution by individual molecules at 0.1-1 mg/mL, micelles at 2 mg/mL, and a combination of both at 10 mg/mL. It is also possible that individual molecules help early on; whereas, micelles may take longer to interact with the membrane. Clearly, further studies should investigate mechanisms of P188-membrane interaction, either as micelles or individual molecules during thermal damage to the plasma membrane. This information will enhance understanding of the fundamental mechanisms and aid in designing better surfactants.

The specificity of P188 action which is not inherent to any high molecular weight molecule was demonstrated by the ineffectiveness of neutral dextran (11 kDa) at 0.5, 2, and 10 mg/mL at 45° C. This finding compares favorably to the results obtained by Lee *et al.*[41] which demonstrated the superiority of P188 over dextran in arresting dye leakage after membrane electroporation. Experiments utilizing PEG (20 mg/mL) and PPG (10 mg/mL), which represent the hydrophilic and hydrophobic constituents of P188, at 45° C have demonstrated these constituents to be ineffective compared to P188. This suggests that both the hydrophilic and hydrophobic portions of P188 must somehow function together to arrest calcein leakage.

The results with dextran indicated that P188 did not simply slow down calcein leakage by reducing the diffusivity of calcein. The similarity of the E_a's in the presence and absence of P188 demonstrated that, although P188 altered the kinetics of calcein leakage, it did not alter the mechanism of the thermal damage process in the plasma membrane. These two results suggest that some type of P188-plasma membrane interaction probably occurred so

P188 may have sealed thermally induced plasma membrane defects. This hypothesis is indirectly supported by the observation that the physical manifestations of electrically induced membrane damage have been shown to be the formation of aqueous pores.[9,17,53] The recently demonstrated effectiveness of P188 by Lee *et al.*[41] in sealing electropermeabilized skeletal muscle membranes suggests P188 may be acting as a sealant of membrane pores in both electrical and thermal damage. This mechanism of action is depicted in Figure 27 where an individual P188 molecule aligns its hydrophobic core with the plasma membrane defect and the flexible hydrophilic tails oppose the aqueous extracellular media. The now sealed plasma membrane arrests calcein leakage. Since the results of the P188 concentration studies showed little effectiveness just above the CMC at 2 mg/mL, it is likely P188 interacted with the thermally damaged plasma membrane as individual molecules and not as micelles. Given the relatively large size of P188 and the similarity in the E_a's in the presence and absence of P188, it probably inserts neither into the defect, provided 30 Å is a typical defect size, nor the cell. It is believed that P188 is adsorbed to the surface and held in place by hydrophobic interactions and hydrophilic interactions with the extracellular media may stabilize this adsorption provided the hydrophilic tails are not too long in which case P188 may be desorbed due to significant hydrogen bonding between extracellular water molecules and the hydrophilic tails of P188.[56] Fluorescently labeled or radioactively labeled ^{14}C P188 should provide qualitative information regarding the presence of P188 at the thermally damaged plasma membrane, within the plasma membrane, or within the cell.

Experiments utilizing the poloxamers P238, P338, and P407 at 10 mg/mL at 45° C have shown these poloxamers to be as effective as P188. These results suggest that relative hydrophilic/hydrophobic content and molecular weight does not significantly alter the effectiveness of these block copolymers. It also suggests that these poloxamers function by a similar mechanism. However, given that the hydrophobic core lengths of all the

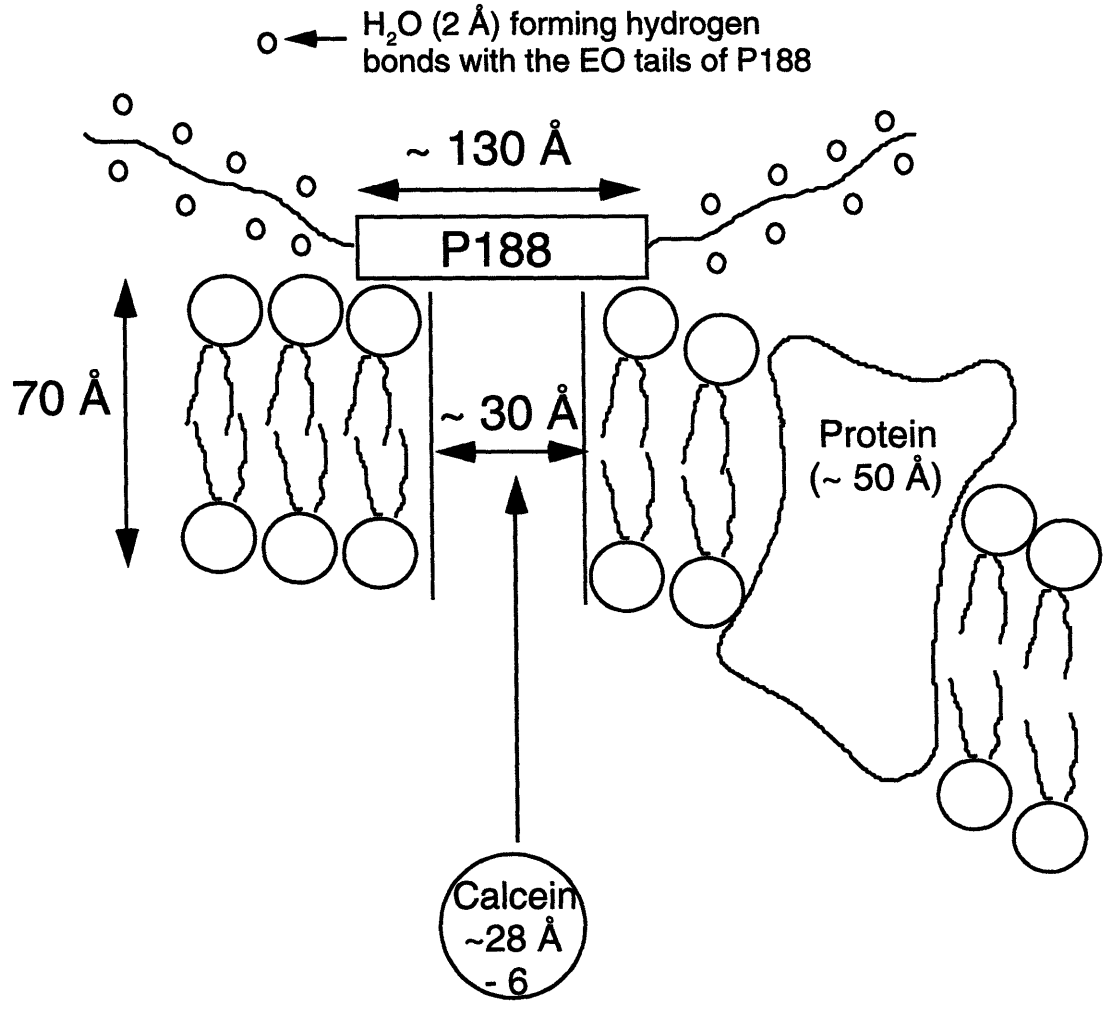

Figure 27. Representation of a possible mechanism of action of P188.

poloxamers used in the study were ≥ 130 Å and calcein has an estimated diameter of 28 Å, this may explain why all the poloxamers worked equally well. It would be informative to utilize a poloxamer with a hydrophobic core length < 28 Å in a future study to obtain evidence that these poloxamers seal defects by hydrophobic interactions.

It is noteworthy to mention that, in this study, cells were exposed to P188 just prior to the thermal insult. Obviously, this is not the case for the clinical application, and further

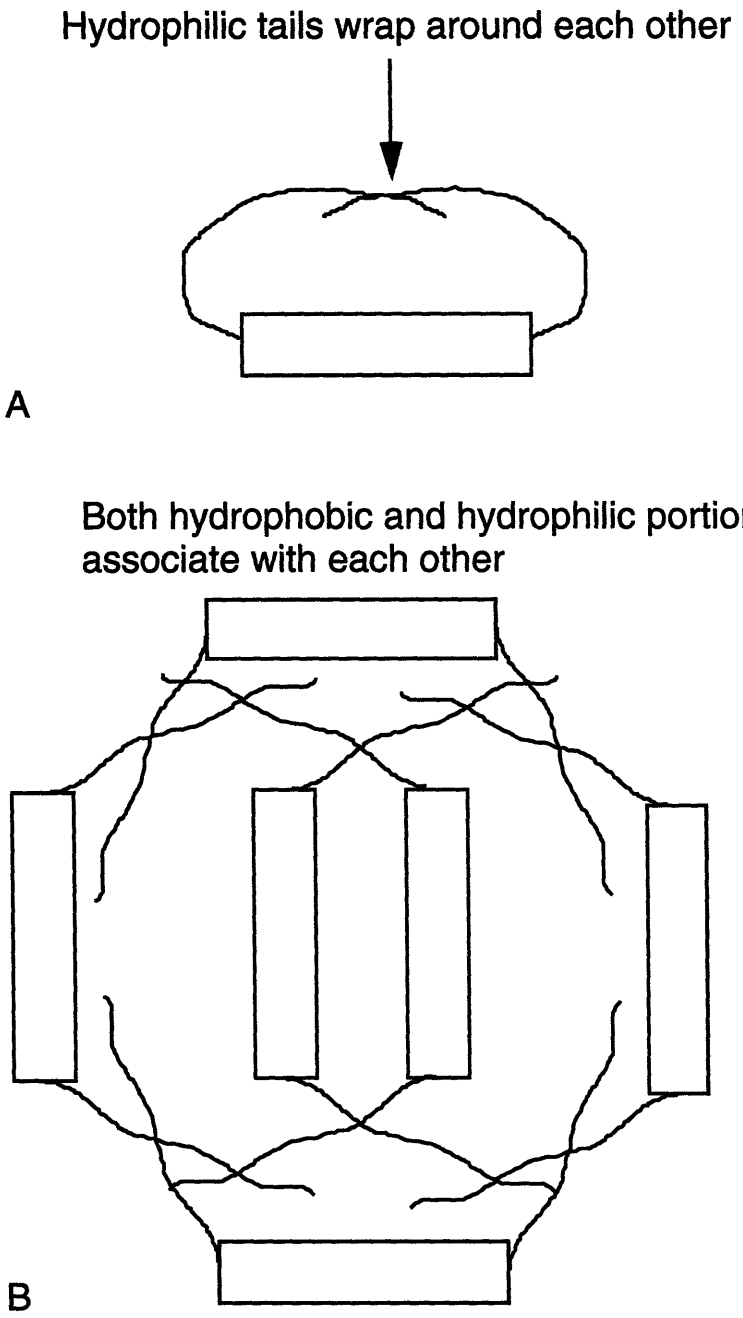

Figure 28. (A) Representation of a unimolecular micelle of P188 which forms at low concentrations when a P188 molecule wraps around itself.
(B) Representation of multimolecular micelles of P188 which form at high concentrations when 2-8 P188 molecules are associate.

studies should investigate the efficacy of P188 infused following a thermal insult. Nevertheless, the success of P188 in sealing both electrically and thermally damaged cell

membranes is very encouraging and certainly merits additional investigation. Also, further studies which can show P188, administered after a heat shock, is capable of maintaining the cell viability up to 24 hours post heat shock are warranted. These results would provide useful information on the ranges of temperatures and the thermal doses in which P188 is effective. It would also strongly support the incorporation of P188 into therapeutic protocols for treating thermally damaged muscle tissue and indicate possible effectiveness in other thermally damaged tissues.

5.3 Conclusions

This study has demonstrated the plasma membrane of skeletal muscle cells to be a major site of thermal injury. The thermally mediated membrane damage may be effected by a number of mechanisms including disruption of the phospholipid bilayer, denaturation of membrane proteins, depolymerization of the cytoskeleton, activation of secondary messenger systems by intracellular free Ca^{2+}, and/or a combination of these mechanisms. The E_a of 32.9 kcal/mole for the time for 40% calcein leakage from skeletal muscle cells suggests the activity of any one of these mechanisms. The mathematical models have demonstrated that the permeability of the plasma membrane at all temperatures except perhaps 45° C was both time and temperature dependent indicating continuous membrane disruption if exposure to elevated temperatures persists.

A concurrent study demonstrated the effectiveness of P188 in arresting and retarding transmembrane calcein leakage from skeletal muscle cells exposed to 40-60° C. These results demonstrate the first successful action of P188 in thermally damaged cells. The specificity of P188 was demonstrated by the ineffectiveness of neutral dextran in arresting calcein leakage as compared to P188. Other studies which showed the ineffectiveness of PPG and PEG as compared to P188 suggested that both the hydrophilic and hydrophobic

components of P188 were needed to arrest calcein leakage. Additional studies conducted at 45° C with the poloxamers P238, P338, P407 indicate no statistically significant difference in effectiveness among them and P188.

These results strongly suggest that further work is needed to determine the precise nature of the thermal damage process and the mechanism of P188 action. This information should aid in the development of better therapeutic treatment schemes for electrical trauma and burn victims and in the design of more effective copolymer surfactants.

References

1. DiVincenti, F.C., Moncrief, J.A., and Pruitt, B.A., Jr. Electrical Injuries: A Review of 65 Cases. *J. Trauma*, 9:672-679, 1969.

2. Hunt, J.L. Soft Tissue Patterns in Acute Electric Burns. *In* Electrical Trauma: The Pathophysiology, Manifestations and Clinical Management. Cambridge University Press, 83-104, 1992.

3. Demling, R.H. Electrical Trauma: Pathophysiology and Clinical Management. *In* Electrical Trauma: The Pathophysiology, Manifestations and Clinical Management. Cambridge University Press, 122-132, 1992.

4. Edison Electric Institute Safety and Industrial Health Committee Summary Report: Non-Fatal, Contact Electric Shock and Burn Accidents, Prepared by: A.B. Vimont and W.B. Rich, Kentucky Utilities Company, 1977.

5. Baxter, C.A. Present Concepts in the Management of Major Electrical Injury. *Surg. Clin. North Am.*, 50:1401, 1970.

6. Artz, C.P. Changing Concepts in Electrical Injury. *Am. J. Surg,* 128:600-602, 1974.

7. Lee, R.C., Gaylor, D.C., Bhatt, D.L., and Israel, D.A. Role of Cell Membrane Rupture in the Pathogenesis of Electrical Trauma. *J. Surg. Res.*, 44: 709-719, 1988.

8. Sances, A., Larson, S.J., Myklebust, J., and Cusick, J.F. Electrical Injuries. *Surg. Gynecol. Obst.*, 149:77, 1979.

9. Lee, R.C., and Kolodney, M.S. Mechanisms of Electrical Injury to Tissues: Electrical Breakdown of Cell Membranes. *J. Plast. Reconst. Surg.*, 80:672-679, 1987.

10. Dalziel, C.F., and Lee, W.R. Let-Go Currents and Voltages. *AIEE Transactions*, 75 (2):49-56, 1956.

11. Lee, R.C., and Kolodney, M.S. Mechanisms of Electrical Injury I: Dynamics of the Thermal Response. *J. Plast. Reconst. Surg.*, 80:663-671, 1987.

12. Tropea, B.I., and Lee, R.C. Thermal Injury Kinetics in Electrical Trauma. *J. Biomech. Eng.,* 114: 241-250, 1992.

13. Moussa, N.A., McGrath, J.J., Cravalho, E.G., and Asimacopoulos, P.J. Kinetics of Thermal Injury in Cells. *J. Biomech. Eng.,* 99:155-159, 1977.

14. Gershfeld, N.L., and Murayama, M. Thermal Instability of Red Blood Cell Membrane Bilayers: Temperature Dependence of Hemolysis. *J. Memb. Biol.*, 101:67-72, 1988.

15. Moussa, N.A., Tell, E.N., and Cravalho, E.G. Time Progression of Hemolysis of Erythrocyte Populations Exposed to Supraphysiological Temperatures. *J. Biomech. Eng.*, 101:213-217, 1979.

16. Lloyd, J.J., Mueller, T.J., and Waugh, R.E. On *in vitro* Thermal Damage to Erythrocytes. *ASME Paper No. 73-WA/Bio. 33*, ASME, 1973.

17. Gaylor, D.C. Physical Mechanisms of Cellular Injury in Electrical Trauma. Ph.D. Thesis, Massachusetts Institute of Technology, Cambridge, MA., 1989. (R.C. Lee, supervisor)

18. Cravalho, E.G., Toner, M., Gaylor, D.C., and Lee, R.C. Response of Cells to Supraphysiological Temperatures: Experimental Measurements and Kinetic Models. *In* Electrical Trauma: The Pathophysiology, Manifestations and Clinical Management. Cambridge University Press, 281-300, 1992.

19. Bischof, J.C., Padanilam, J.T., Lee, R.C., Cravalho, E.G., Tompkins, R.G., Yarmush, M.L., and Toner, M. (unpublished results)

20. Westra, A., and Dewey, W.C. Variation in Sensitivity to Heat Shock During the Cell-Cycle of Chinese Hamster Cells *in vitro*. *Int. J. Rad. Biol.*, 19:467-477, 1971.

21. Harris, M. Criteria of Viability in Heat-Treated Cells. *Expt. Cell Res.*, 44:658-661, 1966.

22. Powell, K.T., and Weaver, J.C. Transient Aqueous Pores in Bilayer Membranes: A Statistical Theory. *Bioelectrochem. Bioenerg.*, 15:211, 1986.

23. Benz, R., Beckers, F., and Zimmerman, U. Reversible Electrical Breakdown of Lipid Bilayer Membranes: A Charge-Pulse Relaxation Study. *J. Memb. Biol.*, 48:181, 1979.

24. Bhatt, D.L., Gaylor, D.C., and Lee, R.C. Rhabdomyolysis Due to Pulsed Electric Fields. *J. Plast. Reconst. Surg.*, 86:1-3, 1990.

25. Sugar, I.P., Forster, W., and Neumann, E. Model of Cell Electrofusion: Membrane Electroporation, Pore Coalescence and Percolation. *Biophys. Chem.*, 26:321-335, 1987.

26. Litster, J.D. Stability of Lipid Bilayers and Red Blood Cell Membranes. *Phys. Lett.*, 53 (A):193-194, 1975.

27. Taylor, G.I., and Michael, D.H. On Making Holes in a Sheet of Fluid. *J. Fluid Mech.*, 58 (4):625-639, 1973.

28. Józwiak, Z., and Leyko, W. Review: Role of Membrane Components in Thermal Injury of Cells and Development of Thermotolerance. *Int. J. Radiat. Biol.*, 62 (6):743-756, 1992.

29. Waddell, W.R., Geyer, R.P., Olsen, F.R., and Stare, J.F. Clinical Observations on the Use of Nonphosphatide (Pluronic) Fat Emulsions. *Metabolism*, 6:815, 1957.

30. Ceresa, R.J. Block and Graft Copolymerization. John Wiley & Sons, Ltd., New York. Volume 2, 1976.

31. O-T-C Topical Antimicrobial Products: Over-The-Counter Drugs Generally Recognized as Safe, Effective, and Not Misbranded. *Fed. Reg.*, 43:1210-1249, 1978.

32. Edlich, R.F., Schmolka, I.R., Prusak, M.P., and Edgerton, M.T. The Molecular Basis for Toxicity of Surfactants in Surgical Wounds. *J. Surg. Res.*, 14:277-284, 1973.

33. Schmolka, I.R., and Raymond, A.J. Micelle Formation of Polyoxyethylene-Polyoxypropylene Surfactants. *J. Am. Oil Chem. Soc.*, 42:1088, 1965.

34. Saski, W., and Shah, S.G. *J. Pharm. Sci.*, 54:71, 1965.

35. Sheth, P.B. *Diss. Abstr.*, 28:974, 1967.

36. Holland, R.J., Parker, E.J., Guiney, K.M., and Zeld, F.R. Fluorescence Probe Studies of Ethylene Oxide/Propylene Oxide Block Copolymers in Aqueous Solution. BASF Corporation, 1992.

37. Rodeheaver, G.T., Kurtz, L., Kircher, B.J., and Edlich, R.F. Pluronic F68: A Promising New Skin Wound Cleanser. *Ann. Emerg. Med.*, 9:572-576, 1980.

38. Schmolka, I.R. A Review of Block Polymer Surfactants. *J. Am. Oil Chem. Soc.*, 54:110-116, 1977.

39. Papadea, C., and Hunter, R. Effect of RheothRx copolymer on blood viscosity related to fibrin(ogen) concentration. *FASEB J.*, 2 (A):384, 1988.

40. Robinson, K.A., Roubin, G.S., King III, S.B., Black, A.J., Stack, J.E., and Hunter, R.L. Inhibition of Coronary Thrombosis after Stent Placement in Swine by Copolymer Poloxamer 188. *Circulation Suppl.*, (in press)

41. Lee, R.C., River, L.P., Pan,F-S., Ji, L., and Wollmann, R.L. Surfactant-Induced Sealing of Electropermeabilized Skeletal Muscle Membranes *in vivo*. *P.N.A.S.* USA, 89:4524-4528, 1992.

42. Lee, R.C. The Pathophysiology and Clinical Management of Electrical Injury. *In* Electrical Trauma: The Pathophysiology, Manifestations and Clinical Management. Cambridge University Press, 33-77, 1992.

43. Butler, E.D., and Grant, T.D. Electrical Injuries with Special Reference to the Upper Extremities. *Am. J. Surg.*, 134:95-99, 1977.

44. Padanilam, J.T. Kinetics of Thermal Injury in Skeletal Muscle Cells. S.B. Thesis, Massachusetts Institute of Technology, 1992.

45. Cosman, M.D., Toner, M., Kandel, J., and Cravalho, E.G. An Integrated Cryomicroscopy System. *Cryo-Letters*, 10:17-38, 1989.

46. Howarth, J.V. The Behaviour of Frog Muscle in Hypertonic Solutions. *J. Physiol.*, 144:167-175, 1958.

47. Parker, I., and Zhu, P.H. Effects of Hypertonic Solutions on Calcium Transients in Frog Twitch Muscle Fibres. *J. Physiol.*, 383:615-627, 1987.

48. Bevington, P.R., and Robinson, D.K. Data Reduction and Error Analysis for the Physical Sciences. Second Edition, McGraw-Hill, Inc., 1992.

49. Lepock, J.R., Frey, H.E., Bayne, H., and Markus, J. Relationship of Hyperthermia-Induced Hemolysis of Human Erythrocytes to the Thermal Denaturation of Membrane Proteins. *Biochim. Biophys. Acta,* 980:191-201, 1989.

50. Tien, H.T. Bilayer Lipid Membranes (BLM). Theory and Practice. Dekker, NY, 1974. Membranes and Transport. Edited by A.H. Martenosi. Plenum, NY, 1:165, 1982.

51. Kotyk, A., and Janacek, K. Membrane Transport. An Interdisciplinary Approach. Plenum, NY, 1977.

52. Chizmadzhev, Yu. A., Chernomordik, L.V., Pastushenko, V.F., and Abidor, I.G. Biofizika Membran. Edited by P.G. Kostyuk. Moscow, USSR, 2:161, 1982.

53. Kaschiev, D., and Exerowa, D. Bilayer Lipid Membrane Permeation and Rupture due to Hole Formation. *Biochim. Biophys. Acta,* 732:133-145, 1983.

54. Welty, J.R., Wicks, C.E., and Wilson, R.E. Fundamentals of Momentum, Heat, and Mass Transfer. Second Edition, John Wiley & Sons, Inc., NY, 1976.

55. Levenspiel, O. Chemical Reaction Engineering. Second Edition, John Wiley & Sons, Inc., 1972.

56. Bridgett, M.J., Davies, M.C., and Denyer, S.P. Control of Staphylococcal Adhesion to Polystyrene Surfaces by Polymer Surface Modification with Surfactants. *Biomaterials*, 13:413-416, 1992.

57. Exerowa, D., and Kaschiev, D. Hole-Mediated Stability and Permeability of Bilayers. *Contemp. Phys.,* 27 (5):429-461, 1986.

58. Wiegel, F.W. Hydrodynamics of a Permeable Patch in the Fluid Membrane. *J. Theor. Biol.*, 77:189-193, 1979.

59. Kanehisa, M.I., and Tsong, T.Y. Cluster Model of Lipid Phase Transitions with Application to Passive Permeation of Molecules and Structure Relaxations in Lipid Bilayers. *J. Amer. Chem. Soc.,* 100 (2):424-432, 1978.

60. Manstch, H.H., Yang, P.W., Martin, A., and Cameron, D.G. Infrared Spectroscopic Studies of *Acholeplasma Laidlawii* B Membranes: Comparison of the Gel to Liquid Crystalline Phase Transition in Intact Cells and Isolated Membranes. *Eur. J. Biochem.,* 178:335-341, 1988.

61. Cruzeiro-Hansson, L., and Mouritsen, O.G. Passive Ion Permeability of Lipid Membranes Modelled via Lipid-Domain Interfacial Area. *Biochim. Biophys. Acta,* 944:63-72, 1988.

62. Cruzeiro Hansson, L., Ipsen, J.H., and Mouritsen, O.G. Intrinsic Molecules in Lipid Membranes Change the Lipid-Domain Interfacial Area: Cholesterol at Domain Interfaces. *Biochim. Biophys. Acta*, 979:166-176, 1989.

63. Melchior, D.L., Morowitz, H.J., Sturtevant, J.M., and Tsong, T.Y. Characterization of the Plasma Membrane of *Mycoplasma Laidlawii* VII: Phase Transitions of Membrane Lipids. *Biochim. Biophys. Acta*, 219:114-122, 1970.

64. Lepock, J.R. Involvement of Membranes in Cellular Responses to Hyperthermia. *Radiat. Res.*, 92:433-438, 1982.

65. Biltonen, R.L., and Lichtenberg, D. The Use of Differential Scanning Calorimetry as a Tool to Characterize Liposome Preparations. *Chem. Phys. Lipids*, 64:129-142, 1993.

66. Leyko, W., and Bartosz, G. Membrane Effects of Ionizing Radiation and Hyperthermia. *Int. J. Radiat. Biol.*, 49:743-770, 1986.

67. Shnyrov, V.L., Orlov, S.N., Zhadan, G.G., and Pokudin, N.I. Thermal Inactivation of Membrane Proteins, Volume-Dependent Na^+, K^+-Cotransport, and Protein Kinase C Activator-Induced Changes of the Shape of Human and Rat Erythrocytes. *Biomed. Biochim. Acta*, 49:445-453, 1990.

68. Lepock, J.R., Frey, H.E., Bayne, H., and Markus, J. Relationship of Hyperthermia-Induced Hemolysis of Human Erythrocytes to the Thermal Denaturation of Membrane Proteins. *Biochim. Biophys. Acta*, 980:191-201, 1989.

69. Lepock, J.R., Frey, H.E., Heynen, M.P., Nishio, J., Waters, B., Ritchie, K.P., and Kruuv, J. Increased Thermostability of Thermotolerant CHL V79 Cells as Determined by Differential Scanning Calorimetry. *J. Cellular Phys.*, 142:628-634, 1990.

70. Welch, W.J., and Suhan, J.P. Cellular and Biochemical Events in Mammalian Cells during and after Recovery from Physiological Stress. *J. Cell. Biol.*, 103:2035-2052, 1985.

71. Coss, R.A., Dewey, W.C., and Bamburg, J.R. Effects of Hyperthermia on Dividing Chinese Hamster Ovary Cells and on Microtubules *in vitro*. *Cancer Res.*, 42:1059-1071, 1982.

72. Roti Roti, J.L., and Laszlo, A. The Effects of Hyperthermia on Cellular Macromolecules. *In* Hyperthermia and Oncology, VSP Utrecht, the Netherlands, 1:13-56, 1988.

73. Cotran, R.S., Kumar, V., and Robbins, S.L. Robbins Pathologic Basis of Disease. Fourth Edition, W.B. Saunders Co., PA, 1989.

74. Brandts, J.F., Erickson, L., Lysko, K., Schwartz, A.T., and Taverna, R.D. Calorimetric Studies of the Structural Transitions of the Human Erythrocyte Membrane. The Involvement of Spectrin in the A Transition. *Biochem.*, 16:3450-3454, 1977.

75. Minetti, M., Ceccarini, M., Distasi, A.M.M., Petrucci, T.C., and Marchesi, V.T. Spectrin Involvement in a 40° C Structural Transition of the Red Blood Cell Membrane. *J. Cellular Biochem.*, 30:361-370, 1986.

76. Campbell, A.C. Intracellular Calcium, its Universal Role as a Regulator. John Wiley & Sons, Inc., NY, 1983.

77. Calderwood, S.K., Bornstein, B., Farnum, E., and Stevenson, M.A. Heat Shock Stimulates the Release of Arachidonic Acid and the Synthesis of Prostaglandins and Leukotriene B4 in Mammalian Cells. *J. Cellular Phys.*, 141:325-333, 1989.

78. Calderwood, S.K., Stevenson, M.A., and Hahn, G.M. Heat Stress Stimulates Inositol Triphosphate Release and Phosphorylation of Phosphoinositides in CHO and Balb C 3T3 Cells. *J. Cellular Phys.*, 130:369-376, 1987.

79. Calderwood, S.K., Stevenson, M.A., and Hah, G.M. Effects of Heat on Cell Calcium and Inositol Lipid Metabolism. *Radiat. Res.*, 113:414-425, 1988.

80. Canaday, D., Li, P., Weichselbaum, R., Astumian, R.D., and Lee, R.C. Membrane Permeability Changes in Gamma-Irradiated Muscle Cells. (in preparation)

81. Bunn, H.F., Forget, B.G., and Ranney, H.M. Human Hemoglobins. W.B. Saunders Company, 1977.

82. Kao, H.P., Abney, J.R., and Verkman, A.S. Determinants of the Translational Mobility of a Small Solute in Cell Cytoplasm. *J. Cell Biol.*, 120:175-1984, 1993.

83. Bird, R.B., Stewart, W.E., and Lightfoot, E.N. Transport Phenomena. 7th Printing, John Wiley & Sons, Inc., NY, 1966.